

## RAUNO TEMMER

Electrochemistry and novel  
applications of chemically synthesized  
conductive polymer electrodes





## **RAUNO TEMMER**

Electrochemistry and novel  
applications of chemically synthesized  
conductive polymer electrodes



The study was carried out at the Institute of Technology, Faculty of Science and Technology, University of Tartu, Estonia.

The dissertation was admitted on May 12, 2014 in partial fulfillment of the requirements for the degree of Doctor of Philosophy (Physical Engineering) and allowed for defense by the Scientific Council of Institute of Technology of the Faculty of Science and Technology of the University of Tartu.

Supervisor: Dr. Tarmo Tamm, Institute of Technology, Faculty of Science and Technology, University of Tartu, Estonia

Opponents: Prof. Hyacinthe Randriamahazaka, Paris Diderot University, France.

Defense: June 20, 2014, University of Tartu, Estonia.

This work has been partially supported by Graduate School “Functional materials and technologies” receiving funding from European Social Fund under project 1.2.0401.09-0079 at the University of Tartu, Estonia.

This research was funded in part by the Estonian Information Technology Foundation, European Social Fund’s (ESF) Doctoral Studies and Internationalization Program DoRa carried out by Archimedes Foundation.



ISSN 1736-3349

ISBN 978-9949-32-585-6 (print)

ISBN 978-9949-32-586-3 (pdf)

Copyright: Rauno Temmer, 2014

University of Tartu Press  
[www.tyk.ee](http://www.tyk.ee)

## ABSTRACT

Chemically synthesized conductive polymer (CP) electrodes were prepared for the following electrochemical modification by electrodeposition or electrochemical (re)doping. The principal goal of the research was to develop methods and tentatively optimize the synthesis conditions to meet the needs of CP application areas with distinctively different expectations for the (physical) structure and ionic mobility of the CP electrodes. Chemical and electrochemical synthesis conditions were optimized for two CP application types: artificial muscles and high specific surface area electrodes. The presented techniques of chemical synthesis of the CP hydrogel electrodes and the novel combined chemical-electrochemical synthesis technique of CPs on nonconductive substrates offer several advantages over traditional electrodes and preparation techniques. The prepared materials and devices, based on widespread CPs polypyrrole (PPy) and poly(3,4-ethylenedioxythiophene) (PEDOT), were characterized using primarily electrochemical methods.

It was shown that metal-free PPy and PEDOT based tri-layer air-operating bending actuators, fabricated using the combination of chemical and electrochemical synthesis methods and novel low-temperature semi-aqueous electrochemical synthesis method, effectively solved the delamination problem and facilitate commercial production by avoiding the usage of precious metals, toxic organic solvents and vacuum techniques. Electro-chemo-mechanical characterization was conducted with the emphasis on ion mobility, frequency response and (voltage) step response of strain difference, strain difference rate and blocking force. The results indicate that the actuation performance of the prepared actuators compares well with ones achieved using alternative techniques. In addition, the developed method was used for the preparation of a new type of liquid-operated tri-layer linear actuators.

Large specific surface area pristine PPy hydrogel electrodes were prepared by oxidative chemical polymerization using affordable environment-friendly compounds and a simple one-step synthesis method. The structure and the electrochemical properties of the prepared hydrogels were characterized. Scanning electron microscopy, energy dispersive X-ray spectrometry, low-temperature N<sub>2</sub> sorption measurements and electrochemical measurements indicated that the structure and chemical composition of the prepared electrodes could be controlled by the synthesis conditions and post-synthesis electrochemical modification. Large specific surface area PPy hydrogels could be used to relieve power density limitations of CP-related energy storage devices, for controlled drug delivery devices, sensors, *etc.* Moreover, using PPy hydrogel as a precursor, derived PPy aerogels and carbonized aerogels were prepared, further widening the number of possible applications.



# TABLE OF CONTENTS

LIST OF ORIGINAL PUBLICATIONS .....	10
ABBREVIATIONS AND NOTATIONS .....	12
1 INTRODUCTION.....	14
1.1 Structure of the thesis .....	14
1.1.1 Overview by chapters.....	14
1.1.2 Overview by articles.....	15
1.2 Motivation .....	16
1.3 Scope .....	17
1.3.1 General goal of the work.....	17
1.3.2 General considerations and limitations .....	18
1.3.3 Conducting polymer actuators .....	18
1.3.4 Polypyrrole hydrogels and derived aerogels .....	19
1.4 General background.....	20
1.4.1 Historic background .....	20
1.4.2 Chemical structures and classes of conducting polymers .....	21
1.4.3 Conductivity mechanism of conducting polymers.....	22
1.4.4 Oxidation, reduction and the related volume changes.....	25
1.4.5 Polypyrrole and PEDOT conducting polymers.....	28
1.4.6 Overview of conducting polymer applications .....	36
1.4.7 Conducting polymer actuators as artificial muscles.....	37
1.4.8 Large surface area conducting polymer electrodes .....	43
1.4.9 Typical characterization methods.....	45
1.5 Review of the state of the art.....	52
1.5.1 Inherent shortcomings of conducting polymers as artificial muscles and large surface area electrodes.....	52
1.5.2 Conducting polymer actuators and combined chemical- electrochemical synthesis methods .....	52
1.5.3 Large surface area conducting polymer electrodes, conducting polymer hydrogels and derived aerogels .....	56
1.6 Problem statement .....	58
1.6.1 Electrochemical synthesis on initially non-conducting surfaces.....	59
1.6.2 Electrolyte-operated linear tri-layer actuators.....	60
1.6.3 Large surface area conducting polymer electrodes with high ionic mobility .....	60
2 EXPERIMENTAL .....	62
2.1 Materials and preparation methods.....	62
2.1.1 Substrates for chemical synthesis.....	62
2.1.2 Chemical synthesis of conducting polymer electrodes .....	63

2.1.3	Electrochemical synthesis, actuator preparation and electrolyte choice considerations.....	66
2.2	Characterization setup .....	68
2.2.1	Electrochemical and ECMD characterization of polypyrrole actuators.....	68
2.2.2	Electrochemical characterization of polypyrrole hydrogel .....	69
2.3	Characterization methods .....	70
2.3.1	Diffusion constant measurements .....	70
2.3.2	Electronic and ionic conductivity measurements.....	71
2.3.3	Physical structure, morphology and chemical composition ....	71
2.3.4	Doping level measurements .....	72
2.3.5	Electro-chemo-mechanical deformation measurements.....	76
2.3.6	Density, specific surface area and pore distribution of aerogels .....	78
2.3.7	Stability assessment.....	79
2.4	Electrochemical modification of hydrogels.....	79
2.4.1	Redoping of hydrogels .....	79
2.4.2	Electrochemical synthesis inside of the hydrogel .....	79
3	RESULTS AND DISCUSSION .....	80
3.1	Layered conducting polymer actuators.....	80
3.1.1	Membranes and substrates characterization .....	80
3.1.2	Chemical synthesis.....	81
3.1.3	Electrochemical synthesis .....	84
3.1.4	Actuator preparation and structure .....	88
3.1.5	Conductivity and doping level .....	90
3.1.6	Electrolytes.....	93
3.1.7	Electrochemical measurements .....	93
3.1.8	Electro-chemo-mechanical deformation measurements.....	95
3.1.9	Stability and mobility of ions .....	102
3.2	Polypyrrole hydrogels and the derived aerogels.....	105
3.2.1	Sodium dodecylbenzenesulfonate colloidal solution formation .....	105
3.2.2	Hydrogel formation .....	106
3.2.3	Polypyrrole aerogel and carbonized aerogel preparation .....	108
3.2.4	Electrochemical properties.....	109
3.2.5	Stability evaluation.....	110
3.2.6	Structure, morphology and doping level.....	110
3.2.7	Density, conductivity and low temperature N <sub>2</sub> sorption measurements .....	114
3.2.8	Control of the doping balance and the electrochemical modification of hydrogels .....	118
4	CONCLUSIONS, FUTURE WORK AND SUMMARY .....	120
4.1	Conclusions .....	120



4.1.1	Combined chemical-electrochemical synthesis method.....	120
4.1.2	Metal-free conducting polymer actuators with electrochemically synthesized working layers .....	122
4.1.3	Electrolyte-operated tri-layer linear actuators .....	123
4.1.4	Polypyrrole hydrogels and derived aerogels .....	124
4.2	Future work .....	125
4.2.1	Combined chemical-electrochemical synthesis method.....	125
4.2.2	Air-operated metal-free bending actuators .....	125
4.2.3	Hydrogels .....	126
4.3	Summary.....	126
4.4	Summary in Estonian .....	127
5	ACKNOWLEDGEMENTS .....	129
6	REFERENCES.....	130
7	PUBLICATIONS .....	145
8	APPENDICES.....	199
8.1	Experiment planning for the ECMD characterization of tri-layer bending actuators.....	199
8.1.1	Bending actuator model for strain difference calculation .....	199
8.1.2	Conversion from tip displacement to strain difference .....	199
8.1.3	Trajectory of chosen point along actuator depending on maximum strain difference.....	200
8.1.4	Actuator's shape at chosen strain difference .....	201
	CURRICULUM VITAE .....	202

## LIST OF ORIGINAL PUBLICATIONS

This thesis is based on the following articles, referenced by Roman numbers. The sequence of the articles follows the structure of the thesis. All articles are reproduced with permission from the publishers and co-authors.

1. **Temmer, R.**; Must, I.; Kaasik, F.; Aabloo, A.; Tamm, T., “Combined chemical and electrochemical synthesis methods for metal-free polypyrrole actuators,” *Sensors and Actuators B: Chemical* 166, 411–418 (2012).
2. **Temmer, R.**; Maziz, A.; Plesse, C.; Aabloo, A.; Vidal, F.; Tamm, T., “In search of better electroactive polymer actuator materials: PPy versus PEDOT versus PEDOT-PPy composites,” *Smart Materials and Structures* 22(10), 104006 (2013).
3. Kiefer, R.; **Temmer, R.**; Aydemir, N.; Travas-Sejdic, J.; Aabloo, A.; Tamm, T., “Electrochemistry of interlayer supported polypyrrole tri-layer linear actuators,” *Electrochimica Acta* 122, 322–328 (2014).
4. **Temmer, R.**; Kiefer, R.; Aabloo, A.; Tamm, T., “Direct chemical synthesis of pristine polypyrrole hydrogels and their derived aerogels for high power density energy storage applications,” *Journal of Materials Chemistry A* 1(48), 15216–15219 (2013).

### Other papers in related field:

1. Kiefer, R.; **Temmer, R.**; Tamm, T.; Travas-Sejdic, J.; Kilmartin, P.A.; Aabloo, A., “Conducting polymer actuators formed on MWCNT and PEDOT-PSS conductive coatings,” *Synthetic Metals* 171, 69–75 (2013).
2. Travas-Sejdic, J.; Tamm, T.; Kilmartin, P.A.; **Temmer, R.**; Aabloo, A.; Kiefer, R. “PEDOT/TBACF<sub>3</sub>SO<sub>3</sub> bending actuators based on a PEDOT-PEDOT sandwich complex,” in *Electroactive Polymer Actuators and Devices (EAPAD) 2013*, San Diego, California, USA (2013).
3. Lee, R.-J.; Tamm, T.; **Temmer, R.**; Aabloo, A.; Kiefer, R., “Two formation mechanisms and renewable antioxidant properties of suspensible chitosan-PPy and chitosan-PPy-BTDA composites,” *Synthetic Metals* 164, 6–11 (2013).
4. Lee, R.-J.; **Temmer, R.**; Tamm, T.; Aabloo, A.; Kiefer, R., “Renewable antioxidant properties of suspensible chitosan-polypyrrole composites,” *Reactive and Functional Polymers* 73(8), 1072–1077 (2013).
5. Kilmartin, P.A.; Travas-Sejdic, J.; **Temmer, R.**; Tamm, T.; Aabloo, A.; Kiefer, R., “PEDOT-PSS/MWCNT coatings on PET for conducting polymer actuators,” *International Journal of Nanotechnology* 11(5–8), 477–485 (2014).

6. Kiefer, R.; Aydemir, N.; Torop, J.; Tamm, T.; **Temmer, R.**; Travas-Sejdic, J.; Must, I.; Kaasik, F.; Aabloo, A., “Carbide-derived carbon as active interlayer of polypyrrole tri-layer linear actuator,” *Sensors and Actuators B: Chemical* (2014 (*Forthcoming*)).
7. Kaasik, F.; Must, I.; Lust, E.; Jürgens, M.; Presser, V.; Punning, A.; **Temmer, R.**; Kiefer, R.; Aabloo, A. “In situ measurements with CPC micro-actuators using SEM,” in *Proceedings SPIE, Electroactive Polymer Actuators and Devices (EAPAD) 2014, San Diego, California, USA* (2014).
8. Kiefer, R.; Lee, R.J.; **Temmer, R.**; Tamm, T.; Aabloo, A., “Chitosan Combined with Conducting Polymers for Novel Functionality: Antioxidant and Antibacterial Activity,” *Key Engineering Materials* 605, 428–431 (2014).

### **Author’s contribution**

In papers **I–II** and **IV**, the author was responsible for majority of research in all phases (including planning and conducting the experiments, data analysis, interpretation and writing of the manuscripts). All co-authors contributed with discussions and participated in writing of the manuscript. Several procedures and measurements were conducted by co-authors and colleagues:

**I:** preparation of the in-house solid polymer gel electrolyte membrane (F. Kaasik); measurement of frequency response of strain difference and blocking force (I. Must);

**II:** ionic conductivity measurements, SEM imaging, sulfur distribution mapping by energy dispersive X-ray spectrometry and participation in ECMD measurements (A. Maziz);

**IV:** SEM imaging (Prof. V. Sammelselg); BET measurements, PPy aerogel carbonization, participation in EIS data interpretation (Dr. A. Jänes), help with aerogel preparation (Dr. A.-L. Peikolainen).

For article **III**, the author participated in chemical synthesis on the PVdF membranes, in conducting electrochemical synthesis, in interpretation of the experimental data and in writing of the manuscript.

# ABBREVIATIONS AND NOTATIONS

*(in alphabetical order)*

Abbreviation	Explanation
AC	alternating current (voltage, sinusoidal)
Ac	propanone (acetone)
APS	ammonium peroxydisulfate
BET	Brunauer-Emmett-Teller (method)
CNT	carbon nanotubes
CP	conducting polymers
CP/dopant	notation of doped CP
CP1 CP2	notation of interface (for layered structures)
CS	chitosan
CV	cyclic voltammetry
DAQ	data acquisition, data acquisition device
DBS <sup>-</sup>	dodecylbenzenesulfonate (anion)
DFT	density functional theory
EAP	electro-active polymer
EC	electrochemical/electrochemically
ECMD	electro-chemo-mechanical deformation
EDL	electrical double layer
EDLC	electric double layer capacitor
EDOT	3,4-ethylenedioxythiophene
EDX	energy dispersive X-ray spectrometry
EIS	EC impedance spectroscopy
EMIm <sup>+</sup>	1-ethyl-3-methylimidazolium (cation)
EtOH	ethanol
EQCM	EC quartz crystal microbalance
ESI	electronic supplementary information
FS	freestanding (film)
FTIR	Fourier transform infrared spectroscopy
IEAP	ionic electromechanically active polymer
IH	in-house (solid polymer gel electrolyte)
IPMC	ionic polymer-metal composite
IPN	interpenetrated network
ITO	indium tin oxide
MEG	ethan-1,2-diol, monoethylene glycol
MEMS	microelectromechanical systems
MeOH	methanol
MFC	microbial fuel cell
MP	4-methylpentan-2-one
MPD	Millipore Durapore
MPI	Millipore Immobilon-P

$n$ M Py-APS	notation of hydrogel from equally $n$ M concentration (regarding to final volume) of Py and APS
OLED	organic light emitting diode
PAn	polyaniline
PC	4-methyl-1,3-dioxolan-2-one, propylene carbonate
PEDOT	poly(3,4-ethylenedioxythiophene)
Py	pyrrole
PPy	polypyrrole
PSS <sup>n-</sup>	polystyrenesulfonate (polyanion)
PTh	polythiophene
<i>p</i> TS <sup>-</sup>	4-methylbenzenesulfonate ( <i>p</i> -toluenesulfonate, anion)
PVdF	poly(vinylidene fluoride)
PVdF-HFP	poly(vinylidene fluoride-co-hexafluoropropene)
RMS	root mean square
RT	room temperature
RTIL	room temperature ionic liquid
SDBS	sodium dodecylbenzenesulfonate
SEM	scanning electron microscopy (microscope)
SPE	solid polymer gel electrolyte
SPS	disodium peroxydisulfate
SS	stainless steel
TBA <sup>+</sup>	tetrabutylammonium (cation)
TFSI <sup>-</sup>	bis(trifluoromethanesulfonyl)imide (anion)
ZRA	zero resistance ammeter

# I INTRODUCTION

## I.1 Structure of the thesis

### *I.1.1 Overview by chapters*

The section “**Overview by articles**” describes in brief the articles, on which the current work is based and the relations between the articles and the current work are explained.

In the sections “**Motivation**” and “**Scope**”, the importance, the goals of the study, the addressed problems are defined, and the limits of the research are outlined.

The section “**General background**” provides a general literature overview from the discovery and development of CPs to their application as actuators and energy storage devices. Both CP-based applications are positioned in the context of the closest alternative approaches. In detail are addressed the properties and concepts, which are equally important in both application areas: origins of conductivity, EC oxidation/reduction processes and related volume changes. In section “**Polypyrrole and PEDOT conducting polymers**” synthesis methods, doping level concept and EC modification methods are described by the example of the two most popular CPs in literature – PPy and PEDOT. The variety of the applications of CPs is briefly referenced in section “**Overview of conducting polymer applications**”. The general literature overview is amended with aspects specific to CP actuators in section “**Conducting polymer actuators as artificial muscles**”. Different design types, materials, preparation processes, actuation principles and key performance indicators are described with emphasis on those related to the current study. In a similar way, in the section “**Large surface area conducting polymer electrodes**”, promising application fields of CP hydrogels are described. For both application types, CP-based devices are compared with similar non-CP alternatives. The most common characterization methods, used throughout the work are described briefly in section “**Typical characterization methods**”.

The section “**Review of the state of the art**” lists the most critical shortcomings of CP actuators and CP-based energy storage devices. The most relevant works and recent advancements related to this study, as well as the origins of the most important concepts are referenced in order to acknowledge the prior achievements, but also the limitations, addressed in the current work, are stated.

In the section “**Problem statement**”, the research questions and the addressed problems are formulated. One out of the several possible solutions to the addressed problems is proposed and hypotheses are set about implications of the proposed approach for the two considered application areas.

In the chapter “**Experimental**”, the experimental part, the used materials, equipment and characterization methods are specified. Due to the novelty and strong emphasis on the synthesis conditions, in the section “**Materials and**

**preparation methods**”, the combined chemical-EC synthesis method and preparation of the pristine PPy hydrogel are described in detail. In the sections “**Characterization setup**” and “**Characterization methods**”, specific characterization conditions and methods, together with appropriate reasoning (more detailed aspects are discussed in chapter “Results and discussion”) will be presented for actuators, hydrogels and aerogels.

The chapter “**Results and discussion**” is partitioned by the covered application areas and internally divided by the most important preparation steps and by the most important characterized parameters. The most significant results of the experiments are presented, interpreted and discussed. Measurement results give an overview of the most characteristic properties. The main emphasis is on implications of usage as electroactive electrodes and possibility of further EC modification of the chemically synthesized electrodes.

In chapter “**Conclusions, future work and summary**”, the most significant results are presented, divided by novel concepts. Novel results and conclusions of the study will be summarized and promising further research directions and implications are predicted.

### ***1.1.2 Overview by articles***

**Paper I** describes the combined chemical-EC synthetic route for the preparation of metal free air operated FS tri-layer bending type PPy/DBS actuators using different types of membranes as separators and electrolyte storage layers. The method solves the delamination problem observed for conventional PPy actuators made layer by layer, without using difficult to commercialize vacuum coating techniques. The paper establishes the concept of the combined chemical-EC synthesis method and chemically synthesized CP electrodes, studies the different ways for such synthesis and characterizes actuators in terms of ion mobility type, strain difference, strain difference rate, blocking force and exchanged charge depending on applied frequency. Low-temperature semi-aqueous synthesis method is introduced.

**Paper II** deals with a comparative study of metal-free air-operated PPy and PEDOT based tri-layer actuators. The work is based on **Paper I**, utilizing the combined chemical-EC synthesis method additionally for novel PEDOT tri-layer actuators and combinations of PPy and PEDOT, as chemically synthesized electrode and EC synthesized working layer materials. The influences of chemically and EC polymerized conductive layers are studied in detail. Four combinations of electronic conducting polymer layers with two different electrolytes are compared.

In **Paper III**, the combined chemical-EC synthesis method (**Paper I**) and chemical deposition of PEDOT (**Paper II**) is used for the synthesis of tri-layer liquid operated linear actuators. The novel concept for linear actuator preparation facilitates their processing and implementation for practical applications. The structure, EC and ECMD properties are characterized. Actuation

mechanism (ion mobility type) dependence on passive interlayer substrate properties and actuation speed is analyzed for two distinctively different interlayer materials.

**Paper IV** presents a simple and direct chemical preparation method of novel pristine PPy hydrogel electrodes and derived polypyrrole and carbonized aerogels, and outlines their characteristic properties – low density, high ion mobility and high specific surface area. Principally, the concept of **Paper I** is followed, using the chemically synthesized PPy hydrogels as electrodes of very different structure, properties and targeted application area. Moreover, the properties of the PPy hydrogels can be tuned by synthesis conditions and post-synthesis EC modification, using the hydrogels as chemically synthesized electrodes.

## I.2 Motivation

Although CPs exhibit variety of properties, making them promising for many applications, and despite the large amount of scientific papers published, CPs have not yet made a break through as commercial products in the context of artificial muscles and large surface area electrodes. After being extensively studied during past decades, CPs still have great potential for further research, development and commercialization. While CPs are easier to manufacture and process than their inorganic analogues, their limited processability, lack of appropriate preparation methods and number of technical issues still make large-scale production difficult. The whole variety of CP properties and tuning options is interconnected with each other in a very sophisticated way, demanding thorough research in order to find the optimal set of conditions for every single application considered.

Challenges, which impede commercial break-through in the most critical development areas are reflected at the European Union level in research and development priorities, set by the European Cooperation in Science and Technology (COST):

- COST Action MP1003: European Scientific Network for Artificial Muscles (ESNAM) priority for ionic EAP artificial muscles: “increase of lifetime and response speed, along with manufacturing in film and fiber form through processes that can be industrialized” [1];
- COST Action MP1004: Hybrid Energy Storage Devices and Systems for Mobile and Stationary Applications: “Multiple interrelated factors have to be satisfied and considered simultaneously: high energy density in combination with high power density, temperature operation range, acceptable level of investment and operational costs at the entire life cycle” [2].

The motivation for the current work is to contribute in both areas using the single concept of chemically synthesized CP electrodes. Many publications



compare the pros and cons of chemical and EC synthesis and modification. CPs are conventionally synthesized either by chemical or EC method depending on the planned application area. Both methods have their advantages and disadvantages depending on the application field. Rarely have these methods been used in combination, which would offer additional synergy, or used for purposes achievable by neither methods separately. In addition, there are only few examples of CP usage as primary electrodes for the EC processes, and the common usage is either as a separate coating material or for the modification of some other primary electrode material. The aim of the current work is to gain additional value from the combined use of chemical and EC synthesis methods and to study CPs as EC electrodes, thereby increasing the potential of CPs for commercial applications. The current work is aimed at value, gained from the synergy between the two methods.

The initial motivation for the current work was the development of a cost-effective metal-free synthesis method for CP actuators without assembly and delamination problems. Research focus was on finding possibilities to synthesize EC CP working layers on initially non-conducting materials. The concept of combined chemical-EC synthesis was formulated as the EC modification of chemically synthesized CP electrodes and adapted for energy storage devices and for electrodes with large surface area in general.

The performance of energy storage devices (as well as that of CPs in many other applications) depends on the permeability and ion mobility inside the electrode material. Very good specific performance indicator values have been achieved, but only for rather small quantities of material. A special class of CP nanostructures, the hydrogels, is an obvious solution to relieve the diffusion limitation issues, retaining the properties of the compact material while still well accessible for ions. To the author's best knowledge to date, there are no reports about CP hydrogels based on single low-cost and well-studied CP and simple production method.

Crosscutting considerations for both application types and all techniques used were low cost, low environmental impact, simplicity and scalability.

## **I.3 Scope**

### ***I.3.1 General goal of the work***

The current work is dedicated to the study of *in situ* chemically synthesized organic CPs for application as electrodes in fabrication of EC and electro-chemo-mechanical devices. The research focuses on finding reproducible synthesis conditions, preparation methods and EC modification possibilities to meet the expectations of two distinctively different application areas with very different requirements. The characterization and the preliminary feasibility study of the resulting materials were conducted for the following purposes:

- presenting a general description of the more or less application-independent properties of the materials in order to estimate their potential for different applications with emphasis on EC characterization methods;
- comparison with alternative approaches and results in scope of two distinctively different application areas – *CP actuators* and *large surface area CP electrodes*;
- pointing out the novelty, the advantages and the disadvantages of the resulting materials and synthesis methods;
- proposing and (re)introducing less traditional (in CP research) characterization methods and metrics.

### **1.3.2 General considerations and limitations**

Where not stated otherwise, only p-doped organic CPs are considered in chapter “Introduction” and if not specified otherwise, PPy is considered as an example. CP synthesis methods used in the current thesis are described for PPy and PEDOT only.

CP electrodes and CP-modified electrodes (not considered in this work) are distinguished based on their role (*e.g.* chemical synthesis on non-conductive surfaces for the following EC deposition), and on the extent of impact to characteristics (*e.g.* PPy hydrogels). Metallic or non-CP conductors are considered as terminals to the main CP material. Only *in situ* chemically synthesized electrodes are considered, excluding *e.g.* electrodes spin-coated from commercial PEDOT/PSS dispersions.

Although the main emphasis of the work is on the EC methods, characterization methods and characterized properties are for consistency not limited to traditional EC ones, and due to the EC origin of the mechanical properties of CPs, ECMD characterization is considered as a subset of EC characterization.

Synthesis and preparation conditions were not fully optimized for any specific application or device. The phrase “novel applications” in the topic should be interpreted as reference to the application areas, where the *chemical-EC synthesis method* and *PPy hydrogels* have the most obvious advantages – CP actuators and energy storage devices.

### **1.3.3 Conducting polymer actuators**

The studied actuators are metal-free ionic EAP-based air-operated tri-layer bending actuators and electrolyte-operated tri-layer linear actuators with PPy, PEDOT or combined electrodes. EC modification was studied as the EC synthesis on chemically synthesized CP electrodes.

ECMD characterization of the actuators does not pretend to be all-inclusive nor specific for some practical application to avoid the increase the bulk of the thesis without increasing the readability or clarity of the original material. There

are many performance characteristics important for actuators: absolute strain, reversible strain, strain rate, stability, force, energy consumption, power to weight ratio, reaction speed, mechanical properties, creep behavior, *etc.* The choice of the investigated characteristics depends usually on the application field considered. The focus of the current work was not the development (including optimization) of actuators for specific application or a comparison with a large number of published actuator descriptions, but rather a qualitative comparison with similar alternatives and the presentation of novel techniques for actuator preparation. The main goal of the characterization was presenting a metal-free chemical-EC synthesis routes and their implications. EC and actuation properties for different electrolytes were neither comprehensively analyzed nor optimized in the current work. Other combinations and materials not included in this work have been studied as well, but the data is in many ways incomparable to those considered in the current work. A minimal amount of unpublished data is included for the sake of integrity.

However, the most common characteristics (with emphasis on reversible strain and strain difference) have been presented, in order to give an idea about the magnitude of the characterized values and to allow to some degree the comparison with freely chosen actuator types from the literature and between separately published original articles.

For the actuators, one of the most important stability criterions in context of the current work is stability against delamination. It is not possible to claim absolute elimination of the delamination problem. Actuators were considered delamination-proof in basis that no delamination was observed during characterization of the other properties to the extent of at least several thousand actuation cycles.

### **1.3.4 Polypyrrole hydrogels and derived aerogels**

Although in some literature sources even electrodeposited CP films, operating in liquid environment, have been regarded as dense gels [3, 4], in the current work, only sparse, jelly-like hydrogels were considered, which are sparse enough to collapse due to capillary forces on conventional drying. Four PPy hydrogels of different densities were characterized in detail and the evaluation of their EC modification was limited to additional doping, redoping and EC synthesis inside of the hydrogel.

For brevity's sake and for better readability, "large surface area" in context of the current work means "large *specific* surface area at commercial level mass loadings".

## **1.4 General background**

By conductivity ( $\sigma$ ) or band gap between valence and conduction band, all materials can be roughly divided into four groups: insulators ( $\sigma < 10^{-7}$  S cm<sup>-1</sup>, band gap usually  $> 3$  eV), semiconductors ( $10^{-4} < \sigma < 10$  S cm<sup>-1</sup>, small band gap), metals/conductors ( $\sigma > 10^3$  S cm<sup>-1</sup>, very small or no band gap) and superconductors. For a long time, organic polymers were used as insulators. After the discovery of organic CPs and the development of the CP-based functionalized materials, CPs rapidly became a popular research field. New CPs are synthesized continuously and CPs find usage in an increasing number of functions. The electrical and optical properties of CPs are approaching those of metals and inorganic semiconductors, retaining many properties of the traditional organic polymers, such as the versatility of synthesis methods and processing options. Among many distinctive properties, from the perspective of the current thesis, some CP properties are more important than others. These are the conductivity, the volumetric changes on reversible reduction/oxidation, the structure, the ion mobility (charge compensation mechanism and rate) and the charge storage ability.

### **1.4.1 Historic background**

Despite an early report about the EC synthesis of doped PAn by H. Letheby in 1862 [5], the chemical composition of the obtained material and its conductivity remained undiscovered. The first chemical oxidative synthesis of low molecular weight Py oligomers was reported in 1888 [6], and the first chemical synthesis of EC active PPy dates back to 1916 [7]. Nevertheless, for a long time organic polymers were generally considered as dielectrics, until the (re)discovery of the conductivity of chemically synthesized PPy ( $\sim 1$  S cm<sup>-1</sup>) in 1963 [8] and of polyacetylenes by the end of 1964 [9]. The first EC synthesis of PPy film on Pt ( $8$  S cm<sup>-1</sup>) was reported in 1968 [10]. Only in 1977 Hideki Shirakawa, Alan G. MacDiarmid and Alan J. Heeger gained broader attention with the high conductivity ( $\sim 10^3$  S cm<sup>-1</sup>) of iodine-doped polyacetylene [11] and were awarded the Nobel Prize in chemistry in 2000 “for the discovery and development of conductive polymers” [12]. Important steps in the research of CPs were the first EC synthesized freestanding, environmentally more stable PPy film [13] and the exchange of dopant anion [14]. Since then, many other characteristic properties, such as optical, magnetic, controllable hydrophobicity, mechanical, ionic *etc.* have been revealed and the CP landscape is rapidly developing. The distinguishable development directions are the synthesis of new CP types and composites with other materials, CP usage in different functions utilizing the different properties of the CPs, and the development of synthesis methods.

### 1.4.2 Chemical structures and classes of conducting polymers

Some examples of the most widespread and extensively studied CPs and their chemical structures are depicted in **Figure 1.1**. Common features of CPs are the backbone consisting of alternating (conjugated) single- and double bonds and the planarity of the conjugated bond system.

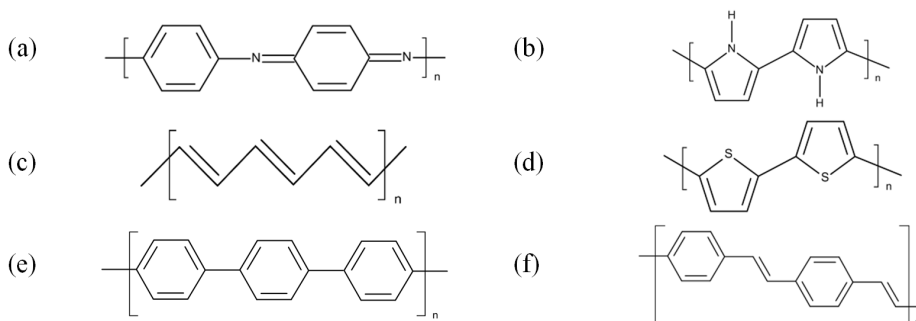


**Figure 1.1.** Examples of the most widespread and well-studied pristine CPs: a) PAN; b) PPy; c) *trans*-polyacetylene; d) polythiophene; e) poly(*p*-phenylene); f) poly(*p*-phenylene vinylene).

The aforementioned basic CPs (among others) can be used as building blocks for substituted polymers (*e.g.* PEDOT in **Figure 1.2a**), self-doped polymers (*e.g.* **Figure 1.2b**, [15]), co-polymers (*e.g.* **Figure 1.2c**, [16]), composites [17, 18], blends [18] and hybrid materials with inorganic macro-ions. Taking into account also CPs doped with different counter-ions, the number of derived CPs and CP-based materials becomes virtually endless. CPs may appear in form of films, fibers, powders/dispersions and different nanostructures.

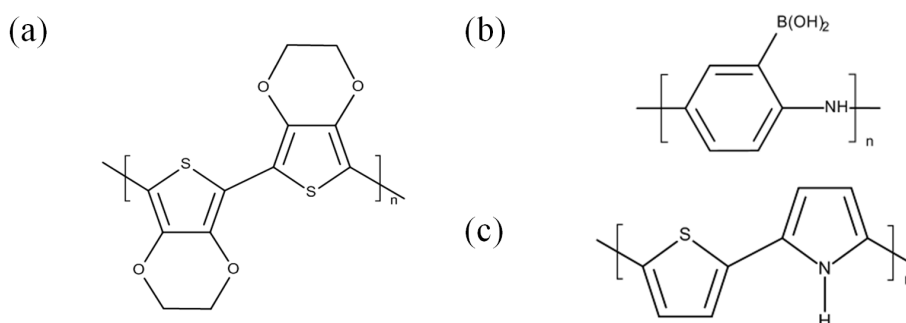


**Figure 1.2.** Characteristic examples of derived CPs: a) substituted PTh (PEDOT); b) self-doped PAN; c) PPy-PTh co-polymer.

Although in literature, derived CPs are often referred based on the corresponding unmodified polymers, like “polypyrroles”, “polythiophenes”, *etc.* [19], a large number of different properties, reported in literature even for the same CP (*e.g.* PPy) depend heavily and in a complex way on many variables, such as synthesis conditions, formulations, measurement conditions and performance metrics [20]. Therefore, very few predictions can be made about most of the properties only by the CP structural formula.

### 1.4.3 Conductivity mechanism of conducting polymers

Pristine polymers are poorly conducting semiconductors or insulators, and for increased conductivity a polymer must be doped by adding (reducing by n-doping) or removing (oxidizing by p-doping) electrons from polymer chains. Charge transport properties of CPs range from insulators to metals. Upon doping, conductivity of conjugated polymers increases several orders of magnitude, reaching the upper range of semiconductors close to the conductivity of metals with additional conductivity control feature by EC changeable oxidation state.

**Table 1.1.** The maximum conductivities of common metals/conductors, CPs, semiconductors and insulators.

Material	Max. conductivity (S cm <sup>-1</sup> , type)	Type by conductivity*
Silver	$6.2 \cdot 10^5$	Metals/conductors
Copper	$6 \cdot 10^5$	
Polyacetylene (CP)	$> 10^5$ (n, p) [16]	
Lead	$4.5 \cdot 10^4$	
Poly(p-phenylene vinylene) (CP)	$10^4$ (p) [16]	
PEDOT (CP)	$> 10^3$ (n, p) [21]	
Polypyrrole (CP)	$10^3$ (p) [16]	
Poly(p-phenylene) (CP)	$5 \cdot 10^2$ (n, p) [22]	
Polyaniline (CP)	$3 \cdot 10^2 \dots 4 \cdot 10^2$ (p) [16]	
<i>Mott's minimum metallic conductivity</i>	$10^2$	
Polythiophene (CP)	$10 \dots 10^2$ (p) [22]	
Germanium	$10^{-2}$	Semiconductors
Silicon	$10^{-5}$	
Glass	$10^{-13}$	Insulators
Quartz	$7.4 \cdot 10^{-19}$	

\* somewhat arbitrary division

Most CP applications utilize p-doping and the incorporated anions are essential for the conductivity and for maintaining of charge neutrality. Due to molecule-wide overlapping of delocalized  $\pi$  molecular orbitals ( $\pi$ -bonds) in defect-free conjugated polymers, electrons removed from these orbitals ( $\pi$ -electrons) create perturbations acting as highly mobile charge carriers along the CP chains. Thus, CPs are called  $\pi$ -conjugated polymers (**Figure 1.3**). The presence of a  $\pi$ -conjugated system is characteristic of only CPs and not of other redox polymers (e.g. poly(vinyl ferrocene)).

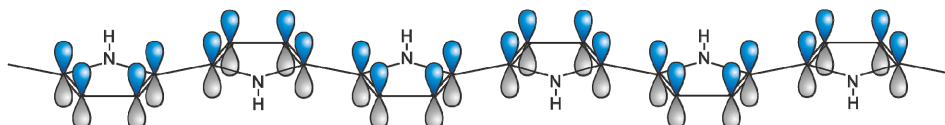


**Figure 1.3.** Conjugated  $\pi$ -orbitals of PPy, forming  $\pi$ -bonds.

Unlike the p-doped inorganic semiconductors, where charge is carried due to electrons removed from the top of the valence band, charge carriers in p-doped CPs are typically referred to as polarons (radical cations with spin  $\frac{1}{2}$ ) and bipolarons (spinless dication) or charged solitons (in *trans*-polyacetylene, spinless) moving in electric field [22]. At lower doping levels polaron conductivity prevails, but with increasing doping level (up to *ca* 0.33 for typical EC synthesized PPy), polarons are replaced by thermodynamically favored bipolarons. At very high p-doping levels (achieved for PTh), metal-type conductivity appears due to the merging of the broadened lower bipolaron band with the valence band [22, 23]. Evolution of charge carriers and electronic bands with increasing doping level in PPy is depicted in **Figure 1.4a** (where CB and VB stand for the conduction band and the valence band, respectively, adapted from [22]). Further oxidation leads to irreversible over-oxidation (**Figure 1.8b**, adapted from [18]).

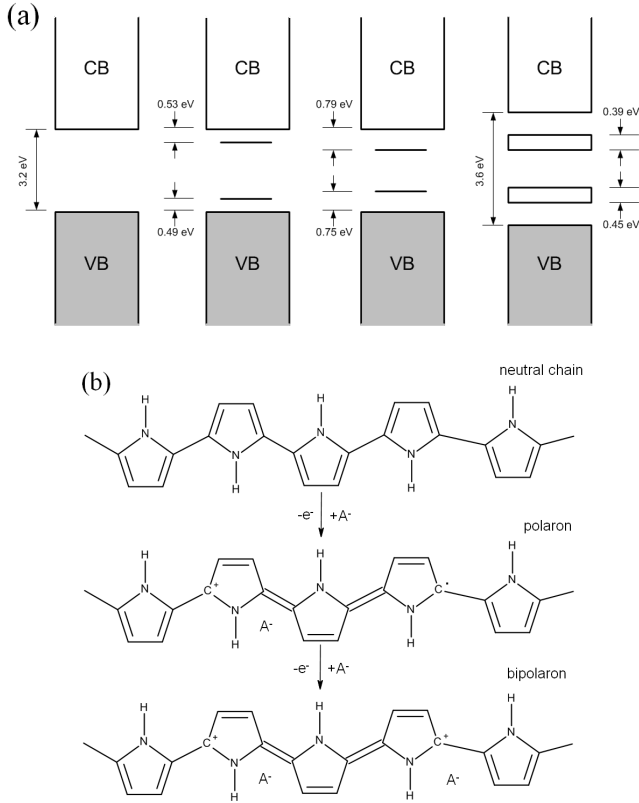


**Figure 1.4.** a) PPy band structure evolution with increasing doping level (from left to right): undoped state, low doping level (*ca.* 15 ... 25%, polaron orbitals form), moderate doping level (bipolaron orbitals form), highly doped state (*ca.* 33%, bipolaron bands form); b) oxidation depending on potential (from top to bottom): undoped PPy, polaron formation; bipolaron formation.

In addition to the conductivity along CP chains, inter-chain hopping mechanism must also be present for macroscopically observable conductivity. This inter-chain hopping/tunneling is considered as a major factor limiting conductance [22]. Conductivity dependence on temperature is often described by equation:

$$\sigma(T) = \sigma_0 \cdot \exp \left[ - \left( \frac{T_0}{T} \right)^k \right], \quad (1.1)$$

where  $\sigma(T)$  is the temperature-dependent conductivity,  $T$  is the temperature,  $\sigma_0$  is the conductivity prefactor,  $T_0$  is the characteristic temperature and  $k$  is a characteristic of the transport process. For metal-type conductivity along

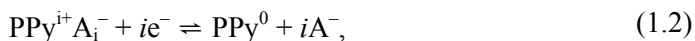


polymer chain, the temperature coefficient is negative (conductivity decreases with increasing temperature), and for semiconductors – positive (conductivity increases with increasing temperature). The exponent  $k$  is interpreted often in terms of variable range hopping (VRH) model or (if  $k = 1$ ) nn-H (nearest-neighbor hopping) type conductivity [24]. For VRH model,  $k = 1 / (d + 1)$ , where  $d$  is the conduction path dimensionality. By literature data [25], one can say that depending on CP, its structure, doping level and temperature, different types of conductivity are manifested both for hopping between CP chains as well as between larger morphology-dependent granular structures. A more general 3D delocalization model is proposed by Zuppiroli *et al.*, explaining the conductivity between chains as adiabatic hopping/tunneling through dopant ions and the conductivity between polaronic clusters by slower nonadiabatic inter-cluster Coulomb gap hopping ( $k = 1/2$ ) [26], characteristic of granular metals [27].

For best conductivity, the conjugation length (defect-free length of the conjugated polymer chain) should be as long as possible and the hopping range as short as possible, which is supported by higher crystallinity degree and chain alignment.

#### **1.4.4 Oxidation, reduction and the related volume changes**

Oxidation means the removal of electrons from CP (p-doping) by applying positive potential, and the availability of anions is needed for balancing the appearing excess positive charge by incorporation of anions. The opposite process, addition of electrons to the oxidized CP, compensates the positive charge of CP chains and if incorporated anions are small and mobile enough ( $\text{Cl}^-$ ,  $\text{Br}^-$ ,  $\text{NO}_3^-$ ,  $\text{ClO}_4^-$ , *etc.*), they move out of the polymer matrix to retain its electroneutrality. Formally, for PPy (left side: oxidized state, right side: reduced state):



where  $\text{PPy}^+$  denotes oxidized PPy, doped with anions  $\text{A}_i^-$ , and  $\text{PPy}^0$  is the undoped, neutral PPy. Usually, as-prepared CPs are already oxidized (and hence conductive) to some degree, and charge neutrality is maintained already by doping anions, incorporated during synthesis of CPs.

Oxidation-reduction process is different, when anions are large (naphtalene-1,5-disulfonate,  $\text{DBS}^-$ , 1,4-bis(2-ethylhexoxy)-1,4-dioxobutane-2-sulfonate,  $\text{PSS}^{\text{H}-}$ , *etc.*) or the motion of anions is hindered for some of several other reasons. In that case, adding electrons still makes the initially oxidized CP chains neutral, but due to the immobility of the anions, their excess negative charge is compensated by the ingress of cations in order to maintain charge neutrality. Formally, for PPy (left side: oxidized state, right side: reduced state):



where  $\text{C}_i^+$  denotes the incorporated cations.

Generally, oxidation-reduction process of CPs is considered as a reversible and quasi-equilibrium process. In both cases, current from the electron flux in response to cyclic potential change (CV) is expressed as a pair of current peaks in opposite directions. Usually the shape of the current-voltammogram is characteristic of the mobility type (**Figure 1.5**).

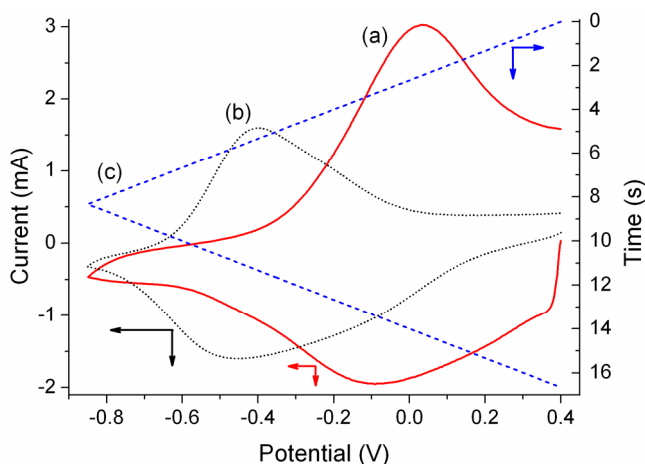
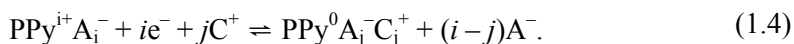


**Figure 1.5.** Current response to the cyclic potential change (synthesis charge  $0.2 \text{ C cm}^{-2}$ , gold substrate): a) anion-active PPy/ $\text{ClO}_4$  in  $0.1 \text{ M LiClO}_4$  electrolyte; b) cation-active PPy/ $p\text{TS}$  in  $0.1 \text{ M NapTS}$  electrolyte; c) potential ( $E = 0.4 \dots -0.85 \dots 0.4 \text{ V}$ , scan rate  $150 \text{ mV s}^{-1}$ ).

Often mixed motion of ions occurs, if anions are of moderate size (benzene sulfonate,  $p\text{TS}^-$ , *etc.*), double-charged ( $\text{SO}_4^{2-}$ ) or of size close to that of cations ( $\text{TFSI}^-$  vs.  $\text{EMIm}^+$ ). Anions and cations have usually different diffusion speed and often the motion of solvent molecules is involved. The type of the dominant mobile ion depends on synthesis conditions, electrolyte, solvent, applied stress, potential scan rate, *etc.* Moreover, conditions influencing ion mobility can be changed by redoping with anions of different size or charge distribution, changes in structure or density of the CP, by altering the supporting electrolyte, potential shape, *etc.* Formally, for PPy (left side: oxidized state, right side: reduced state):



The working principle and the key performance indicator values of CP-based energy storage devices rely on the CPs' charge storage ability and oxidation/reduction rate.

Characteristic of CPs is the volume change due to ingress or egress of ions. Swelling and the connection between dopant concentration and the applied mechanical stress of CP was predicted by the intercalation model of Baughman, Hsu *et al.* in 1978 [28, 29] and experimentally measured by Francois 1981 [30]. The first CP actuator is attributed to Baughman *et al.* in 1987 [31]. Based on the observation that the permeability of CP membrane to certain ions depends on the polarization potential (Burgmayer and Murray, 1982 [32]), Otero *et al.* (1992, [33]) synthesized an anion-active bi-layer CP actuator (**Figure 1.6a**). Using the bending beam method, Pei and Inganäs developed a mathematical method, binding the volume and the structural change of the CP due to ion fluxes in and out of CP with the macroscopically expressed bi-layer curvature change [34, 35].

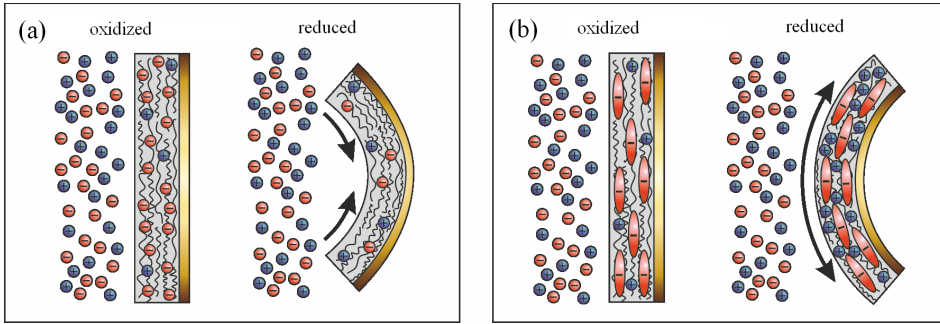


**Figure 1.6.** Bi-layer curvature change on bending of: a) an anion-active film on oxidation; b) a cation-active film on reduction. Reduction of anion-active and cation-active bi-layer causes bending into opposite directions.

Although contributions from alternative mechanisms, such as the electrostatic repulsion between charged CP chains have been suggested [36], the vast majority of the volume change is attributed to ion movement. Otero *et al.* has shown that if only one type of ions (cations or anions) is moving then the volume change, caused by ion motion, is proportional to the exchanged charge [37]. His model, derived largely based on unimorph bending bi-layer in electrolyte, explains the connection between redox processes and volume changes. Having the number of moving ions:

$$n = \frac{Q_{red(ox)}}{z}, \quad (1.5)$$

where  $Q_{red(ox)}$  is the exchanged charge during reduction or oxidation and  $z$  is the ion charge, then

$$\Delta V_{red(ox)} = n \cdot \frac{4}{3} \cdot \pi \cdot r^3 + \Delta V_{sol}, \quad (1.6)$$

where  $\Delta V_{red(ox)}$  is the total volume change during reduction or oxidation,  $r$  is the crystallographic radius of the ions and  $\Delta V_{sol}$  is the volume change, caused by ingress or egress of solvent molecules. Using EQCM and EIS methods, Plieth *et al.* [38] have shown that cations are solvated and carry different numbers of solvent molecules. In addition, motion of solvent molecules can be caused by maintaining equilibrium between chemical potentials and (at a slower rate, [39]) osmotic pressure of the polymer and electrolyte [3, 4]. In case of anion mobility in PEDOT, anion insertion is accompanied by the expulsion of solvent molecules (except  $\text{SO}_4^{2-}$ , which due to the double charge and high charge density is carrying water) [38].

#### 1.4.5 Polypyrrole and PEDOT conducting polymers

In the current work, PPy (**Figure 1.1b**, the respective Py monomer in **Figure 1.7a**) and a substituted derivative of polythiophene – PEDOT (first synthesized by Heywang *et al.* 1992 [40], **Figure 1.2a**, the respective EDOT monomer in **Figure 1.7b**) were used as industrially promising model materials. Both have certain similarities and differences and in many cases can substitute each other. Both PPy and PEDOT can be prepared chemically (as coatings, dispersions, powders, in solutions, solution-gas interfaces or in vapor phase) or EC as coatings or freestanding films (after peeling off from the electrode), allowing the tuning of properties by synthesis conditions. In many cases, they can be synthesized under similar conditions, allowing comparison with each other. Significant differences are the conductivity, the aqueous solubility of the monomers, the mechanical properties, the stability, and the monomer price.

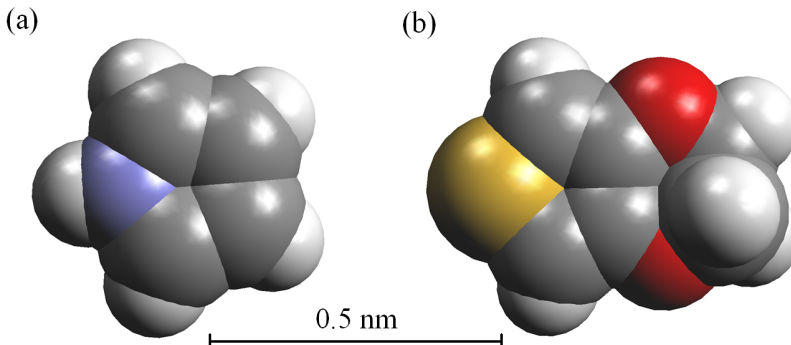


**Figure 1.7.** Space-filling model images of monomers: a) Py; b) EDOT.

As mentioned before, the number of different CPs is virtually unlimited. Nevertheless, among many others, PPy remains one of the first discovered and the most thoroughly studied CPs. PPy is attractive because of the good conductivity, biocompatibility (including with mammalian cells [41]), environmental stability at ambient conditions, versatility of the synthesis methods and broad range of synthesis conditions. PPy is also attractive as a model CP material for scientific research due to the low oxidation potential of the Py monomer, large variety of applications, and huge commercial potential due to the ease of EC synthesis in aqueous solutions and affordable price of the monomer. PPy can also be used in its non-conducting over-oxidized form (**Figure 1.8a**) as permselective membrane for biosensors [42, 43], and anti corrosion protection [44]. PPy can be polymerized at neutral pH and it retains its conductivity up to pH 10 [45].

PEDOT belongs to the class of substituted thiophenes. PEDOT gained attention relatively recently due to its high conductivity, biocompatibility, chemical and thermal stability. Transparency in its oxidized state has made it especially attractive for photovoltaic and OLED applications. Comparing to PPy, PEDOT is mechanically softer, while even chemically synthesized PEDOT has usually higher conductivity due to fewer defects, as the  $\beta$ -positions of the thiophene rings are blocked with dioxyethylene groups. These groups inhibit structural disorders such as  $\alpha$ - $\beta'$  couplings (branching and cross-linking of PPy chains, **Figure 1.8b**) and over-oxidation (**Figure 1.8a**) at  $\beta$ -positions [46, 47], characteristic defects of PPy. Positive charges on the conjugated PEDOT chain are stabilized by oxygen atoms at  $\beta$ -positions [48].

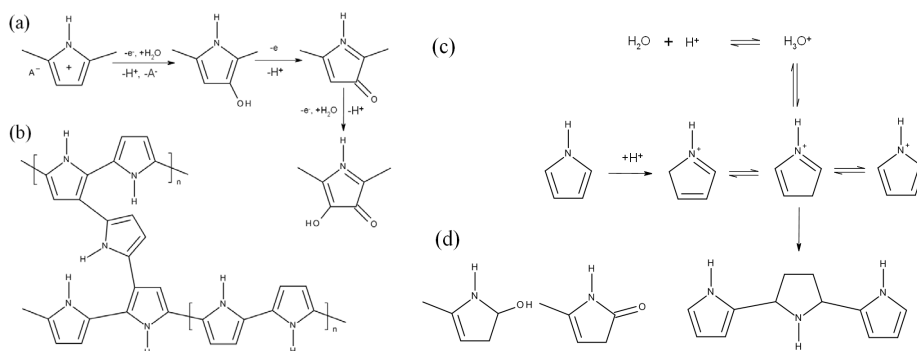


**Figure 1.8.** Structural and conjugation defects of PPy: a) over-oxidation at  $\beta$ -position; b) branching and cross-linking; c) non-conjugated trimer containing pyrrolidine [49]; d) chain termination.

Py and especially EDOT are hydrophobic and have limited solubility (0.67 and 0.01 ... 0.015 M [15, 48], respectively at RT) in aqueous media, forming not true solutions, but rather emulsions, colloidal solutions or micellar solutions.

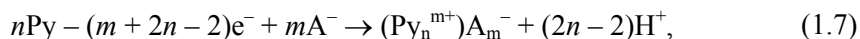
Water as the solvent also limits the synthesis potential window, the synthesis temperature range and the choice of electrolyte salts to ones sufficiently soluble in water. Despite these limitations, water remains the solvent of choice for industrial polymerization due to economic, environmental and safety issues. Despite the low solubility of EDOT in water, limiting the available synthesis conditions, chemically synthesized PEDOT/PSS in form of aqueous dispersion is perhaps the most commercially successful CP industrial raw material.

Both PPy and PEDOT can be synthesized by chemical or electrochemical oxidative polymerization [16, 50]. Both methods have many variations and as for most polymers, the structure of the synthesized CP is difficult to determine. Properties of the resulting polymer depend in a complex way on many synthesis conditions (and their combinations), such as synthesis media (usually solvent), the chosen supporting electrolyte salt, its concentration and oxidant (in case of chemical synthesis), synthesis temperature, different additives, modifications of the chemical composition or structure of the resulting polymer, *etc.*

#### 1.4.5.1 Synthesis mechanisms

During synthesis, two oxidative processes occur simultaneously: the oxidation of the monomer, oligomers or polymer chains into polymerizing radical cations and balancing the charges on the chains with counterions [15]. The result of the polymerization is an oxidized (charged) polymer, where the positive charges on the polymer backbone are compensated by dopant anions, originating from supporting electrolyte or oxidant.

A simplified polymerization reaction (with the example of PPy and assuming idealistic, single, defect-free continuous polymer chain, doped with monovalent anions) can be formulated as:



where  $m$  is the number of anions  $A^-$  from the electrolyte or oxidant,  $n$  is the number of Py monomers,  $e^-$  is the electron taken away by the oxidant (chemical polymerization) or by anodic current (electropolymerization),  $\text{Py}_n^{m+}$  is the polycation of the resulting PPy polymer. Assuming a one-compartment synthesis vessel, a significant difference between the chemical and EC method is in the resulting pH of the synthesis solution. In case of EC synthesis, protons released during the polymerization are reduced to hydrogen at the cathode. The release of a big quantity of protons, confirmed by the decreasing pH during polymerization [51] could be used for the evaluation of the efficiency or the progression of the chemical polymerization.

Due to the better control over the polymerization rate, predominantly electrochemical polymerization process is studied in the literature. Despite extensive research, there is no widely accepted agreement about the whole electropolymerization mechanism. It is generally accepted that the mechanism

(in example of PPy in **Figure 1.9**) is similar for PPy and PEDOT [51, 52], starting from the oxidation of a monomer on the electrode surface (**Figure 1.9a**), forming a radical cation that has several resonance forms (not depicted in **Figure 1.9**). The second step is the polycondensation of radical cations by the coupling of radicals and the elimination of  $2\text{H}^+$  from the  $\alpha$ -positions of the two heterocycles to form a neutral dimer (**Figure 1.9b**) followed by the oxidation of the dimer. The nature of the following polymerization process remains controversial. According to Heinze's "*oligomer approach*", a PPy chain grows by the sequential coupling of dimers to tetramers, tetramers to octamers *etc.* [15]. Perhaps the most admitted mechanism is that proposed by Diaz [51] (**Figure 1.9c**) with some minor modifications. According to Diaz, the polymerization proceeds as the progressive coupling between an oligomer or polymer chain and monomeric cations. Some authors believe that the coupling occurs in the reaction layer in the solution near the electrode, until the oligomers become too large to remain soluble and precipitate on the electrode [18]. According to Otero and Rodríguez, the "polymerization takes place through active species grafted to the electrode surface" [53], according to Marandi *et al.* [54], the polymerization in aqueous solution begins from the adsorbed layer of the monomer on the electrode. According to Heinze, both mechanisms may be involved [15]. In all cases, when a neutral polymer (chain) oxidizes to a polycation, anions are incorporated to balance the positive charge of the polymer; the resulting polymer is finally doped with the anions, which give the polymer the conductive properties.

There are disagreements also regarding the processes ending the polymer chain propagation. By Diaz [51], Otero and Rodríguez [49], chain propagation in aqueous media ends with over-oxidation at  $\alpha$ -position. By Street in [16], chain propagation ends due to sterical blocking or it becoming too unreactive.

Within the framework of the chosen monomer and synthesis method (chemical or EC), choice of the doping anion influences the conductive properties of the resulting material the most. Having other conditions equal, variation of the doping anion alone may alter the conductivity by two orders of magnitude [55, 56] and cause "very dramatic changes in topology" of the resulting film [56]. The resulting polymer has usually one anion per 3–5 repeating units, which corresponds to a doping level of 0.2–0.33.

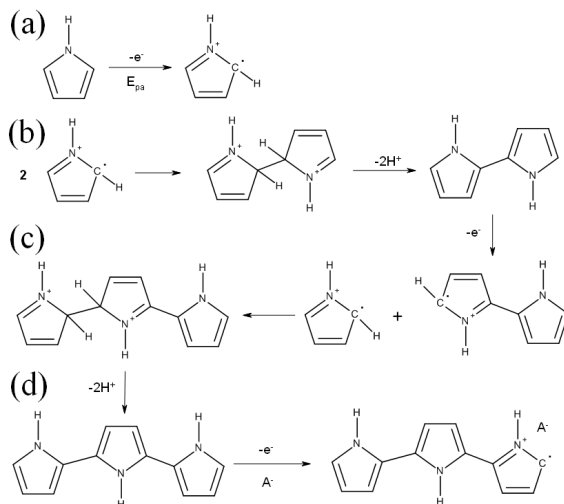


**Figure 1.9.** Simplified (first steps) PPy polymerization according to Diaz *et al.*: a) monomer oxidation; b) radical-radical coupling and deprotonation; c) dimer oxidation, coupling and deprotonation; d) doping of trimer.

The synthesis mechanism depends on the synthesis conditions in a complex way and remains poorly understood. The electrical, mechanical, electrochemical, optical, structural properties depend on many factors, such as:

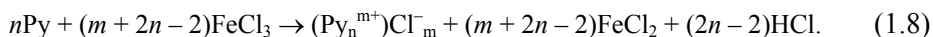
- monomer(s);
- electrolyte/dopant ion;
- solvent (including water content);
- synthesis method and regime;
- pH;
- additives;
- temperature;
- concentrations;
- substrate properties;
- formulation (dimensions, thickness, powder/nanoparticles/films/gels);
- *etc.*

Due to the absence of a widely recognized methodology, the results reported in literature sources are seldom comparable and can neither be easily interpreted nor generalized. There have been efforts toward the standardization of methods and limiting the number of model materials for fundamental research, but with limited success [20, 57].



### 1.4.5.2 Chemical synthesis

Both PPy and PEDOT can be synthesized by chemical oxidative polymerization. The most common method for the chemical synthesis is the mixing of monomer and oxidant in a solution. Depending on the synthesis conditions and additives, the resulting polymer is usually in form of a flocculated precipitate, powder, coating film, polymer dispersion or different nanostructures [58]. Less often used are interfacial polymerization methods: between monomer-swollen solid and oxidant solution, between two immiscible solutions, one of them containing the monomer and the other the oxidant, polymerization from monomer vapor on the surface, coated with thin layer of oxidant [59] *etc.* Solvent is usually chosen according to the solubility of the monomer, oxidant, different additives, type of substrate (if present) and the chosen synthesis temperature. Usually a small amount of water is added to organic solvents (accordingly water vapor in vapor phase synthesis) to facilitate deprotonation. Different oxidants can be used, such as APS, SPS, FeCl<sub>3</sub>, Fe<sub>3</sub>TS, CuCl<sub>2</sub>, SbF<sub>5</sub>, Br<sub>2</sub>, H<sub>2</sub>O<sub>2</sub>, Fe<sub>2</sub>(SO<sub>4</sub>)<sub>3</sub>, *etc.* Formally (for FeCl<sub>3</sub> oxidant):



Often additives are used to introduce different doping anions. In addition, different surfactants are widely used to influence the structure of the polymer through micelle formation, in order to increase solubility of the monomer or for emulsion polymerization. Surfactant micelles are widely used for the soft-template synthesis of various dispersions, nano-particles and nano-structures.

The conductivity of chemically synthesized PPy is usually several orders of magnitudes lower than that of EC synthesized PPy [16] and limits the choice of a sole dopant, because the (residual) oxidant anion participates in doping of the CP. At the same time, chemical polymerization is preferred for the large-scale production of polymeric material, the production of nanoparticles and for the coating of nonconductive surfaces. The chemical synthesis process is less controllable and has low yield when used for surface coating in solutions. In addition, the CP layer has low quality and the thickness is not always reproducible.

### 1.4.5.3 Electrochemical synthesis

Usually, EC synthesis is preferred due to the higher conductivity of the resulting material (usually in form of film or electrode coating), reproducibility and more precise control over the synthesis rate, morphology and deposition area.

Over a wide range of synthesis conditions, the EC polymerization is a highly effective process, and in the literature, efficiency of 100% is usually assumed (*e.g.* [60]). Therefore, EC polymerization allows good control over the polymerization process and thickness of the resulting film.

EC synthesized films are considered chemically and mechanically stable and often biocompatible. EC synthesis is carried out by the oxidation on the anode of the EC cell, containing a supporting electrolyte. Solvent is usually chosen based on the solubility of the monomer and the electrolyte salt at the required synthesis temperature and stability at the synthesis potential. Doping with the electrolyte anions (for PPy typically 33 mol% of repeating units) occurs during electropolymerization.

EC polymerization can be done in different regimes: galvanostatic (monitored using the chronopotentiometry technique), potentiostatic (monitored using the chronoamperometry technique) or using dynamic methods as potentiodynamic, sequential polymerization [61], *etc.* Whatever the synthesis regime, the amount of the synthesized polymer (and usually thickness of the deposited film) is generally determined by the synthesis charge (assuming 100% synthesis efficiency and including part of the charge spent for doping of the CP):

$$Q_s = \int i(t)dt, \quad (1.9)$$

where  $Q_s$  is the synthesis charge,  $i(t)$  is the synthesis current and  $t$  is time.

Most of the properties, such as the structure, the conductivity, the elasticity *etc.* depend on a number of synthesis conditions, such as temperature, deposition rate, substrate, synthesis duration *etc.* However, it is generally agreed that in order to obtain homogeneous, flexible and well conducting films, synthesis should be conducted at low temperatures, at low deposition rate [62, 63] and high concentration of monomer [53, 63] and the supporting electrolyte [64]. Aqueous synthesis allows a much wider choice of supporting electrolyte salts, but prohibits synthesis at temperatures significantly below the melting point of water. To non-aqueous electrolytes, usually 1 ... 4 v.% water is added in order to facilitate proton transport away from the electrode. At low temperatures, the limiting factors are typically the melting point of the electrolyte, the crystallization of water additive, and the solubility of the electrolyte salt and that of the monomer, high viscosity, high electrolyte resistance and slow diffusion speed of the monomer. These conditions lead to high synthesis potential (for galvanostatic synthesis), over-oxidation and diffusion limited aggregation regime (as opposed to charge transfer limited deposition), which causes dendritic growth of the polymer, and hence, formation of low quality film. In addition, at very low deposition rates the 100% synthesis efficiency assumption is not valid anymore. Monomer solubility problem (especially for EDOT) is sometimes relieved with surfactant additives [65, 66], increasing solubility or enabling polymerization in micellar medium.

Perhaps due to dependence of the electropolymerization process on synthesis conditions [64, 67], the initial steps of the electropolymerization process are not fully understood, but despite different opinions [68–71], several mechanisms are widely recognized. These comprise of the primary nucleation process,

divided to the induction period (monomer oxidation and oligomerization) and instantaneous or progressive steady nucleation, followed by 2D layer-by layer deposition or 3D growth [72, 73].

#### 1.4.5.4 Doping level and electrochemical modification

PPy and PEDOT can be prepared only in their doped (conducting/oxidized) form. The extent of doping is expressed by the dimensionless doping level, which may have different meanings, depending on the context of research. Analytical doping level, sometimes also “dopant level” is (also here) the ratio of the number of charge-compensating dopant ions to the number of repeating units in polymer [74] and is determined usually using elemental analysis. Doping level may be alternatively defined as the ratio of the positive charge of the polymer to the number of repeating units in polymer (especially when multi-charged anions or polyanions are involved) and it then expresses the oxidation level of the polymer (“doping ratio” in [75]). Using notations and assumptions from (1.7):

$$d_a = \frac{m}{n}, \quad (1.10)$$

where  $d_a$  is the analytical doping level,  $n$  is the total number of polymer units, and  $m$  is the number of dopant ions, neutralizing the positive charge of polymer. For an anion-active doped polymer and monovalent anions, the analytical doping level is equivalent to the oxidation state. EC doping level (also formal or effective doping level) is expressed through the exchanged charge during EC oxidation or reduction (“redox activity”):

$$d_e = \frac{Q_{red(ox)}}{n \cdot e}, \quad (1.11)$$

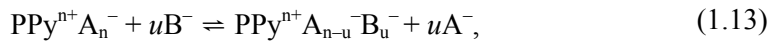
where  $d_e$  is the EC doping level,  $Q_{red(ox)}$  is the reduction or oxidation charge and  $e$  is the electron charge. EC doping level is close to the analytical one for thin films, but decreases with increased deposition charge (film thickness), increases with increasing deposition current density, and for single-charged anions always  $d_a > d_e$  [76]. EC doping level is often expressed as:

$$d_e = \frac{2 \cdot Q_{red(ox)}}{Q_s - Q_{red(ox)}}, \quad (1.12)$$

where  $Q_s$  is the synthesis charge, consumed during the EC synthesis. EC doping level is somewhat ambiguous, depending on timeframe, film thickness, and

density. In addition, oxidation and reduction occur at different rates. Therefore, the measurement conditions must be defined very precisely beforehand and results are rarely comparable between different authors. Oxidation level depends on potential, therefore, higher synthesis potentials (still lower than those, causing extensive over-oxidation) lead to higher doping levels of the polymer.

In order to modify the properties of an existing polymer after synthesis, for polymers doped with small or medium-sized anions, it is possible, at least partially, to replace the initial doping ion for another by soaking in a different electrolyte, polarization or EC cycling in an electrolyte containing other anions. Formally:



where  $u$  is the number of dopant ions  $\text{B}^-$  after redoping. Depending on the redoping method,  $m$  may or may not be equal to  $u$  and the new doping level is

$$d_a = \frac{u}{n}. \quad (1.14)$$

#### **1.4.6 Overview of conducting polymer applications**

After decades of extensive research, conducting polymers have a direct or indirect connection with virtually every branch of science and technology. CPs are considered mature enough to replace their nonconductive, inorganic or non-polymeric predecessors in many fields, including information technology. Although initially considered as low-weight conductors, by now they are able to function in variety of devices as:

1. materials for electrically conducting textiles [16], transparent conductive coating [16];
2. chemical [16] (*e.g.* artificial nose, artificial tongue), biological [16], mechano-electrical [77, 78], temperature [79] and humidity sensors;
3. energy storage (*e.g.* super-capacitors and rechargeable batteries [19, 80]);
4. energy harvesting (mechanical, photovoltaic, thermoelectric [81]) and generation (fuel cells) devices;
5. medical applications such as tissue engineering [41], implanted stimulators, sensors [79, 82], drug delivery and controlled release devices [83], bio-compatible *in vivo* electrodes [83] and other implantable devices;
6. electrochromic devices [84], electronic display applications components [16], camouflage;
7. organic (micro)electronics [16] (*e.g.* OLED, since 1999, [85]), field-effect transistors [86], and information processing [87];

8. surface modifications for anti-static and anti-corrosion [16] coatings, electromagnetic interference shielding, superhydrophobic (*e.g.* self-cleaning) surfaces [88];
9. functional (*e.g.* ion selective, enantioseparation and gas-liquid separation) membranes [16, 83];
10. robotics, manipulators [89], Braille screens [90], and in general – actuators [3, 4, 31, 33, 34, 36, 83, 90–109].

Suggested device dimensions and working environments span from MEMS and lab-on-chip devices to macroscopic devices for aviation, car manufacturing, and space applications. CPs are used in complete full-CP devices or as one of materials or components. Most successful and widespread among commercial applications are probably OLED displays and antistatic coatings.

## **1.4.7 Conducting polymer actuators as artificial muscles**

### **1.4.7.1 Artificial muscles in general**

Artificial muscles (term first used in 1849 by Smee, [110]) are materials or devices with characteristics similar to or able to substitute natural muscles. Actuators with muscle-like structure or functionality are desirable in many classes of devices and working environments, and their properties are often compared with those of mammalian muscles. Actuators mimicking natural muscles are essential in robotics, medicine, biotechnology and in many fields where properties, such as longitudinal movement, volumetric effect, miniaturization, silent operation, biocompatibility, high power-to-weight or power-to-volume ratio are required.

### **1.4.7.2 Electroactive polymer actuators**

Materials are considered electromechanically active, if they change their mechanical properties (usually volume, shape, stiffness or stress) in response to external electrical stimulus or respond with electric signal to mechanical stimulus. Polymeric electroactive materials, EAPs (often and also in the current thesis used in a narrower sense as “electromechanically active polymers” [77]), possess also a number of intrinsic properties, making them attractive as artificial muscles [77, 93–95, 111], such as elasticity and processability.

These properties are utilized to construct actuators with longitudinal (linear), bending or twisting type of motion. EAP actuators can be used in many application areas, especially where their advantages, such as simplicity, softness, tunable properties, lightness and ease of miniaturization are paramount – prosthetics, bio-mimetics, implantable and wearable [112] devices *etc.* They have several advantages over other artificial muscles: typically simple yet flexible design, adaptability for different applications, simultaneous sensing

properties [113], inherent scalability, silent operation, potential energy harvesting ability [77, 96], and usually low cost. The versatility of the EAP actuators can be further improved by implementing different, usually layered or coaxial configurations. Due to the simple construction and with some limitations, EAPs and their key properties are easily scalable (up-, down- and out-scalability) with geometrical dimensions, including miniaturization [97, 114] by cutting into smaller pieces, bundling, and production using micromachinery, photolithography, dry etching [97] and laser ablation [98], making them ideal candidates for MEMS and lab-on-chip devices.

EAP actuators can be further divided into two large groups: field-activated actuators (electronic EAPs) and ionic EAP actuators (IEAP) [99]. The working principles of typical electronic and ionic EAPs are illustrated in **Figure 1.10**.

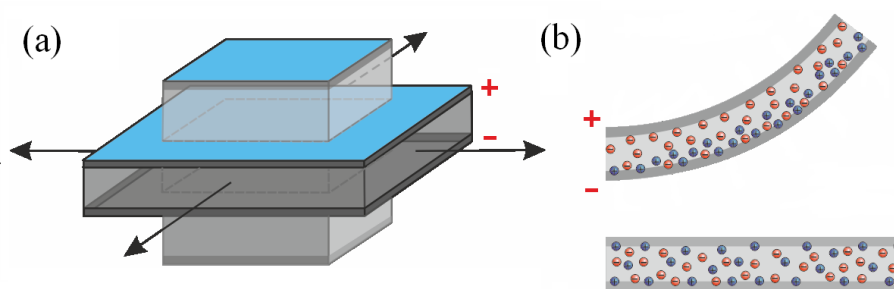


**Figure 1.10.** Working principles of a) electronic (dielectric elastomer) EAP; b) IEAP.

In case of electronic EAPs, the actuation is caused by various charging effects or electrostatic forces. Electronic EAPs typically have high stress and energy density, they are fast and efficient and do not need electrolytes. A serious disadvantage is the high driving voltage and non-reversibility by polarity. Representative classes in this group are liquid crystal elastomers [115], dielectric elastomers [116], electrostrictive polymers [117], piezoelectric polymers [118], and CNT aerogels [119].

In case of ionic EAPs, the electrically driven motion of ions or molecules causes actuation. IEAPs could be divided further into conducting polymers [100], ionic polymer-metal composites [120], polymer gels [121] and carbon-based ionic actuators (*e.g.* CNT, carbide-derived carbon) [122]. Typical representatives of ionic EAP actuators are based on EDL charge transfer, for example, IPMC, activated carbon or CNT based actuators. In CP actuators, additionally to the double layer charging-discharging, redox processes are involved. By the widely accepted taxonomy of artificial muscles (**Figure 1.11**, [77]) CP actuators belong to the ionic branch of the electromechanically active polymer artificial muscles.

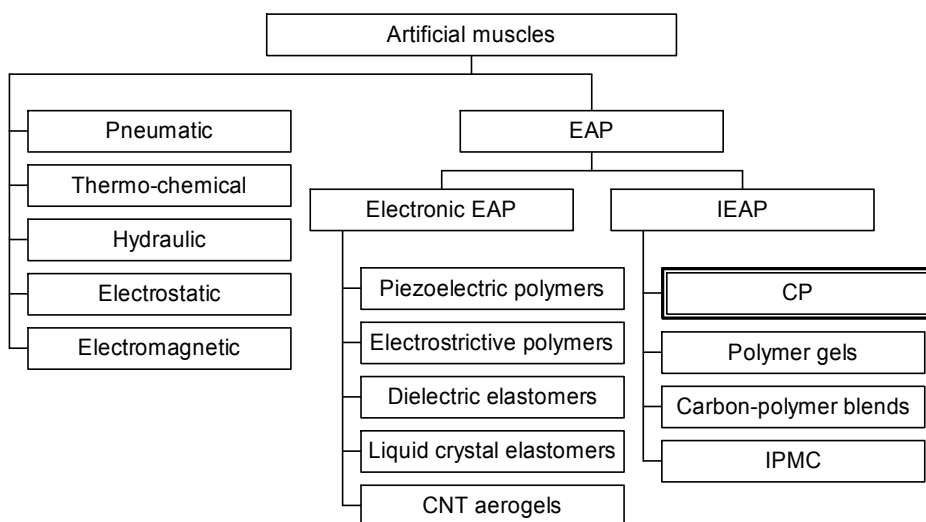


**Figure 1.11.** Taxonomy of artificial muscles.

All EAP classes have distinctive advantages, disadvantages, and properties optimal for different applications. Most of the EAP actuators can be used simultaneously as sensors, responding electrically to mechanical (mechano-electrical sensors) or environmental changes (*e.g.* humidity sensor). A significant difference of several EAP actuator types, comparing to mammalian muscles, is the “catch state” property – ability to maintain position under constant load without energy consumption [100]. Nowadays, EAP actuators are in phase of transition from fundamental and applied research into commercial products. Perhaps the most commercially successful representatives are polymeric piezoelectrics and dielectric elastomers [123, 124].

### 1.4.7.3 Conducting polymer actuators

Besides the applications, associated solely with the conductive properties, CPs can be utilized as chemically or electro-chemo-mechanically active materials. The low voltage (0.5... 3 V) needed for actuation is at least an order of magnitude lower than that needed for electronic EAPs, making them competitive for applications, where low driving actuation voltage is needed. The advantages of CP actuators over other ionic EAP actuators are good conductivity, catch states, flexibility of synthesis conditions and larger stress, when compared to IPMC and CNT actuators [94].

Actuation, caused in most cases and mostly by ion diffusion, classifies the vast majority of CP actuators to the IEAP group. The working principle of CP actuators typically relies on the EC change of oxidation state by oxidation or reduction (removal or addition electrons from polymer chains, respectively) [33,

125]. Concomitant ingress or expulsion of ions (often together with solvent molecules) between the polymer matrix and the associated electrolyte to balance the charge causes swelling or contraction of the polymer [34, 35, 100, 101], alters the mechanical properties of the CP and leads to macroscopic volume change, which can be converted into mechanical work. Conformational changes [94] of polymer chains and chemically [101] triggered changes can also contribute to volume change. Therefore, in order to function, CP (hereafter electro-chemo-mechanical) actuators must have at least two electrodes (at least one of them containing an active CP material), an electrolyte, and a power source.

CP actuators can be classified by a number of characteristics:

1. by active CP material: PPy, PEDOT, PAn, combined from different CPs and/or other materials, such as CNTs, carbide-derived carbon, *etc.*;
2. by operating environment: electrolyte, air, vacuum, ambient environment, containing ions, such as living body, sea water *etc.*;
3. by motion type: linear (longitudinal), bending, twisting;
4. by electrolyte: salts, dissolved in water, organic solvents or RTIL, RTIL;
5. by number of layers: freestanding, bi-layer, tri-layer, *etc.*;
6. by membrane type: none, IPN, SPE, porous non-CP membrane, ionomers;
7. by type of dominant mobile ion: anion-active, cation-active, mixed-type;
8. by geometry: beam, tubular/coaxial, non-uniform;
9. by dimensions and scale of operation: starting from nano- and microscale;
10. by number of actuation directions relative to neutral position: unimorph, bimorph, *etc.*

Virtually all the aforementioned actuator types can be combined with other types or bundled together for scale-up. All types have their advantages and disadvantages depending on the targeted application. Actuator types used in the current work are depicted in **Figure 1.12**.

Most literature sources deal with freestanding actuators of linear (longitudinal) actuation. Longitudinal actuators change their volume due to the flux of ions, utilizing linear movement (usually) in one direction (**Figure 1.12a**). Longitudinal actuators are usually operated in electrolyte environment and they require a separate counter electrode (the same requirements are shared by most of the bi-layer actuators). Nevertheless, tri-layer air-operated linear actuators, having two layers with different ion mobility types and separator membrane are possible as well. In addition, the actuation type may depend on the assembly tactics and effectively convert bending type motion to longitudinal or *vice versa*.

Another widespread actuator type is the layered actuator. Layered actuators can be divided into air-operated (also in vacuum) and electrolyte-operated actuators (common for bi-layer actuators). Layered actuators with bending type movement (**Figure 1.12b**) became popular due to the relatively small strain of the CP material, along the lines of IPMC actuators. Most of the bending tri-layer actuators are able to operate outside electrolyte media and are therefore



more attractive from the perspective of practical applications. Such design allows the transformation of relatively small strain into large deflection, which is easier to visualize and measure, and optimal for some applications where large forces are less important than large strokes. A typical CP actuator is based on layered (typically bending) or coaxial design. The layered design requires good electrical and mechanical contact between the layers and between the active material and the driving power supply. Typical CPs used for such actuators are PPy and PEDOT. The actuation mechanism of a bending tri-layer actuator is based on the volumetric change difference between the two active layers on the ingress and expulsion of ions. For air-operated actuators, the design must contain an ion reservoir and for tri-layer air-operated actuators, the membrane acts as an electronic separator and electrolyte storage layer. Air-operated actuators often suffer from electrolyte solvent evaporation and need encapsulation for long-term operation; or a RTIL, having negligible vapor pressure, should be used as the electrolyte [126]. For CP actuators, typically non-ionic SPE [127] or commercial membranes are used as the electrolyte storage layer.

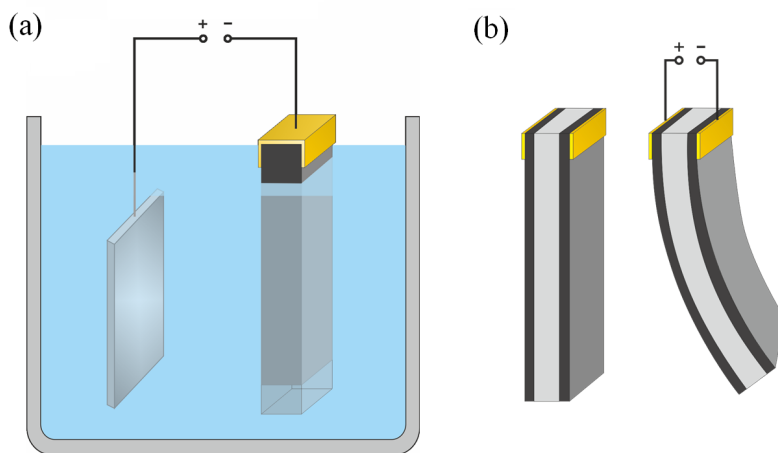


**Figure 1.12.** CP actuators: a) electrolyte-operated linear layer actuator; b) air-operated bending tri-layer actuator.

Depending on the relative sizes of anions and cations (including the solvation shells), driving voltage shape, anion charge, density of the CP structure, *etc.*, CP actuators can be anion-active, cation-active or mixed type. Usually large or multi-charged anions have low diffusion speed or are immobile inside the polymer matrix, and the redox process charges are compensated by the more mobile cations (**Figure 1.13b**). Otherwise, electroneutrality is maintained by anions entering and leaving the active CP material (**Figure 1.13a**).

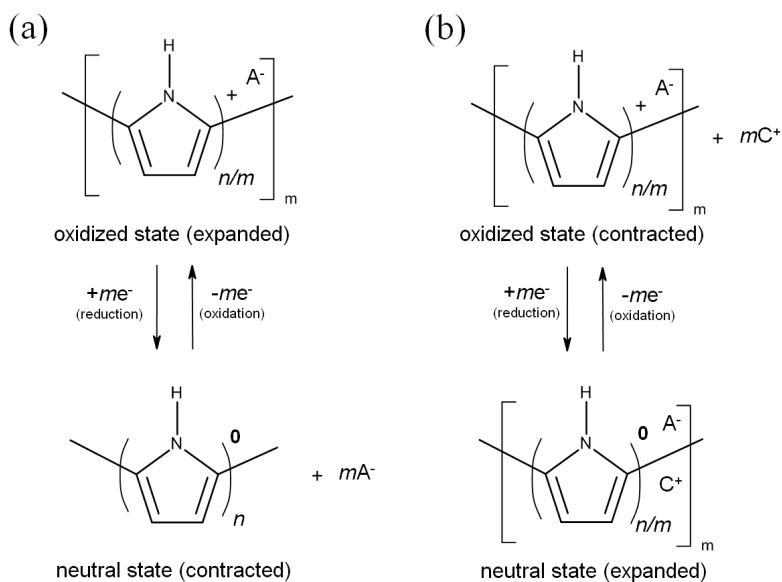


**Figure 1.13.** Electro-chemo-mechanical processes of: a) anion-active; b) cation-active CP actuator (adapted from [18]).

CP actuators share most of the disadvantages of other IEAPs: low electro-mechanical coupling and efficiency [106], need for encapsulation when actuating in air or non-electrolyte environment [94], low diffusion dependent actuation speed and high current consumption [102], but due to low driving voltages they are promising for bio-mimetic or bio-interacting applications. Besides many other applications, CP-based actuators are promising in medicine and for applications, where mammalian-muscle-like actuation is needed, due to similarities with natural muscles (*e.g.* silent longitudinal or bending movement, softness, elasticity, sensing properties, scalability, and biocompatibility). In addition, they have several advantages over alternative electromechanical transducers (*e.g.* high tensile strength [100], large stresses, high stiffness [102], control by oxidation state [103], low driving voltage [34, 36, 62, 90, 100–102, 104, 106–108], high work density, scalability). Comparison with natural mammal skeletal muscles is given in **Table 1.2**.

**Table 1.2.** Comparison of mammalian muscle and CP actuators (adapted from [94] and references therein, where not referenced otherwise).

Property	Typical for natural muscle (maximum value)	CP actuators value (maximum value)
Strain (%)	20 (>40)	2 (40, [128])
Stress (MPa)	0.1* (0.35)	5 (100, [129])
Work density (kJ m <sup>-3</sup> )	8 (40)	100 (190, [61])
Density (kg m <sup>-3</sup> )	1037	
Strain rate (% s <sup>-1</sup> )	(>50)	1 (12)
Specific power (W kg <sup>-1</sup> )	50 (284)	(150)
Efficiency (%)	(40)	<1 (18)
Coupling		(0.1)
Cycle life	(>10 <sup>9</sup> )	2.8 · 10 <sup>4</sup> (8 · 10 <sup>5</sup> )
Modulus (MPa)	10 ... 60	0.8 (3)

\* sustainable

### **1.4.8 Large surface area conducting polymer electrodes**

Although large surface area CP electrodes are useful for a number of applications, some of them are more obvious in the context of current study. These are energy storage, sensors and controlled drug delivery devices, where large surface area and good mechanical, electronic and ionic contact with the working environment are paramount.

#### **1.4.8.1 Energy storage**

CPs are used in several types of energy storage devices. Perhaps the most thoroughly studied are CPs in supercapacitor applications, but also in context of rechargeable batteries [130] mostly for cathode (on discharge, [131]), but (seldom) in the n-doped form also as anode material [132]. Based on the weight of undoped dry material, CPs have usually high theoretical specific charge storage capacity (*e.g.* 420 mA h g<sup>-1</sup> for PPy, [132]), and therefore, hybrid and full-CP batteries [19] are seen as promising research direction for energy storage applications, especially for flexible devices.

The traditionally solely carbon-based EDL capacitors increasingly benefit from the additional pseudo capacitance from redox reactions [133]. While EDLC capacitance is stored in EDL near to the interface between the carbon and the electrolyte, the pseudo capacitance is expected to utilize the bulk of the redox-active material. One possibility for the pseudo capacitance of such hybrid devices is the reversible doping and dedoping of CPs [134–136]. Madden has estimated the capacitance of PPy to be  $1.30 \pm 0.05 \cdot 10^8$  F m<sup>-3</sup> and the energy

density  $10^5 \text{ J kg}^{-1}$ , which are respectively 5 and 10 times higher than the corresponding values of tantalum capacitors [106]. CPs can increase the specific energy, but due to the slower Faradaic processes, the specific power decreases.

The most common method for comparison of energy storage properties, the Ragone plot [137, 138], originates from the automotive industry and relates specific energy (driving range,  $\text{Wh kg}^{-1}$ ) and specific power (speed and acceleration of electric vehicle,  $\text{W kg}^{-1}$ ) curve(s). The Ragone plot allows the comparison of a single electrode of an energy storage device, for single device or different devices with different working principles (**Figure 1.14**, adapted from [74, 134]). As a shortcoming, Ragone plots do not account for mass loading and often very impressive values are achieved only for rather small devices and material quantities.

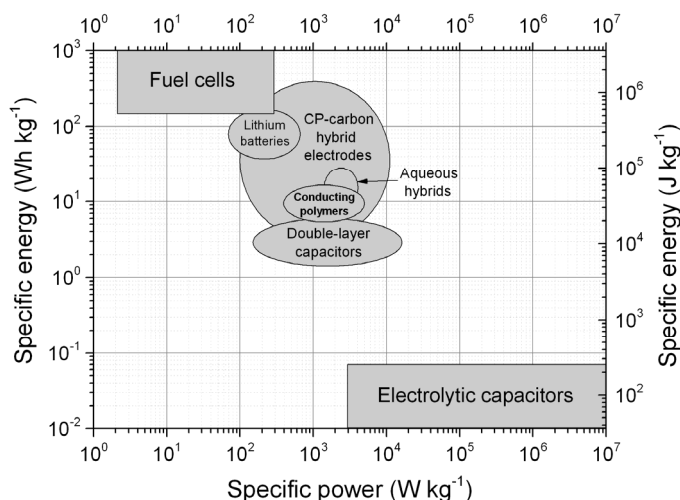


**Figure 1.14.** Ragone plot of common types of energy storage devices and electrodes.

#### 1.4.8.2 High sensitivity sensors and controlled drug delivery devices

Another promising application field for CPs is the biocompatible electrodes for *in vivo* data acquisition and electrical stimulation devices. Similar biocompatibility requirements are needed for drug carrying or controlled drug release devices. For both functions, such electrodes are required to be biocompatible, stable and mechanically compatible with tissues, and could be combined with electrodes with anti-inflammatory drug carrying properties [87].

Ryan *et al.* have shown that anionic drugs (sodium diclofenac) [139] can be incorporated as dopant during the EC synthesis of PPy. For the drug carrying function, large surface area is desirable and thus, for example, biocompatible CS hydrogels can be used for drug delivery and prolonged release [140], but using EC active materials allows additional control over the drug release rate.

CPs are good candidates for controlled drug delivery, but usually rigid, mechanically less compatible formulations of CPs have been used (*e.g.* for ciprofloxacin delivery, [141]). CP hydrogel electrodes combine the most essential properties of CPs and hydrogels: biocompatibility, large surface area, mechanical compatibility with soft tissue and the possibility of EC drug release control.

For the best sensing and drug carrying properties, the freedom of dopant choice is required as drugs are incorporated to CP based devices as anionic dopants or cations, when anionic dopant is too large to leave the CP on reduction, and charge neutrality is maintained by cations. Although dopant of choice can be introduced during the chemical synthesis, possible side reactions may influence on drug composition or EC and mechanical properties of the resulting polymer. Usually ions of drug molecules are too large to be mobile in thick and dense CP layers, but despite the large size of ions, the surface and outer layers of CPs can be additionally doped or redoped with drug ions of choice by means of dopant exchange under either diffusion control or by EC cycling in appropriate electrolyte.

### 1.4.9 Typical characterization methods

Selection of the most traditional characterization methods, most relevant for this work is presented.

#### 1.4.9.1 Electronic and ionic conductivity

The most important characteristic of a CP material is its electronic conductivity. Usually a four-point probe (**Figure 1.15**) is used for the measurement, and depending on circumstances such as sample size, geometry and homogeneity, conductivity, sheet resistivity or apparent (effective) conductivity is presented. Separation of current supply terminals and voltage measurement terminals mitigates the influence of wiring resistance and contact resistance, caused by poor electrical and mechanical compatibility between CP and metal terminals.

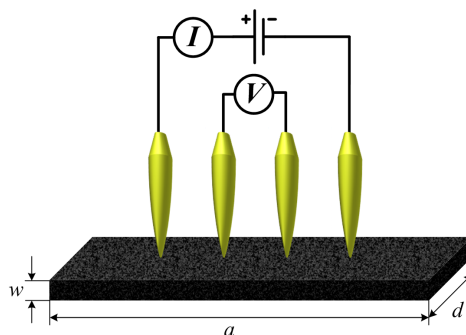


**Figure 1.15.** Four-point probe setup for conductivity measurement.

Constant current is passed through the outer terminals of evenly spaced probe contacts and the voltage between the inner contacts is measured. The electronic conductivity of a homogeneous sample with well-defined geometry can be calculated using Smits' equation [142]:

$$\sigma_e = i \cdot [C'(a, d, s) \cdot F(w, s) \cdot w \cdot V]^{-1}, \quad (1.15)$$

where  $\sigma_e$  is the electrical conductivity,  $C'(a, d, s)$  and  $F(w, s)$  are correction factors [142], depending on the sample length  $a$ , the sample width  $d$ , the probe contact spacing  $s$ , and the sample thickness  $w$ ,  $i$  is the constant current, applied to the outer contacts, and  $V$  is the voltage drop between the inner contacts.

An important parameter for CP applications, where ion motion is involved, is the ionic conductivity. Ionic conductivity can be measured by EIS, using the equation [143]:

$$\sigma_i = \frac{w}{Z_{re} \cdot A}, \quad (1.16)$$

where  $\sigma_i$  is the ionic conductivity,  $Z_{re}$  is the real part of the complex impedance at high frequency plateau,  $w$  is the sample thickness and  $A$  is the sample area.

#### 1.4.9.2 Cyclic voltammetry and electrochemical impedance spectroscopy

Cyclic voltammetry is an EC method, based on potential scanning, and allows gaining a lot of information even for very complicated electrode reactions. During CV, potential is scanned linearly in time over a certain potential range and concomitantly the current value is measured. Repeated scan cycles allow the observation of the same process several times and finding non-reversible changes. The varied parameters are only the potential range and the scan rate.

Analysis is done from current vs. potential graphs. In a three-electrode EC cell setup, the working electrode potential is measured against a reference electrode, placed as near as possible to the working electrode. CV allows the distinction between anion- and cation-driven redox processes at the electrode. In a two-electrode setup, where the counter electrode and reference electrode terminals are connected together, as are the working electrode and sense electrode (if present) terminals, it is difficult to separate the processes taking place on either electrodes. Nevertheless, the redox peak currents, the total exchanged charge and their dependence on scan rate and voltage range can still be measured. CV of CPs gives information about the mobile ion type and several characteristic values can be calculated, depending on scan rate. Typical voltammograms of CP film in three-electrode setup and tri-layer actuator in two-electrode setup are depicted in **Figure 1.16a** and **Figure 1.16b**, respectively.

Important features for the CV analysis are the anodic/cathodic peak currents, the potentials corresponding to the anodic/cathodic current peaks, oxidation/reduction charges integrated over positive/negative current values, respectively, and their dependence on scan rate. Often, current values are divided by scan rate providing pseudo capacitance, allowing concise comparison of CVs at different scan rates. By the CV driven dimensional change (ECMD), it is possible to conclude which mobility type dominates in volume change.

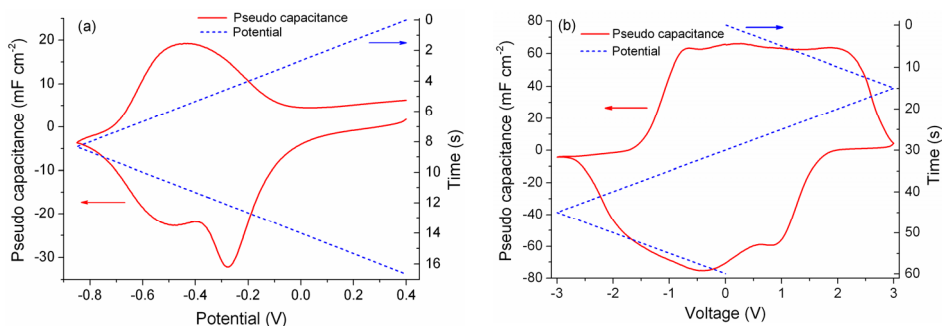


**Figure 1.16.** Cyclic voltammograms of: a) PPy/*p*TS film; b) PPy|PEDOT/TFSI actuator in three-electrode and two-electrode configurations, respectively.

The EIS method is based on the dependence of the response of the current of the EC system on the frequency of the exciting voltage signal (typically AC 5 ... 25 mV RMS in frequency range  $10^{-3}$  ...  $10^6$  Hz). The total complex impedance  $Z(f)$  depends on the configuration and the values of the resistive, capacitive, inductive *etc.* components of the system. Typical factors, contributing to the impedance of an EC system are the double layer capacitance, the kinetics of the electrode process (*e.g.* charge transfer resistance), diffusion, solution resistance *etc.* Analysis is predominantly done from the Nyquist plot ( $-Z_{im}$  vs.  $Z_{re}$ ), the Bode impedance plot ( $\log_{10}(|Z|)$  vs.  $\log_{10}(f)$ ) and/or the Bode phase plot (phase shift  $-\varphi$  vs.  $\log_{10}(f)$ ). The results are fitted against a presumable equivalent circuit in order to determine the characteristic values of individual components, each representing observed phenomena from experiments. The simplest, Randles equivalent circuit for CPs, the Nyquist and Bode plots of a CP electrode are depicted in **Figure 1.17**. A characteristic difference between the CV and EIS methods is the state of the system – while CV assumes and studies the dynamic behavior of the system (the processes), then EIS assumes a (more or less) steady state of the EC system and studies system's structure.

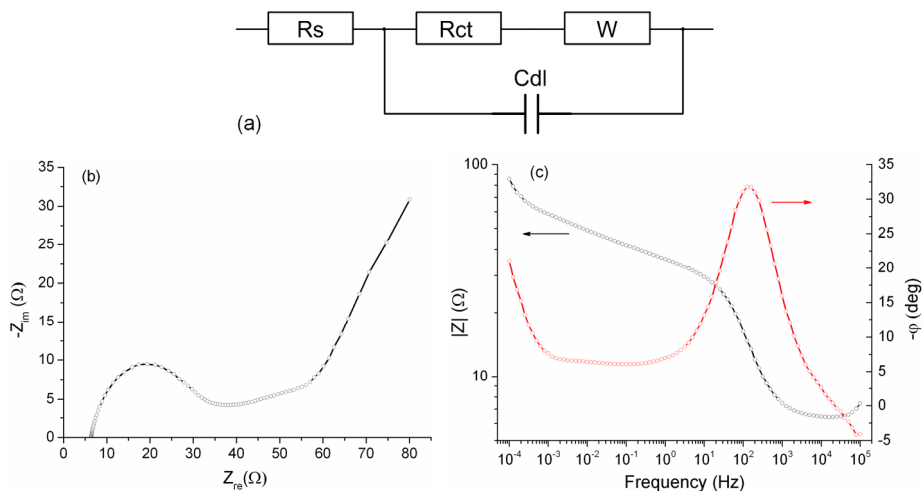


**Figure 1.17.** Typical a) (Randles) equivalent circuit ( $R_s$  – solution resistance,  $R_{ct}$  – charge transfer resistance,  $C_{dl}$  – double layer capacitance,  $W$  – Warburg element); b) Nyquist plot; c) Bode plots of a CP electrode (PPy hydrogel (0.1 M SDBS, 0.3 M Py-APS) electrode in 0.2 M NapTS electrolyte).

### 1.4.9.3 Electro-chemo-mechanical deformation characterization of actuators

Due to different designs, characteristics optimized for different applications and production methods, and lack of widely accepted standards, it is difficult to compare actuators with each other. Nevertheless, definitions of some characteristics, measurement methods and comparison principles have been more or less well established and generalized to cover both CP and non-CP actuators of different designs. The characterization and the comparison of actuators is often based on similar characteristics of commercially widespread transducer types and mammalian muscles.

The movement and force characteristics, often used to describe both linear and bending type actuators are the stroke, the strain, and the stress, caused by ion flux in the same manner as described by Eq. (1.6). For bulk CP material and linear actuators, the strain is defined as the relative linear length change and empirically found to be proportional to charge density up to strains of about 1% (until a considerable influence of back-relaxation and creep) [94]:

$$\varepsilon = \frac{\Delta L}{L} \text{ and} \quad (1.17)$$

$$\varepsilon = \frac{\sigma}{E} + \alpha \cdot \rho, \quad (1.18)$$



where  $\varepsilon$  is the strain (usually measured in per cents),  $\Delta L$  is the length change,  $L$  is the initial length of the actuator,  $E$  is the elastic modulus,  $\alpha$  is the strain to charge ratio and  $\rho$  is the charge density. Stress  $\sigma$  is defined as the force per cross section area:

$$\sigma = \frac{F}{A}, \quad (1.19)$$

where  $\sigma$  is the stress (unit Pa),  $F$  is the force, and  $A$  is the cross section area. Actuation speed is expressed by the bandwidth (in case of periodical movement at different frequencies), defined as the frequency of strain decrease from maximum low frequency value by 50% [94] or by strain rate:

$$\varepsilon_r = \frac{d\varepsilon}{dt}. \quad (1.20)$$

For periodically moving actuators, the strain rate is often expressed as the average over a full actuation cycle [108].

Important characteristics for autonomous actuator devices and mechanical energy harvesting devices are the efficiency and the electromechanical coupling. In case of actuators, the former describes the ratio of the external work to the total electrical energy consumption, and the latter includes the work spent for the internally generated mechanical potential energy. The maximum extracted mechanical energy in expense of internal mechanical potential energy is not more than 50% of the electrical energy spent to store the internal mechanical potential energy [94].

Several models exist for describing the behavior of bending actuators. The most sophisticated of them account for the finite speed of the strain propagation along the actuator, the viscoelasticity, the back-relaxation and overshooting phenomena. A model proposed by Alici *et al.* [89] has been widely used for tri-layer CP actuators and adopted for other types of bending tri-layer actuators (*e.g.* [144]). The model accounts for the structure of the actuator and expresses the electrode strain (assuming constant thickness, no distortion of cross-sections and elastic behavior of the materials) and the blocking force (assuming  $1/R \approx 0$ ) at the tip of the bending tri-layer actuator as:

$$\varepsilon = \frac{E \cdot I}{R \cdot E_e \cdot W \cdot w_e \cdot (w_e + w_m)} \text{ and} \quad (1.21)$$

$$F = \frac{E_e \cdot W \cdot \varepsilon \cdot w_e \cdot (w_e + w_m)}{L}, \quad (1.22)$$

where  $\varepsilon$  is the strain of the electrode,  $E \cdot I$  is the flexural rigidity of the actuator,  $R$  is the bending curvature radius,  $E_e$  is the Young's modulus of the electrode layer,  $W$  is the width of the actuator,  $L$  is the length of the actuator,  $w_e$  and  $w_m$  are the thicknesses of the electrode and membrane layer, respectively.

Perhaps the simplest model for the characterization of bending tri-layer actuators, proposed by Sugino *et al.* (**Figure 1.18**, adapted from [127]), allows the measurement of the strain difference between the electrodes instead of strain and assumes constant thickness and uniform curvature of the actuator.

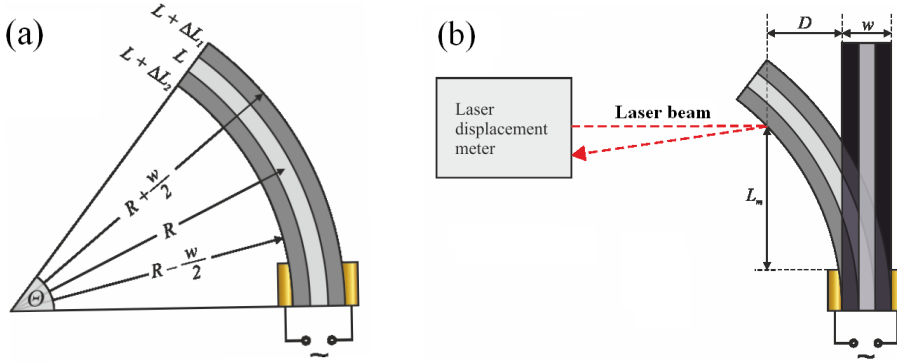


**Figure 1.18.** Sugino's *et al.*: a) model; b) displacement measurement setup of bending tri-layer actuator.

For tri-layer bending actuators, the strain difference is calculated as [127]:

$$\varepsilon = \frac{\Delta L_1 - \Delta L_2}{L} = \frac{w}{R} \cdot \left( 1 + \frac{\Delta L_1 + \Delta L_2}{2 \cdot L} \right), \quad (1.23)$$

where  $\Delta L_1$  and  $\Delta L_2$  are the length changes of the two electrodes of the bent actuator (**Figure 1.18**),  $w$  is the thickness of the actuator,  $R$  is the curvature radius of the actuator and  $L$  is the free length of the actuator. Strain difference allows quantitative comparison of the deflection ability of bending type actuators. For easier measurement with a laser displacement meter, the second term of the right side is considered negligibly small. Using the relation of Pei and Inganäs [34]:

$$k = \frac{1}{R} = \frac{2 \cdot D}{L^2 + D^2}, \quad (1.24)$$

where  $k$  is the curvature of the actuator,  $D$  is the half of the peak to peak displacement, Sugino *et al.* obtained from equations (1.23) and (1.24) for strain difference [127]:

$$\varepsilon \cong \frac{2 \cdot D \cdot w}{L_m^2 + D^2}, \quad (1.25)$$

where  $L_m$  is the distance between the fixed end of the actuator and the projection of the laser beam to plane parallel to the actuator's middle position (**Figure 1.18**). As one can see, strain difference is proportional to the curvature and approximately proportional to the displacement, if the measurement distance is significantly larger than displacement. In addition, Pei and Inganäs [35] have shown that the curvature change of bending bi-layer is proportional to linear strain. Strain difference is principally calculated from the maximum deflection from the neutral position in range  $0 < \theta \leq \pi/2$ , but due to creep and in order to reduce the measurement error, the half peak-to-peak displacement is often used instead.

Strain difference would not be the best choice for engineering of practical applications and precise control, but one of the most robust tools for qualitative and semi-quantitative comparison of bending ability of similar bending actuators with different working layers. To some extent, also bending actuators of different structures and geometries can be compared by calculating strain difference from published displacement data.

#### 1.4.9.4 Characterization of large surface area conducting polymer electrodes

There are many parameters for hydrogel and aerogel characterization. These are a number of physical and mechanical properties, chemical properties, EC characteristics, stability *etc.*, depending on the targeted application. The most important characteristics specific to hydrogels and aerogels in context of the current work are the structure, the density, the chemical composition, and the formation mechanism. Due to the conductive properties and EC activity, most of the already mentioned methods can be used for characterization.

The methods, more specific for sparse hydrogels and aerogels structures were SEM and low temperature N<sub>2</sub> sorption analysis.

## **I.5 Review of the state of the art**

### ***1.5.1 Inherent shortcomings of conducting polymers as artificial muscles and large surface area electrodes***

The same problems are present in most of the CP applications where the working principle and is related to redox processes and ion mobility in bulk material. These are the limited ion transport rate, the narrow EC potential window, the inefficiency due to friction and ohmic drop, the chemical degradation due to unwanted side-reactions and the mechanical degradation, caused by repeated swelling and shrinking accompanied with ion and solvent motion. One can say that the CP competitive advantages are also the root causes of the inherent shortcomings. The Faradaic nature of the redox processes, offering low operating voltages, at the same time reduces the operating speed, yields inefficiency in energy transmission, limits the operating voltages, and for many applications, requires the isolation from the surrounding environment. The utilization of the bulk volume of the material, manifested in high energy density, at the same time limits the mechanical durability and power density. The flexibility in the preparation methods and the large number of property tuning options also yields not so well defined CP materials, demanding massive dedicated applied research and optimization for every application considered. Being so different from the widespread metal conductors and non-conducting polymers often causes compatibility issues (electrical, mechanical and chemical) on interfacing with other materials.

From the processing perspective, most of the CP formulations differ from conventional non-conducting polymers in many ways, such as different synthesis methods, lack of thermoplasticity, limited solubility, rigidity, processing scalability problems and often the price of raw materials. Therefore, researchers and engineers are still facing severe challenges in transforming the full potential of CPs to commercial value and applied research is largely dedicated to solving the most acute problems, different for every application.

### ***1.5.2 Conducting polymer actuators and combined chemical-electrochemical synthesis methods***

Expectations on CP actuators and problems differ from the perspective of the proposed application and actuator design, but one can list those, related to each other and encountered most often:

- low energy conversion efficiency;
- low actuation speed;
- high stiffness;
- poor durability;
- limited scalability;
- high price;

- poor reproducibility;
- need for encapsulation;
- difficult optimization;
- difficult to industrialize preparation methods;
- controlling and modeling problems;
- different configuration-dependent design issues.

Although some of the CP actuators' performance values in the literature and **Table 1.2** are impressive and comparable to those of natural muscles, these have either been achieved on resonance conditions, not achieved concurrently or on the same device, without sacrificing acceptable values of some other property or are not yet achievable on macroscopic scale in a cost-effective manner.

### 1.5.2.1 Electrochemically synthesized bending conducting polymer actuators

One of the most important areas where high electro-mechanical coupling is required is CP actuator development (besides mechano-electrical sensors and mechanical energy harvesting devices). The performance of the actuators is directly connected to ion mobility inside of the polymer. Too much free volume for ion motion results in smaller dilatometric response at the same exchanged charge and causes back relaxation of the actuator, making it less controllable.. It has been established that on other conditions equal, strain to charge ratio is proportional to the radius of the moving ion. Additionally, it has been shown that for anion-active actuators, strain is improved when the moving anion is somewhat larger than the one used in the synthesis of the polymer.

Considering the relatively small strains and strain rates of macroscopic CP films, layered actuators, transforming relatively small strain to visually observable stroke, become popular and from the perspective of practical applications, air operated actuators are preferred. A common problem with bending type CP layered actuators is delamination, caused by the poor adhesion and mechanical properties of CPs. One of the proposed solutions to the delamination problem is the use of IPN, where the monomer is diffused into a non-porous SPE layer and polymerized chemically afterwards by soaking in an oxidant solution [92]. With the exception of the IPN CP actuators, the best results in terms of conductivity, response speed, efficiency, elasticity and durability have been achieved with CP films, synthesized EC at low temperatures and at low deposition rates. EC synthesis is also preferred due to the better control over synthesis conditions and better reproducibility of the results. The CPs synthesized EC at such conditions have a more ordered structure, fewer conjugation defects and larger actuation displacements [145]. Therefore, EC synthesis is often conducted at lowered temperatures [146] (even as low as  $-50^{\circ}\text{C}$ ). Aqueous synthesis is preferred due to environmental concerns, but it is

limited to electrolytes based on water-soluble salts and difficult at temperatures significantly below the melting point of water. Another restriction, limiting aqueous synthesis, is the monomer's solubility in water, which is especially restricting for EDOT and limits the choice of dopant anion. There have been no reports about semi-aqueous synthesis using salts, which are water-soluble and not soluble in organic solutions at low temperatures (significantly less than 0 °C).

The simple method of separately synthesizing CP layers EC on metal substrate, peeling them off, and attaching to a membrane layer [108] usually suffers from delamination. In addition, one of the CP-specific issues is the decrease of conductivity on reduction, which limits the part of the material participating in actuation [147] and affects negatively the performance of the actuators. EC deposition directly on the membrane requires an electrode and the common method for obtaining a conducting surface for the EC deposition as well as for retaining conductivity of the reduced CP film is vacuum evaporation [148] or sputtering [89, 149] of a noble metal coating on the insulating middle layer.

Smela and co-workers observed the delamination of EC deposited PPy from thermally in vacuum evaporated gold electrodes [150, 151]. In addition, Pyo *et al.* deposited a thermally evaporated Au electrode layer in vacuum on polyimide and observed poor adhesion between Au and the EC synthesized PPy. Nevertheless, they achieved good adhesion by EC deposition of rough Au inter-layer ensuring mechanical interlocking between Au and the EC deposited PPy [152]. Because of the poor metal-CP compatibility manifested through high contact resistance and delamination, several methods have been proposed to avoid delamination and improve adhesion, *e.g.* metal surface roughening by electroplating or etching [153], modifications after synthesis at low pH, treatment with toxic additives and solvents, and doping with biomolecules (*e.g.* dopamine, [154]). Smela *et al.* also used chemical modification of the Au layer to improve adhesion [155].

Au electrodes, prepared by radio frequency magnetron sputtering were first used for actuators in 1987 by Baughman and co-workers [100], not as electrodes for the EC deposition, but as electrical contacts, sputtered onto an existing CP layer. Au, sputtered on SPE still suffered from delamination [92]. Lewis and co-workers used Pt sputter-coated PVdF film as an electrode for the EC synthesis of PPy and no delamination problems were mentioned. Very good adhesion and conductivity can be achieved with Au sputter coated on porous PVdF membrane [156, 157], where delamination happens rarely and only at high strains.

### 1.5.2.2 Polypyrrole vs. PEDOT vs. polypyrrole-PEDOT composites

PPy is the most widespread CP actuator material, but PEDOT is increasingly used due to the higher conductivity and softness [158, 159]. The actuation properties of PPy and PEDOT have been compared by several authors. One of

the causes of inefficiency is the heat dissipation due to the  $iR$  drop on CP electrodes, caused by the resistance of the electrode and high charging current. Several authors have attempted to improve the PPy actuation properties by the more conducting PEDOT, thereby also reducing  $iR$  drop on electrodes. Zanuideen *et al.* compared the electromechanical properties of the EC synthesized combined PPy/DBS and PEDOT/DBS bi-layer (PPy|PEDOT) and tri-layer (PPy|PEDOT|PPy) freestanding actuators with PPy films [160]. They found that in 0.1 M NaCl aqueous solution, the bi-layer structures have higher strain at higher strain rates and the tri-layer films are stronger and faster than pure PPy film with half the thickness of the composite structure. Zanuideen *et al.* also showed that PPy and PEDOT are compatible, can be synthesized EC on top of each other, are delamination-proof and ions are mobile through the interface of the two polymers [161], thus, utilizing PEDOT for the improvement of PPy conductivity. Gaihre *et al.* compared the displacements of EC synthesized PPy, chemically synthesized PEDOT and EC synthesized PEDOT bi-layer actuators. They found that the largest displacements were achieved by PPy actuators synthesized EC at  $-32$  °C, followed by PEDOT actuators, synthesized EC at RT. Lowered EC synthesis temperature ( $-30$  °C) decreased the displacement of PEDOT actuators and the chemically synthesized PEDOT actuators had the lowest displacement [145].

### 1.5.2.3 Combined chemical-electrochemical synthesis method

Chemical synthesis in solutions (including with surfactants as soft templates) is widespread. The products are usually different powders, nanoparticles and composites. Besides the CP particles synthesized chemically in solutions, CPs can be synthesized chemically on both conducting and non-conducting surfaces. In addition, the purely chemical synthesis of CP (actuator) materials is well known. There have been reports about PAn and PPy actuators, fabricated chemically using biopolymer microfibers and nanofibers as templates, though EC generated films are commonly used. A recent (2012) review by Omastova and co-workers [162] addressed the chemical polymerization of CPs on different non-conductive polymers, but not on PVdF used in the current work. To the author's best knowledge, there have been no earlier reports about the chemical synthesis of neither PPy nor PEDOT on PVdF surface.

Although CP actuators have been successfully prepared both chemically and EC, there have been no reports about using *in situ* chemically deposited CPs in the role of electrodes for the following EC deposition on initially non-conducting material. To date, *in situ* chemical synthesis for CP actuators (without the EC synthesis step) has been used only for IPN actuators and not for layered actuators with a porous membrane.

The use of EC synthesized PAn CP as an electrodes has been known since 1980 [163], but neither for PPy nor for electrodeposition. A relatively new branch of research is that of CPs in role of primary electrodes, as opposed to

CP-modified electrodes, for the following EC deposition, modification and study using EC methods. The typical approach is to compress/compact chemically synthesized PPy powder (so called “polypyrrole black”) together with some binding agent.

Other types of metal-free actuators have been made by Fukushima, Takeuchi and co-workers [164, 165] using SWNTs to form the electrodes for their air-operated bending actuator. Starting from an Au electrode, Xu *et al.* carried out simultaneous chemical-EC synthesis of PPy in order to obtain superhydrophobic surfaces [88].

Usually, the chemical and EC synthesis of CPs are not combined, but rather either of them is used, depending on application. Moreover, interfacial synthesis only on conducting surfaces has been considered for long time a problem inherent to electrochemistry [53] and chemically prepared conducting coatings on initially non-conducting surfaces have not been used as electrodes for EC synthesis. EC synthesis on electrolessly deposited PPy has been reported in 2009 by Lee and co-workers [105], but it was not specified, whether *in situ* chemical oxidative deposition method was used for the first step and also not for air-operated actuator devices. Other less similar methods for EC synthesis have used traditional conducting electrodes (ITO or metal) to deposit CP *inside* of the intermediate non-conducting materials. As an example, ITO working electrode was used for the EC synthesis of PEDOT into nitrile butadiene rubber IPN by Fabre-Francke (2012) and co-workers [84] for an optical device. Later (2013), the combined synthesis method was used by Esrafilzadeh and co-workers to deposit PPy on a conducting fiber prepared from a mixture of commercial *ex situ* prepared PEDOT/PSS aqueous solution and CS, dissolved in acetic acid [141]. To author’s best knowledge, the combined chemical-EC synthesis method, described in **I**, can be considered novel.

### **1.5.3 Large surface area conducting polymer electrodes, conducting polymer hydrogels and derived aerogels**

In energy storage field, disadvantages, inherent to most of the CP applications are present, manifested in low power density, narrow operating voltage range, processing issues, chemical and mechanical instability. Therefore, carbon-based energy storage devices dominate. For CP-based devices, the achieved pseudo capacitance values are significantly lower than the theoretical pseudo capacitances due to limited diffusion speed and hence ions’ penetration depth in CP material. In addition, CPs have poor cyclic stability due to mechanical degradation and loss of contact on cyclic volumetric changes and over-oxidation [166]. Considering the theoretical limits to charge storage capacity as a fundamental constraint of CPs, one can see from **Figure 1.14** that the main bottleneck for using CPs in energy storage applications is the low power density at commercial level ( $\geq 10 \text{ mg cm}^{-2}$ , [133]) mass loading. While very high



specific performance indicator values for CPs in energy storage field have been presented in the literature, these are in most cases limited to rather small quantities and very thin layers of the active material, and low mass loading [167, 168]. The limited diffusion speed (and hence, limited diffusion depth) of ions inhibits the scale-up of CP-based devices and in order to solve the problem, a number of nanostructures have been proposed [58, 166], which are often difficult to produce industrially, and do not meet the requirements of the bulk material in many commercial applications.

Hydrogels are three-dimensional networks consisting of two phases – mostly continuous (water) and non-continuous (particles, linked chemically or physically). Polymers are capable of gelation by forming networks of polymer chains. In CP hydrogels, the properties of hydrogels and those of CP's are joined together to form a qualitatively new class of materials. CP hydrogels are promising material candidates in fields such as molecular electronics, electrical displays, biomedical sensors [82] and scaffolds, and drug delivery. Therefore, CP hydrogels have been studied by many workers ([79, 169–179]). For a long time, the production of CP hydrogels has been considered difficult and very sophisticated methods and/or expensive ingredients or supporting compounds have been used to achieve this goal.

In earlier reports, hydrogels have been made conductive using another polymeric [174, 180] or non-polymeric [181, 182] binder to form the hydrogel structure, a separate cross-linker [82], or ionic binding [170] (decomposes in alkaline solutions). Such routes commonly introduce restrictive limitations for the applicability (specific monomers of otherwise poor properties, price, redox cycling ability, pH stability *etc.*). These limitations prevent the utilization of the whole diversity of the properties of conducting polymers. Using multivalent metal cations [177, 179, 183], for example, limits the biocompatibility and electronic conductivity [177, 179], cross-linking by polyanionic dopants limits the stability in alkaline solutions and on EC reduction. The reported single-component hydrogels have several limitations in terms of synthesis complexity and the availability of monomers [173, 184].

Producing CP hydrogels from surfactant micellar solutions of monomers can be regarded as a special case of soft-template method, widely used for the production of nanoparticles. Generally, soft-templates and self-assembled nanostructures have several advantages over hard templates, such as simplicity and lower material costs [25]. From the same components and of similar concentrations (as in the present work) DeArmitt and Armes succeeded for the first time in preparing stable colloidal dispersions of surfactant-stabilized PPy nanoparticles, but due to the different handling methods, no hydrogel was obtained, despite the attempts with different preparation methods [185]. To date there have been no reports of successful hydrogel formation solely from these components for some reason.

To the author's best knowledge, there was only one group (Ghosh and Inganäs 1999 ... 2000 [177, 179]), who used CP hydrogel as an electrode for

the following EC synthesis. In their case, the hydrogel was prepared by ionic cross-linking of commercial PEDOT/PSS by bivalent  $Mg^{2+}$  ions in 0.25 M  $MgSO_4$  electrolyte. As PEDOT is not a perfect material for energy storage devices due to high price, low energy density (due to high molecular weight) and low mechanical strength, the properties of the hydrogel were improved by the EC synthesis of PPy/ $SO_4$  inside the hydrogel matrix. For the small quantity of prepared hydrogel (1.25 ... 2.5 mm<sup>3</sup>) and low active layer thickness (50 ... 100 μm), energy density  $\sim 5.5$  W h kg<sup>-1</sup> in power density range  $10^2$  ...  $10^4$  W kg<sup>-1</sup> (taking into account the dry mass of the electrode) was measured.

Aerogels are obtained by the supercritical drying of hydrogels to avoid the collapse of the gels due to capillary forces occurring on conventional drying. Preparation of carbonized aerogels from organic hydrogels (most often from resorcinol-formaldehyde) by critical point drying followed by pyrolysis is a well-known method (Pekala *et al.* [186]). An *et al.* [187] modified resorcinol formaldehyde-derived carbon aerogel with PPy synthesized by chemical soft template method (using sodium lauryl sulfate surfactant) and in combination, the large surface area aerogel EDLC and the pseudo capacitance of PPy achieved 433 F g<sup>-1</sup>. The first attempts to combine the EC properties of CP's and aerogels were based on composites with other gel-forming materials, like V<sub>2</sub>O<sub>5</sub> [188] (0.1 ... 0.2 g cm<sup>3</sup>, 150 ... 250 m<sup>2</sup> g<sup>-1</sup>). First conducting polymer aerogels were made from sodium 4-(2,3-dihydrothieno[3,4-b][1,4]dioxin-2-yl)-methoxybutane-1-sulfonate hydrogels [189]. To the author's best knowledge, pristine PPy hydrogels and aerogels have not been made previously.

Recently, Wei *et al.* obtained high surface area activated carbon by pyrolysing chemically synthesized PPy powder [190]. To the author's best knowledge, no attempts have been made to prepare carbonized aerogels from CP aerogels.

## 1.6 Problem statement

Traditionally, chemical and EC synthesis and modification methods have not been used in combination. The research task was to develop combined synthesis methods and to optimize the synthesis conditions to meet the needs of two application fields without sacrificing the properties beneficial for both applications – performance, stability, and suitability for industrial production.

The primary research problem was to study the properties of *in situ* chemically synthesized electrodes using mainly EC methods. Chemically synthesized electrodes were characterized in order to elucidate benefits for two major types of CP applications: the ones requiring large CP surface area and high ionic mobility and those, where EC synthesized CP coating on non-conducting surface was required. In order to provide comparison with alternatives, the concept of chemically synthesized electrodes in combination with EC synthesis and EC modification of the electrodes was utilized for CP actuators and for PPy hydrogel electrodes. These CP applications have distinctively different

expectations for CP structure, ionic mobility and electro-chemo-mechanical coupling.

The current work aims at answering the question, which are the advantages and the disadvantages of the concept of chemically synthesized electrodes and the combined synthesis method for the chosen applications.

### ***1.6.1 Electrochemical synthesis on initially non-conducting surfaces***

Tri-layer air-operated bending actuators were used as an application for the chemical-EC synthesis method with the goal to find the solution to the delamination problem using the chemical synthesis step in place of vacuum techniques, while retaining the advantages of EC prepared actuators. Resulting methods were intended to increase the technological suitability for commercialization and biocompatibility by avoiding the usage of noble metals and vacuum technologies. The prepared actuators had to be characterized mostly by means of EC methods. Comparison of the actuators of different designs and CPs was aimed at studying the implications of the developed method and identifying possible ways for further development. Expectations to the outcome of the research were:

- finding possibilities and suitable chemical synthesis methods for the preparation of the EC synthesized working layers on a initially non-conducting membrane layer for air-operated metal-free actuators and electrolyte-operated linear actuators, considering also:
  - different chemical synthesis methods for the preparation of the electrode layer;
  - properties of the chemical synthesis substrates, such as hydrophobicity/hydrophilicity, porosity/homogeneity (including SPE membranes), resistance to chemical synthesis media and oxidants;
  - applicability of different CPs for chemical and EC layers and their combinations in order to control the structure and the properties of the actuators;
  - need for EC synthesis in organic as well as aqueous media at lowered temperatures;
  - availability of the materials, suitability for industrial production and the environmental impact;
  - avoiding drawbacks in performance characteristics (comparing with alternative methods);
- obtaining characterization results, allowing considerations of the chemical-EC synthesis method for other applications where EC coating is preferred on non-conducting surfaces.

### ***1.6.2 Electrolyte-operated linear tri-layer actuators***

CP actuators operate either in electrolyte or in air (also in vacuum). According to the application, the design could be radically different. In an electrolyte, freestanding single-layer CP films have been considered enough for linear actuation, and additional polymer membrane has not been considered necessary to operate in an electrolyte bath. In air application, a membrane in role of an ion reservoir is necessary.

Linear CP electrolyte-operated freestanding actuators are typically prepared as films, synthesized EC on a conducting substrate and peeled off afterwards. To author's best knowledge there have been no reports of truly stable actuation, either in terms (of lack) of creep or mechanical durability. Bending creep and the related issues are inherent to asymmetrical materials, deposited on an electrode and then removed, as the inner and outer layers are different in terms of structure and electroactivity. Linear creep behavior and ion mobility type depend solely on strain and internal stress of the CP material.

There are also the considerations of speed and force. For single-layer freestanding films, only the outer layer of the film is active due to the diffusion limitations of the ions. Thus, it would be beneficial to produce very thin actuators to ensure fast response. Such actuators would be fragile and difficult to handle. In case of thicker freestanding films and/or increased actuation speed – only the outer layer is accessible to ions, the inner part is passive and must be stretched (reminding the generally poor elasticity of CPs) by the outer layers.

The optimal linear actuator should be inherently symmetric, have the whole CP material accessible to ions and the thickness of the actuating CP layer should be related to the expected actuation speed and force output. Parts of the actuator, not participating in actuation, should have mechanical properties required by the intended application (typically better/different from those of CPs) and therefore tunable. The mechanical properties of this passive part should be able to suppress creep and retain the intended ion mobility type. The preparation method should ensure precise control over the mechanical, EC and ECMD properties. Development of the actuator, satisfying these requirements was intended as a proof of concept of the chemical-electrochemical synthesis method.

### ***1.6.3 Large surface area conducting polymer electrodes with high ionic mobility***

The research goal was to prepare large surface area CP hydrogels using the most classical and extensively studied components for chemical synthesis – polypyrrole, ammonium peroxydisulfate and sodium dodecylbenzenesulfonate for the traditional chemical synthesis. To date, for some reason, there have been no reports of successful hydrogel formation solely from such components.

Moreover, to author's best knowledge, there are no reports that CP hydrogels have been used for carbonized aerogel formation.

Chemically synthesized large surface area electrodes were studied and characterized mainly in context of high power density CP energy storage devices with the goal to relieve the diffusion speed and the resulting power density limitation, inherent to CP energy storage applications. The following key properties were expected from results of the study:

- preliminary study of the ranges of the suitable synthesis conditions and further EC modification options;
- EC and environmental stability of the chemically synthesized CP hydrogels;
- avoiding the disadvantages of alternative approaches;
- environmental concerns, availability of the materials and simplicity (preferring single-component hydrogels) of the preparation methods;
- acceptable control over the structure, chemical composition, mechanical, electrical and electro-chemo-mechanical properties.

While the main emphasis was on properties beneficial for energy storage devices, the prepared hydrogels and their EC modification options were characterized in order to evaluate their feasibility and potential for other applications requiring biocompatibility and exchange of the doping anions, expected for controlled drug delivery devices, *in vivo* and optionally anti-inflammatory electrodes and biocompatible anodes in microbial fuel cells. As a proof of concept, the prepared hydrogels were used as electrodes for the following EC synthesis inside of the hydrogel and as starting material for the high surface area PPy aerogels and carbonized aerogels.

## 2 EXPERIMENTAL

This chapter describes the used materials, preparation and measurement methods, technical set-ups and procedures for polymer synthesis and characterization. Although several materials and methods for both chemical and EC synthesis step were used (detailed description in papers I–IV), only those leading to the most representative and reproducible results are described in the experimental section. Detailed information about the used reagents and equipment can be found in papers I–IV (referenced in text).

### 2.1 Materials and preparation methods

A combined chemical-EC synthesis method was used to prepare the actuators. Working layers of the actuators were prepared in two steps. The chemically synthesized CP formed an electrode surface for the following EC deposition of the main actuating layer. The chemically synthesized electrode material remained mostly in the outer layer of the membrane, and the amount of chemically synthesized CP decreased sharply towards the centre of the membrane. The EC synthesis on this electrode resulted in the formation of tri-layer actuators.

All solutions, used in the preparation of the materials, EC and ECDM measurements were deaerated by ultrasonication and by saturation with Ar, where possible (no surfactants in solution) in order to reduce the amount of dissolved oxygen in solution, as at positive potentials the dissolved oxygen accelerates PPy degradation [191].

#### 2.1.1 Substrates for chemical synthesis

Substrates were used as middle layers of the actuators in two different roles: as electrolyte storage and electronic separator layer for tri-layer air-operated bending actuators and as a mechanically supporting interlayer for electrolyte-operated tri-layer linear actuators.

Membranes used for the bending actuators were based on the PVdF polymer and PVdF-HFP co-polymers:

1. Commercial Millipore Immobilon-P (MPI, from product datasheet: PVdF, hydrophobic, thickness 125  $\mu\text{m}$ , pore size 0.45  $\mu\text{m}$ , porosity 70%);
2. Commercial Millipore Durapore (MPD, from product datasheet: PVdF, hydrophilic, thickness 110  $\mu\text{m}$ , pore size 0.1  $\mu\text{m}$ , porosity 70%);
3. In-house (IH) solid polymer gel electrolyte (SPE) membrane was prepared similarly to the procedure of Sugino *et al.* [127]. RTIL EMImBF<sub>4</sub> (200 mg, 8 wt.%) and PVdF-HFP (200 mg, 8 wt.%) were dissolved in a mixture of MP (2 ml, 64 wt.%) and PC (500 mg, 20 wt.%). The mixture was stirred over night at 70 °C and poured into mold. SPE film was obtained after the MP

solvent evaporated. Membrane porosity, estimated as electrolyte volume (EMIImBF<sub>4</sub> in PC) ratio to total membrane volume after MP solvent evaporation was 83%. Initial membrane thickness, calculated from the electrolyte and PVdF-HFP volumes was 273  $\mu\text{m}$ .

For electrolyte-operated tri-layer linear actuators, two substrate types were used as interlayer:

1. porous commercial MPD membranes;
2. non-porous chitosan (CS) substrate prepared by dissolving CS polymer powder (2 wt.%) in 2% acetic acid aqueous solution. The solution was poured into mold, dried in air followed by soaking in 0.2 M NaOH and drying in the oven at 60 °C overnight. Thickness of the film was approximately 110  $\mu\text{m}$ .

### **2.1.2 Chemical synthesis of conducting polymer electrodes**

Chemical synthesis was in the current work used for the preparation of conductive electrodes of application-specific structure and properties for the following EC modification. PPy aerogels and carbonized aerogels were prepared from hydrogels for the characterization of the structure and the chemical composition using SEM and EDX and for low temperature N<sub>2</sub> sorption measurements, including comparison with resorcinol formaldehyde-derived carbonized aerogels.

#### **2.1.2.1 Chemical synthesis on non-conducting surfaces for tri-layer actuators**

Details of several chemical synthesis methods, used for the chemical synthesis of PPy on porous surfaces are described in papers **I**, **II** and **IV**. For different membrane types, different methods gave the most reproducible results.

For PPy synthesis on IH SPE (membrane preparation is described in section 2.1.1) the synthesis was carried out at RT ( $22 \pm 2$  °C) in an aqueous solution of 0.044 M Py, 0.015 M SDBS and 0.1 M SPS. Membrane, cooled down to  $-30$  °C was immersed in solution with gentle stirring until the membrane become black from the deposited PPy (about 200 s). The membrane was washed between fingers to remove unbound PPy deposit and dried.

For PPy synthesis on porous commercial Millipore PVdF membrane, three different methods were used:

1. *Synthesis in solution (on liquid-liquid and solid-liquid interfaces)*: For PPy chemical synthesis on hydrophobic MPI membrane, solution with the same concentrations as for SPE was used. PVdF membrane was permeated with pyrrole monomer and immersed in solution at temperature 70 °C for 20 s, until membrane turned black from the polymerizing monomer, diffusing out

from the surface pores of the membrane. Polymerization was terminated by washing in cold MeOH. For PPy synthesis on hydrophilic MPD membrane, synthesis time was reduced to 15 s, temperature lowered to 60 °C. The optimal synthesis solution was 0.075 M APS and 0.006 M SDBS.

2. *Vapor phase synthesis I (on liquid-vapor interface)*: PVdF membrane permeated with 0.5 M FeCl<sub>3</sub> solution in PC, were swept with filter paper and exposed on glass plate between two Petri dishes to Py vapor at 40 °C until the membrane turned black (about 15 min). After turning over, the membrane was swept clean again and the exposure was repeated for the other side. The resulting membrane was then thoroughly rinsed with MeOH.
3. *Vapor phase synthesis II (on solid-vapor interface)*: commercial PVdF membrane was painted with 0.5 M FeCl<sub>3</sub> oxidizer solution in mix of water and MeOH (80:20 v/v.%), followed by exposition to Py vapor identically to the previous method.

The chemical synthesis of PEDOT on hydrophilic MPD membrane was carried out in a similar way as for PPy: membrane, permeated with monomer, was wiped dry with filter paper and immersed in 1.5 M FeCl<sub>3</sub> aqueous solution at 60 °C for 120 s, until the membrane became dark blue.

A different approach was chosen for the linear tri-layer actuator. Commercial MPD membrane and CS film were soaked in EDOT solution in PC with 4 v.% water added and then immersed in hot (60 °C) 0.2 M FeCl<sub>3</sub> solution in PC for 1 min.

The chemical synthesis was terminated by washing in cold MeOH and wiping off detached remains of the CP deposit. The substrate was washed with water and MeOH and dried (weighted down) in vacuum oven (except IH SPE membrane containing PC solvent).

### 2.1.2.2 Polypyrrole hydrogel, aerogel and carbonized aerogel preparation

The synthesis solution was prepared in two beakers, containing the same volume of water. Except the synthesis utilizing 0.1 M SDBS and 0.1 M APS solution (**Table 3.4**), in one beaker the SDBS surfactant and Py monomer were dissolved, with the oxidant in the second beaker. Both solutions were clear, without visible opalescence or turbidity at all tried concentrations. Both solutions were mixed together while actively stirring until the resulting solution turned dark gray (approximately 3–10 s) due to the chemical polymerization of PPy. The solution was immediately spilled into a glass mould and held still overnight to complete gelation.

After gelation, hydrogels were carefully removed from mould and washed with deionized water during 1 week to remove unreacted Py, detached Py oligomers, residues of oxidant and its reaction residues and the remains of SDBS. Hydrogels were washed by immersing in water, which was replaced



every 12 h until the initially yellowish water remained colorless and not foaming upon shaking due to the remains of SDBS.

For EC measurements, 0.2 M Py-APS and 0.3 M Py-APS hydrogel was gelatinized in a cylindrical cup (diameter 48 mm, top surface area 18 cm<sup>2</sup>, hydrogel volume 15 cm<sup>3</sup>) above a sparse platinum wire ( $\varnothing$  75  $\mu$ m) mesh with surface area 2.7 cm<sup>2</sup>. The hydrogel was washed by holding it for a long time in actively stirred and periodically replaced deionized water.

For aerogel preparation, hydrogels were washed first with water and after that with MeOH and/or Ac. The hydrogels were immersed in washing liquid, which was replaced every 12 hours. Solvent exchange (water to Ac or MeOH) was carried out by immersing hydrogels in a beaker with the target solution and holding them above the bottom using a SS mesh sheet, allowing water, as the higher density solvent to spill down into the bottom of the beaker. Yellowish or light blue color of liquid in bottom part of the beaker confirmed solvent exchange. This procedure was repeated 5–7 times until the yellowish color (in water) disappeared and the initially dark blue color became pale (Ac or MeOH). The dark blue residue was collected and dried in N<sub>2</sub> atmosphere for elemental analysis. After solvent exchange, the hydrogels were dried by supercritical CO<sub>2</sub> extraction similarly to the procedure described by Perez-Caballero *et al.* [192]. Solvent extraction was carried out in continuous extraction regime. The detailed procedure of supercritical CO<sub>2</sub> extraction consisted of four steps:

1. At CO<sub>2</sub> pressure 200 bar and at constant temperature 25 °C, the hydrogel was held in extractor (with closed output valve) for 20 min, allowing blending of CO<sub>2</sub> with hydrogel's solvent;
2. Output restrictor of the extractor was carefully opened and after reaching CO<sub>2</sub> pressure 100 bar and at constant temperature 25 °C, the mixture of the hydrogel's solvent and CO<sub>2</sub> was during 4 h slowly exchanged to pure CO<sub>2</sub>. Speed of the exchange was observed and controlled visually by intensity of CO<sub>2</sub> bubbling from a submerged-in-EtOH hose from the output valve of the extractor;
3. Temperature of the extractor was raised up to 45 °C, at pressure 100 bar and with opened output restrictor, CO<sub>2</sub> was transferred into supercritical state and kept for 2 h, continuing solvent exchange;
4. At 45 °C with closed input valve and slightly opened output restrictor, the pressure was left to decrease slowly down to normal pressure (4 ... 6 h), after pressure equilibration, extractor was left to cool down at room temperature. After reaching room temperature, the aerogel was removed from extractor.

PPy aerogel was further carbonized by pyrolysis. Pyrolysis was carried out under vacuum at 350 °C for 12 h.

## 2.1.3 Electrochemical synthesis, actuator preparation and electrolyte choice considerations

### 2.1.3.1 Electrochemical synthesis

The main working layers of the actuators were synthesized EC in either aqueous or PC solutions. The EC synthesis was carried out galvanostatically to allow precise control over the deposition rate, easier interpretation of the dynamics of the synthesis and consistent reproducibility. Potentiostat/galvanostat PARSTAT 2273 was used as the constant current source for the one-compartment two-electrode EC cell (**Figure 2.1**) at current density  $0.1 \text{ mA cm}^{-2}$  and at lowered temperatures ( $-28 \dots -31.5 \text{ }^\circ\text{C}$ ). For chemical-EC synthesis, CP was deposited simultaneously on both sides of the membrane using chemically synthesized CPs as the anodes, connected as the working electrode and sense electrode of the potentiostat/galvanostat. For the synthesis of freestanding films, a SS plate was used as the anode. Symmetrically and parallel to the anode, SS (AISI316L) mesh sheets (cathodes) were placed, and connected as the counter electrode and reference electrode of the potentiostat/galvanostat.

DBS<sup>-</sup>-doped CPs were synthesized from 0.2 M monomer and 0.2 M SDBS solution in mix of water and MEG (50:50 v/v.%). TFSI<sup>-</sup>-doped CPs were synthesized from 0.2 M monomer and 0.2 M LiTFSI solution in PC with 2 v.% water added.

Actuators for the comparison of chemically synthesized electrodes with sputter-coated (Au, thickness 50 nm) electrodes were synthesized with charge density  $2.2 \text{ C cm}^{-2}$  and at current density  $0.11 \text{ mA cm}^{-2}$ .

EC synthesis of the linear actuators was carried out in a conventional three-electrode EC cell at RT with a SS sheet counter electrode and Ag/AgCl wire as the reference electrode.

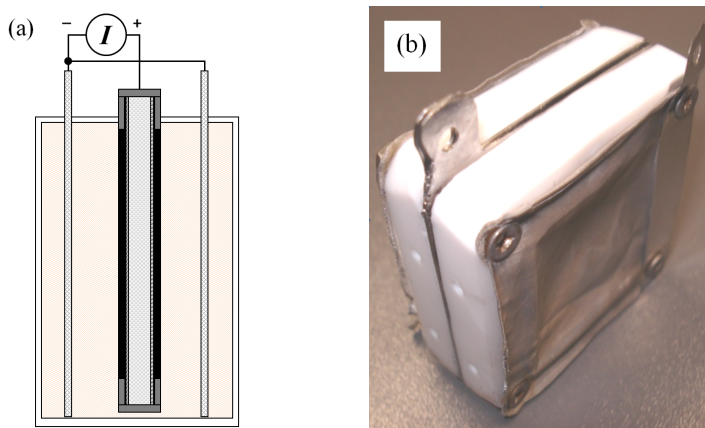


**Figure 2.1.** EC synthesis cell: a) conceptual schema; b) photo.

**Table 2.1.** Designations and synthesis conditions of the EC synthesized films.

Designation in publications	Substrate	Chemical layer	EC layer	EC synthesis solution	$T$ (°C)	Charge density (C cm <sup>-2</sup> )
–	MPD	PEDOT/Cl	PEDOT/DBS	0.2 M monomer, SDBS in H <sub>2</sub> O:MEG (50:50 v/v.%)	-25	4
IH-immersion	IH	PPy/(DBS,SO <sub>4</sub> )	PPy/ DBS		-23	4
MPI-immersion	MPI	PPy/Cl			-23	8
MPI-vapor					-23	2
Sample B	CS	PEDOT/Cl			-18	4
Sample A	MPD	PPy/SO <sub>4</sub>	PPy/ TFSI	0.2 M monomer, LiTFSI in PC (2 v.% H <sub>2</sub> O)	-31.5	2
PPy PPy		PEDOT/Cl				
PEDOT PPy	SS	n/a	PEDOT/TFSI			
PPy-FS*						
PEDOT-FS*						
PPy PEDOT	MPD	PPy/SO <sub>4</sub>	PEDOT/TFSI			
PEDOT PEDOT		PEDOT/Cl				

\* Freestanding film used for reference

### 2.1.3.2 Actuator preparation

After polymerization, the resulting films were washed with water or MeOH and dried (weighted down) in vacuum oven (except IH membrane containing PC solvent). For actuator preparation, the edges of the EC synthesized sheets were trimmed off and the remainder of the sheets was cut into 3 × 20 mm (PPy/DBS<sup>-</sup>), 4 × 20 mm (TFSI<sup>-</sup>-doped CPs) or 3 × 10 mm (linear actuator) strips. Before measurements, actuators were held for at least 48 h in target electrolyte. Electrolytes, used in this work are listed in **Table 2.2**.

**Table 2.2.** Electrolytes used for CP actuators (concentrations in referenced sources may differ).

Electrolyte	Description
1 M LiTFSI in PC	Widespread electrolyte for high strain and strain rate air-operated PPy actuators with porous membrane, similar to ones used in this work ( <i>e.g.</i> [98, 149, 156])
1 M EMImBF <sub>4</sub> in PC	Initial electrolyte in IH SPE membrane prepared according to [127]. Usage of electrolyte decreases due to hydrophilicity and environmental issues. Used for different actuator types ( <i>e.g.</i> [144, 164])
EMImTFSI (3.89 M)	Hydrophobic, stable. Common RTIL for IPN actuators. Used in ( <i>e.g.</i> [92, 145, 164]).
0.1 M TBACF <sub>3</sub> SO <sub>3</sub> in PC	Used in this work for tri-layer linear actuator ECMD measurements and also in [193, 194]

\* Concentrations in the literature sources may differ.

### 2.1.3.3 Actuator electrolyte concentration considerations

In order to operate in air, the quantity and the concentration of the electrolyte had to be sufficient to compensate the actuation charge in the electrode(s) without a significant influence on the conductivity of the remainder of the electrolyte. Assuming full oxidation of the fully reduced electrode, the oxidation charge from (1.12):

$$Q_{ox} = \frac{d_a \cdot Q_s}{d_a + 2}. \quad (2.1)$$

Amount of dopant ions (mol) is then:

$$n_{mol} = \frac{Q_{ox}}{F}, \quad (2.2)$$

where  $F$  is the Faraday constant. The available free volume in the membrane is:

$$V = p \cdot h \cdot A, \quad (2.3)$$

where  $p$  is the porosity of the membrane,  $h$  is the thickness of the membrane and  $A$  is the area of one side of the membrane. Replacing synthesis charge  $Q_s$  with synthesis charge density  $\delta$  ( $C\ m^{-2}$ ), combining equations (2.1) ... (2.3), estimating the expected doping level (usually *ca.* 0.33) and assuming 100% synthesis efficiency, the minimal concentration (M) of the electrolyte in the porous membrane to compensate the charge of one electrode can be calculated as:

$$c = \frac{d_a \cdot \delta}{p \cdot h \cdot (d_a + 2) \cdot F}. \quad (2.4)$$

## 2.2 Characterization setup

### 2.2.1 Electrochemical and ECMD characterization of polypyrrole actuators

Electro-chemo-mechanical parameters of the bending actuators were typically characterized using an in-house setup (**Figure 2.2**) consisting of custom NI Labview software interfaced through PCI-6036E DAQ (National Instruments) with a laser displacement meter LK-G82/LK-G3001P (Keyence) and an isometric force transducer MLT0202 (ADInstruments). The current of the actuation signal was measured using an in-house current amplifier/ZRA. Actuators were mounted side-ways (2 mm clamped, free length 18 mm)

between flat gold contacts. The displacement measurement distance from the clamped end of the actuator was adjusted using an XY-micrometer stage. The voltage at the actuator clamp, the current, and the displacement or the blocking force were measured simultaneously. The displacement signal was shifted by 2 ms in order to compensate for the measurement delay of the displacement meter.

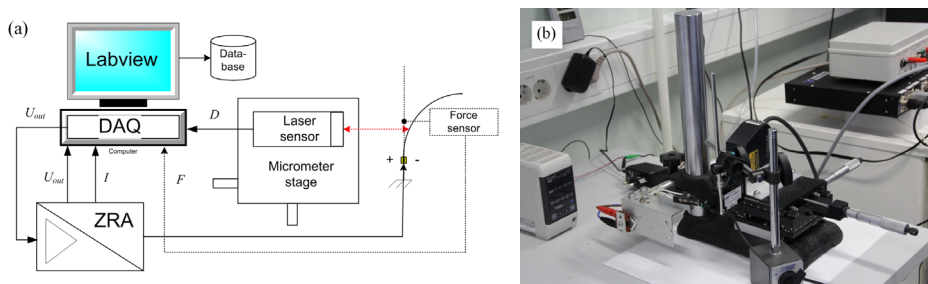


**Figure 2.2.** Actuator characterization setup: a) schematic of experimental measurement system (ZRA is integrated with current amplifier); b) photograph.

EC measurements of bending actuators were conducted in two-electrode configuration with potentiostat/galvanostat PARSTAT 2273. Chemically or chemically-EC coated membrane sides, clamped between gold plates were used as electrodes connected to working/sense and counter/reference inputs, respectively. In order to exclude the effect of evaporation of solvent, the EC measurements were only performed using the RTIL EMImTFSI as the electrolyte.

EC and ECDM characterizations of linear actuators were carried out in a three-electrode configuration, using CHI650C EC workstation (CH Instruments) and 611A Dynamic Muscle Analysis (Aurora Scientific Inc.). Actuators, clamped vertically between polyvinyl chloride holders with SS sheets as contacts at the bottom end (free length of the actuator 1 mm) were used as working electrodes and a Pt sheet as the counter electrode. All potentials were measured against a Ag/AgCl (3 M KCl) reference electrode. Actuator samples were immersed in 0.1 M TBACF<sub>3</sub>SO<sub>3</sub> in PC electrolyte 2 h before measurements and preloaded with a constant force 20.3 mN. EC and ECDM measurements were conducted with CV experiments ( $\pm 1.0$  V, scan rates 5, 10 and 50 mV s<sup>-1</sup>) and square wave potentials ( $\pm 1.0$  V, frequency 0.1 Hz).

### 2.2.2 Electrochemical characterization of polypyrrole hydrogel

A hydrogel electrode was used as the working electrode in a one-compartment three-electrode EC cell, where a carbon rod was used as the counter electrode. Experiments were carried out using the potentiostat/galvanostat PARSTAT 2273 and the potentials were measured vs. a reference electrode (Ag/AgCl, 3 M

KCl or SCE), placed in proximity of the working electrode surface. The hydrogel was EC cycled in electrolyte for 96 h after electrolyte change and before measurements. EC characterization was performed for 0.3 M Py-APS concentration hydrogel in 0.2 M NaBF<sub>4</sub> (also in 0.2 M LiClO<sub>4</sub> for redoping experiments) electrolyte.

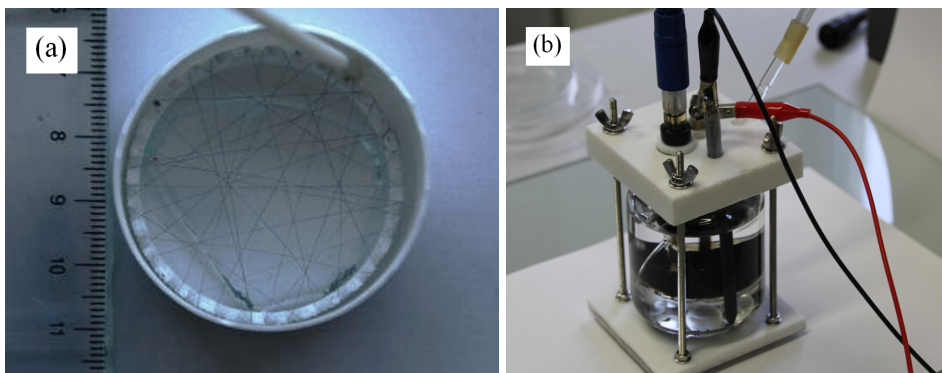


**Figure 2.3.** Hydrogel characterization setup: a) the electrode; b) the electrochemical cell.

## 2.3 Characterization methods

Both gels and actuators have many characteristics. The choice of the characterization methods depends on the targeted application area. In the current work, hydrogels were characterized by their density, conductivity, porosity and EC properties. The characterization methods were chosen so that they were as much as possible applicable for both actuator and hydrogel/aerogel characterization. The main parameters influencing the properties relevant to this work were the doping level, the conductivity, the mechanical properties, the permeability, the surface area.

### 2.3.1 Diffusion constant measurements

Apparent diffusion constant measurements for actuators were conducted using the CV technique in two-electrode connection of the potentiostat and derived from the slope of the  $j_p$  vs.  $v^{1/2}$  graph according to the Randles-Sevcik equation:

$$j_p = 0.4463 \cdot n \cdot F \cdot c \cdot \sqrt{\frac{n \cdot F \cdot v \cdot D_{app}}{R \cdot T}}, \quad (2.5)$$

where  $j_p$  is the absolute value of redox current density peak (A cm<sup>-2</sup>),  $D_{app}$  is the diffusion constant,  $n$  is the number of electrons participating in the redox event,

$F$  is the Faraday constant,  $c$  is the concentration,  $v$  is the scan rate,  $R$  is the gas constant, and  $T$  is the temperature.

### **2.3.2 Electronic and ionic conductivity measurements**

Electrical sheet resistances of the chemically synthesized layers and the electrical conductivities of the final electrodes were typically measured in dry state with an in-house setup based on the four-electrode potentiostat/galvanostat PARSTAT 2273. Using the chronopotentiometry technique, constant current was passed through the working electrode and counter electrode, connected to the outer contacts of the four-terminal probe. Potential between the inner contacts was measured using the reference and sense electrode terminals of the potentiostat/galvanostat. Conductivities were calculated using Eq. (1.15). Sample thickness was measured with a digital micrometer or from a SEM micrograph of the cross-section of the sample. Effective conductivities of the electrodes with different PPy and PEDOT combinations for chemical and EC layer and with different spatial distributions were calculated using effective thickness, defined as the thickness of the EC synthesized CP, assuming uniform density and 100% synthesis efficiency. Thickness, corresponding to the CP-dopant combination, similar synthesis conditions and used synthesis charge density, were taken from literature ([195] and [196] for PPy/TFSI and PEDOT/TFSI, respectively).

The ionic conductivities were measured by means of EIS using a VSP potentiostat (Biologic SA). PVdF membranes were permeated with electrolyte and fixed in a cell with SS pressure contact electrodes. The ionic conductivity was calculated from Eq. (1.16).

### **2.3.3 Physical structure, morphology and chemical composition**

Structure and morphology of the chemically synthesized actuator electrodes, EC synthesized working layers and aerogels was qualitatively studied using SEM Hitachi TM3000 (with back-scattered electron detector and acceleration voltage 5 or 15 kV), CARLZEISS AG-ULTRA 55 GEMINI (with secondary electron detector and acceleration voltage 15 kV), Helios NanoLab 600 SEM and CM-Instrument JCM-6000. For cross-section micrographs and sulfur distribution mapping by EDX spectrometer (SwiftED 3000, connected to Hitachi TM-3000 SEM), the actuator samples were broken between tweezers at boiling nitrogen temperature. Before imaging, the aerogels were sputter coated with gold.

For the MPD membrane, the tortuosity was quantitatively characterized by the comparison of the ionic conductivity of the electrolyte with and without the membrane. Tortuosity coefficient, describing the ratio of the average actual path length to the shortest path between membrane sides, was calculated using equation [197]:

$$t = \sqrt{\frac{\sigma_0}{\sigma_i} \cdot p}, \quad (2.6)$$

where  $\sigma_0$  is the ionic conductivity of the electrolyte,  $\sigma_i$  is the ionic conductivity of the membrane, permeated with the electrolyte,  $p$  is the porosity of the membrane, and  $t$  is the tortuosity.

Roughness of the inner (attached to the membrane) surface of the chemically-EC synthesized CP bending actuators and the structure of the hydrogels was quantitatively characterized using the CV technique and the fractal dimension method [198]. The fractal dimension was calculated as:

$$d_f = 2 \cdot \alpha + 1, \quad (2.7)$$

where  $d_f$  is the fractal dimension and  $\alpha$  is the Faradaic charge transfer coefficient.  $\alpha$  is calculated as the slope of the least-square fit of the  $\log(j_p)$  vs.  $\log(v)$  graph, where  $j_p$  is the redox current density peak ( $\text{mA cm}^{-2}$ ) and  $v$  is the scan rate.

The CV experiments to estimate the fractal dimension of the hydrogels were conducted in 0.2 M  $\text{NaBF}_4$  electrolyte in potential range  $E = 0.4 \dots -0.85 \dots 0.4 \text{ V}$  (vs.  $\text{Ag/AgCl}$ , 3 M  $\text{KCl}$ ) at scan rates 0.1 ... 0.45  $\text{mV s}^{-1}$  and in pure EMImTFSI in case of bending actuators. For the EC synthesis inside of the hydrogel, fractal dimension was measured in 0.2 M  $\text{LiClO}_4$  in MEG electrolyte in potential range  $E = 0.4 \dots -0.85 \dots 0.4 \text{ V}$  (vs. SCE) at scan rates 10 ... 50  $\text{mV s}^{-1}$ .

In order to characterize the structure of hydrogels EC, EIS experiments were conducted in 0.2 M  $\text{NaBF}_4$  electrolyte with the excitation voltage AC 25 mV RMS in frequency range from  $1 \cdot 10^{-4} \text{ Hz}$  to 25 kHz at a constant potential of  $E = 0.4 \text{ V}$  using potentiostat/galvanostat PARSTAT 2273.

In order to analyze and compare the adhesion mechanisms and quality of the chemically synthesized PEDOT electrodes on PVdF and CS, Raman spectra (Renishaw System 1000 microprobe, 785 nm excitation line obtained by Renishaw solid state diode red laser) and FTIR spectra ( $4000 \dots 600 \text{ cm}^{-1}$ , Bruker Alpha with Platinum ATR) were measured.

### 2.3.4 Doping level measurements

#### 2.3.4.1 Doping level from the weight of freestanding films

For thick freestanding films, doping level was calculated from the films' dry weight and the synthesis charge, assuming 100% synthesis efficiency. The amount of the EC polymerized repeating units (mol) is:



$$n_{mol} = \frac{Q_s}{F \cdot (d_a + 2)}, \quad (2.8)$$

where  $Q_s$  is the consumed synthesis charge,  $F$  is the Faraday constant, and  $d_a$  is the analytical doping level. The total mass of the doped polymer is:

$$m = n_{mol} \cdot (M_{CP} + d_a \cdot M_d), \quad (2.9)$$

where  $M_{cp}$  is the molar mass of a CP repeating unit and  $M_d$  is the molar mass of the dopant anion. Substituting  $n_{mol}$  from Eq. (2.8) to Eq. (2.9) and solving for  $d_a$  gives:

$$d_a = \frac{2 \cdot F \cdot m - Q_s \cdot M_{CP}}{Q_s \cdot M_d - F \cdot m}. \quad (2.10)$$

The obtained formula can be considered analogous to that of Bay *et al.* [60], who used the same assumptions for doping level calculation, but synthesis current and EQCM frequency change at microscopic level instead of the total synthesis charge and the weight of the resulting macroscopic film.

#### 2.3.4.2 Doping level by energy dispersive X-ray spectrometry

EDX was used for the elemental analysis of PPy aerogels and dried hydrogels. The analytical doping by sulfate and sulfonate anions could be separately quantified, knowing that the prepared gel contains only PPy  $(C_4H_3N)_n$ , doped with either  $DBS^-$  ( $C_{18}H_{29}SO_3^-$  from the SDBS surfactant) or  $SO_4^{2-}$  anions (from APS). Both anions contain one S atom and the analytical doping level is then ( $S$ ,  $N$ ,  $O$ ,  $C$ ,  $B$ ,  $Cl$  are atomic ratios of the respective elements in per cents,  $d_a$  is the analytical doping level, and subscript is reference to a specific anion):

$$d_a = d_{DBS} + d_{SO_4} = \frac{S_{DBS} + S_{SO_4}}{N}. \quad (2.11)$$

The total number of  $O$  atoms is the sum from both anions and the total number of  $S$  is the sum from both anions:

$$O = 3 \cdot S_{DBS} + 4 \cdot S_{SO_4}, \text{ and} \quad (2.12)$$

$$S = S_{DBS} + S_{SO_4}. \quad (2.13)$$

Solving equations (2.12) and (2.13) for  $S_{SO_4}$  and equalizing the results one can obtain

$$S - S_{DBS} = \frac{O - 3 \cdot S_{DBS}}{4}. \quad (2.14)$$

Solving Eq. (2.14) for  $S_{DBS}$  yields

$$S_{DBS} = 4 \cdot S - O. \quad (2.15)$$

Replacing Eq. (2.15) into Eq. (2.12) gives

$$S_{SO_4} = O - 3 \cdot S. \quad (2.16)$$

Redoping with  $BF_4^-$  gives an additional doping component

$$d_{BF_4^-} = \frac{B}{N}. \quad (2.17)$$

For gels, redoped with  $ClO_4^-$ ,  $O$  in Eq. (2.15) and Eq. (2.16) is substituted with  $O - 4 \cdot Cl$ . Then

$$d_{DBS^-} = \frac{4 \cdot (S + Cl) - O}{N}, \quad (2.18)$$

$$d_{SO_4^{2-}} = \frac{O - 4 \cdot Cl - 3 \cdot S}{N}, \text{ and} \quad (2.19)$$

$$d_{ClO_4^-} = \frac{Cl}{N}. \quad (2.20)$$

Since the results of elemental analysis using EDX were not always reproducible (probably due to the roughness of the samples), the reliability of the results was improved through repeated experiments and by the elimination of results, which were not consistent with the C ratio. Reliability check was based on the reasoning that a PPY unit has 4 C, one N, and a  $DBS^-$  has 18 C atoms. Then for  $DBS^-$  ions remains  $C - 4 \cdot N$  carbon atoms and

$$S_{DBS} = \frac{C_{DBS}}{18} = \frac{C - 4 \cdot N}{18}. \quad (2.21)$$

### 2.3.4.3 Electrochemical doping level and energy storage properties

Using the redox charges from cyclic voltammetry experiments, EC doping level was calculated using Eq. (1.12).

To measure hydrogel's maximum charge storage capability, linear sweep (0.1 mV s<sup>-1</sup>) technique was applied to the fully oxidized or fully reduced electrode, followed by chronoamperometry at the final potential until the decay of the redox current. The experiments were conducted in 0.2 M NaBF<sub>4</sub> aqueous electrolyte (in 0.2 M LiClO<sub>4</sub> in MEG electrolyte for experiments of the EC synthesis inside the hydrogel). During oxidation or reduction, the total exchanged charge was measured. Specific (gravimetric) capacitance was calculated as [199]:

$$C_m = \frac{Q_{ox} + Q_{red}}{2 \cdot m \cdot \Delta E}, \quad (2.22)$$

where  $Q_{ox}$  and  $Q_{red}$  are the oxidation and reduction charges, respectively,  $m$  is the dry mass of the CP and  $\Delta E$  is the potential window. Differential specific (gravimetric) capacitance (using CV technique in the same 0.2 M NaBF<sub>4</sub> electrolyte at scan rate of 0.25 mV s<sup>-1</sup>) was estimated as:

$$C_m = \frac{i_{peak}}{v \cdot m}, \quad (2.23)$$

where  $i_{peak}$  is the peak redox current and  $v$  is the scan rate. Low scan rates were intentionally chosen in order to limit the otherwise high redox currents, caused by the large inner surface area of the hydrogel electrode. Frequency dependent specific (gravimetric) capacitance was calculated from the slope of the  $-Z_{im}$  vs.  $f^{-1}$  graph of EIS measurements at low frequencies as in [200]:

$$C_m = -\frac{1}{m \cdot 2 \cdot \pi \cdot f \cdot Z_{im}}, \quad (2.24)$$

where  $f$  is the frequency, and  $Z_{im}$  is the imaginary part of the complex impedance. The maximum specific capacitance depending on doping division of PPy hydrogel was calculated as:

$$C_m = \frac{(d_{DBS} + 2 \cdot d_{SO_4}) \cdot F}{\Delta E \cdot (M_{Py} + d_{DBS} \cdot M_{DBS} + d_{SO_4} \cdot M_{SO_4})}, \quad (2.25)$$

where  $d_{DBS}$  is the doping level from DBS<sup>-</sup> anions,  $d_{SO_4}$  is the doping level from SO<sub>4</sub><sup>2-</sup> anions,  $M_{Py}$  is the molar mass of PPy repeating unit,  $M_{DBS}$  is the molar mass of DBS<sup>-</sup> anion,  $M_{SO_4}$  is the molar mass of SO<sub>4</sub><sup>2-</sup> anion,  $\Delta E$  is the potential window and  $F$  is the Faraday constant. The specific (gravimetric) energy density was calculated as:

$$E_m = \frac{C_m \cdot \Delta E^2}{2}, \quad (2.26)$$

where  $E_m$  is the specific (gravimetric) energy density and  $\Delta E$  is the charge-discharge potential window. The specific (gravimetric) power density was calculated as:

$$P_m = \frac{E_m}{\Delta t}, \quad (2.27)$$

where  $P_m$  is the specific (gravimetric) power density and  $\Delta t$  is the charge-discharge duration.

### **2.3.5 Electro-chemo-mechanical deformation measurements**

In the current work, actuators were characterized for comparison with the most similar actuators, reported in literature. For all types of characterization experiments (step response, frequency response of the strain difference and blocking force) and different electrolytes, different actuators were used for minimizing the impact of the previous measurements.

#### **2.3.5.1 Identification of the moving ions**

The identity of the moving ions was assessed using the ECMD strain measurements. The dominant mobile ion was identified by the sign of the strain (or strain difference). CP expansion on oxidation referred to anion-dominated ion transport and expansion on reduction was interpreted as cation-dominated ion transport. The mobility of various ionic species was studied using ECMD response in course of CV experiments as well as by strain difference response to potential steps.

#### **2.3.5.2 Strain, strain difference and blocking force measurement**

Strain and strain difference were measured in order to characterize the actuation properties of the actuators as well as for the determination of the ion mobility type (anion or cation) based on Eq. (1.6).

Bending actuators, used in this work, can achieve high curvature values, at which the actuators curl up and the largest displacement values do not correspond to the largest values of the consumed charge. Therefore, strain difference, instead of tip displacement was chosen for actuator characterization. Strain difference was calculated from the displacement, measured near the clamped end of the actuator. Strain difference under few assumptions

unambiguously determines the actuator's position and shape at every given moment. Equations in Appendix 5 were used for planning ECMD experiments with bending actuators. Based on the expected maximum strain difference  $\varepsilon_{\max}$  and actuator's thickness  $w$ , the measurement distance  $L_m$  and the free length  $L$  were in Eq. (1.25) chosen so that laser points at the actuator as far as possible from the clamped end (to reduce measurement error). At the same time, the free length of the actuator and the measurement distance were chosen to be small enough to avoid the actuator from shading the laser or bending away from the intersection with the laser beam. The maximum measurement distance and the maximum free length were calculated from equations (8.6) and (8.5), respectively:

$$\max(L_m) = \frac{w}{\varepsilon_{\max}}, \text{ and} \quad (2.28)$$

$$L_{\max} = \max(L_m) \cdot \frac{\pi}{2}. \quad (2.29)$$

The displacement for the strain difference calculation was measured typically at 5 mm distance (adjusted using a XY-micrometer stage) from the clamped end of the actuator and at 3 mm for the high curvature values.

Equations (1.17) and (1.25) were used for the calculation of strain (relative change in thickness or relative linear length change of tri-layer actuator) and strain difference (bending actuators, see also **Figure 1.18**), respectively. The thickness of the actuators for strain difference calculations was measured with a micrometer after swelling in electrolyte.

Blocking force was typically measured at 5 mm distance from the clamped end of the actuator.

### 2.3.5.3 Step response, frequency response of strain difference, strain difference rate and blocking force

Actuators' response to step voltage was measured as an average of four voltage steps in alternating direction at step voltages 0 V ... 1 V with 0.1 V intervals. Displacement for strain difference calculation according to Eq. (1.25) was measured relatively to the actuators' position in the beginning of every step (**Figure 3.13a**).

For frequency response measurements, the mirrored logarithmic sweep sine (0.001 ... 65 Hz, 0.8 V, duration 524 s, **Figure 3.14a**) signal was applied to the actuators and the response of strain difference or blocking force was recorded. Frequency response was calculated as the Fourier transform of the strain difference response, divided frequency-wise by the Fourier transform of the applied voltage, and the results were presented in units of % V<sup>-1</sup> (for strain

difference, calculated from displacement according to Eq. (1.25)) or  $\text{mN V}^{-1}$  (for blocking force).

For cyclically moving bending actuators, strain difference rate was calculated as the average over a full bending cycle (full cycle of applied potential):

$$\varepsilon_r = 4 \cdot \varepsilon \cdot f, \quad (2.30)$$

where  $\varepsilon$  is the strain difference,  $f$  is the frequency of the applied potential, and the constant 4 is the number of movements (passages) between the neutral and the utter position during the full cycle of the actuation (and applied potential).

Blocking force was measured analogously to frequency response of strain difference with actuators blocked at 5 mm distance from the clamped end.

### **2.3.6 Density, specific surface area and pore distribution of aerogels**

The densities of the aerogels were estimated on basis of the volume of the extraction basket and the measured weight of the aerogel. Semi-theoretical densities of the aerogels were estimated using the doping levels measured using EDX and assuming that the polymerization yield is limited by the available oxidant only. Since molar concentrations of pyrrole and the oxidant are equal, then the number of polymerized Py units is less than the number of the available monomer (subtraction in (2.31) first brackets) units by the number of electrons, spent for doping of the hydrogel, divided by two (for every two electrons, spent for doping, one monomer unit remains unpolymerized). Therefore, semi-theoretical density is:

$$\rho = C_{\text{Py}} \cdot \left[ 1 - \frac{d_{\text{DBS}^-} + 2 \cdot d_{\text{SO}_4^{2-}}}{2} \right] \cdot (M_{\text{Py}} - 2 \cdot M_{\text{H}} + M_{\text{DBS}^-} \cdot d_{\text{DBS}^-} + M_{\text{SO}_4^{2-}} \cdot d_{\text{SO}_4^{2-}}), \quad (2.31)$$

where  $\rho$  is the density of aerogel,  $C_{\text{Py}}$  is the Py concentration,  $d_{\text{DBS}^-}$  and  $d_{\text{SO}_4^{2-}}$  are the  $\text{DBS}^-$  and  $\text{SO}_4^{2-}$  analytical doping levels, and  $M_{\text{Py}}$ ,  $M_{\text{H}}$ ,  $M_{\text{DBS}^-}$ ,  $M_{\text{SO}_4^{2-}}$  are the molar masses of Py, hydrogen,  $\text{DBS}^-$  and  $\text{SO}_4^{2-}$ , respectively.

The pore size distribution and the specific surface area were characterized using low-temperature  $\text{N}_2$  sorption measurements, conducted at the temperature of boiling nitrogen ( $-195.8 \text{ }^\circ\text{C}$ ) using the ASAP 2020 system (Micromeritics). The specific surface area was calculated using BET [201] and the pore size distribution was obtained using non-local DFT with a slit-shaped pore model [202].

### **2.3.7 Stability assessment**

Stability of the actuators was qualitatively assessed by the reproducibility of the ECMD experiments. In terms of stability regarding delamination, actuators were considered stable if no delamination was observed for any actuators during any characterization experiment in extent of at least several thousand actuation cycles, including large strains and strain differences.

Stability of the actuators, hydrogels and aerogels was not quantitatively measured. Hydrogels were tested against decomposition in respect to the pH, EC cycling and stability in different organic solvents.

## **2.4 Electrochemical modification of hydrogels**

In order to elucidate the feasibility of further functionalization (*e.g.* for ion sensing applications or drug delivery devices), redoping and electrochemical synthesis inside the chemically synthesized hydrogels were conducted.

### **2.4.1 Redoping of hydrogels**

Redoping was conducted either:

- by using CV (50 cycles) for the 0.3 M Py-APS hydrogels in 0.2 M NaBF<sub>4</sub> and 0.2 M LiClO<sub>4</sub> aqueous electrolytes ( $E = 0.4 \dots -0.85 \dots 0.4$  V) and 0.2 M Py-APS in 1 M H<sub>2</sub>SO<sub>4</sub> electrolyte ( $E = 0.4 \dots -0.3 \dots 0.4$  V) at scan rate 0.25 mV s<sup>-1</sup>;
- under diffusion control by long-term immersing of hydrogel electrodes in electrolytes, containing the target anion and by replacing the electrolyte several times.

### **2.4.2 Electrochemical synthesis inside of the hydrogel**

Electrochemical synthesis was conducted in a 0.15 M Py-APS hydrogel after exchanging water for 0.2 M LiClO<sub>4</sub> solution in MEG (several exchange cycles). CV measurements were carried out before adding Py into solution (0.2 M regarding to final concentration). After Py diffusion of Py into hydrogel, the solution was exchanged for a solution without monomer; the Py, remaining in hydrogel was partially polymerized with charge 2 C (charge density 0.11 C cm<sup>-2</sup> regarding the top surface area of the electrode). The solution was replaced several times (0.2 M LiClO<sub>4</sub> in MEG without monomer) after deposition and before repeating the CV measurements in order to remove the remaining monomer from the hydrogel. Diffusion progress was monitored by the change of the open circuit potential.

## 3 RESULTS AND DISCUSSION

### 3.1 Layered conducting polymer actuators

#### 3.1.1 Membranes and substrates characterization

The ionic conductivities were measured for MPD membrane (**Figure 3.1a**), permeated with 1 M LiTFSI or EMImTFSI. The measured ionic conductivity values were  $5.37 \cdot 10^{-4}$  and  $7.83 \cdot 10^{-4}$  S cm<sup>-1</sup>, respectively. The tortuosity of the membrane was calculated using the ionic conductivities for pure 1 M LiTFSI ( $5 \cdot 10^{-3}$  S cm<sup>-1</sup>, [203]) and EMImTFSI ( $7.69 \cdot 10^{-3}$  S cm<sup>-1</sup>, [204]) in Eq. (2.6). The measured tortuosity  $2.59 \pm 0.05$  is lower than that of typical nanoporous SPEs (3.2 ... 3.7, [197]). The lower tortuosity of the commercial membrane looks promising from the perspective of actuation speed, but the limited choice of suitable commercial membranes with different thickness remains a serious disadvantage. Nevertheless, a commercial membrane is preferred, if the main goal is the characterization of CP electrodes and only reproducible characteristics are expected from the membrane.

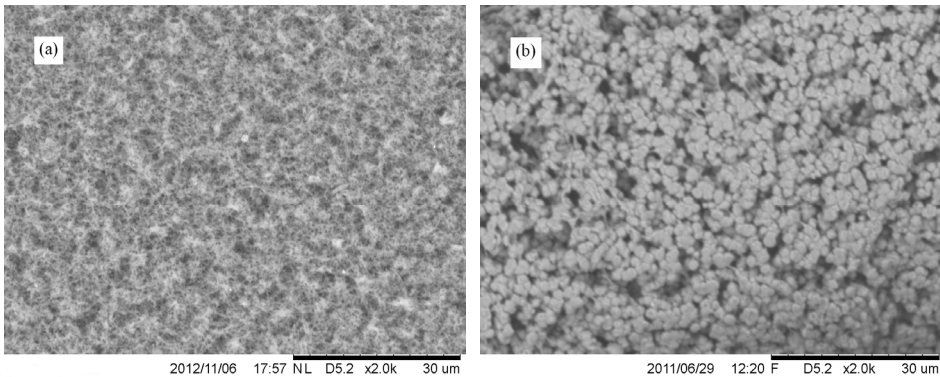


**Figure 3.1.** SEM images of the membranes: a) MPD; b) IH SPE membrane.

For linear electrolyte-operated actuators, two polymeric membrane types were chosen – MPD and CS. These two membranes have distinctively different properties, allowing the qualitative comparison of different circumstances. Neither PVdF nor CS are known to be highly stretchable. In addition, they are not used in role of ion reservoir and CS has to be prepared in a special way (as SPE) to be useful as an ion reservoir. However, for different applications, also different mechanical properties are required. In the current work, two different passive middle layers with different elasticity and structure (homogeneous *vs.* porous) were chosen to find qualitative differences depending on the passive layer properties.



While out of scope of the present study, the properties of both PVdF and CS films (including elasticity) can be tuned in a very broad range (*e.g.* [205] for CS and [127, 197] for PVdF) to meet the requirements of specific applications.

### **3.1.2 Chemical synthesis**

The goal of the chemical step is to obtain adhesion of the conducting polymer layer to the membrane and to create a conductive surface. Chemical synthesis was conducted concurrently for both membrane sides and the deposition conditions for both, PPy and PEDOT were optimized to comply with the following requirements:

1. CP layer had to be conductive enough for the initial step of the following EC synthesis;
2. CP layer had to have negligible pseudo capacitance, compared to the EC deposited layer to avoid influence on the characterization of the prepared actuator;
3. CP synthesis time and rate had to be short enough to prevent the appearance of short circuits between the membrane sides.

All methods, described in the experimental part resulted in adhere CP layers, conductive enough for the following EC synthesis. Four types of membranes were used: commercial hydrophobic MPI, hydrophilic MPD (**Figure 3.1a**), IH SPE (**Figure 3.1b**) and CS film. For the synthesis of PPy on porous and hydrophobic commercial MPI PVdF membrane, different methods were tried. Although both vapor phase synthesis methods gave satisfactory results, in practice it was more convenient to synthesize in the aqueous solution despite the possibility of short circuit development, which became the main concern for the aqueous chemical synthesis. SEM micrographs of the membranes with chemically synthesized PPy/DBS and PEDOT/Cl electrodes are depicted in **Figure 3.1**.

Synthesis conditions were optimized for both types of the commercial PVdF membranes and for both monomers due to different pore size and hydrophobicity/hydrophilicity, and elevated temperatures (60 ... 70 °C) were chosen despite the lower conjugation length, in order to increase the polymerization rate, and hence, to reduce the synthesis time. At longer synthesis durations, short circuits between the membrane sides appeared. While CP polymerized mostly in the outer layers of the membrane, due to the uneven tortuosity, there were still pores having lower tortuosity, and with longer synthesis times, the appearing short circuits were presumably caused by the oxidant penetrating too deep through the less tortuous paths between the two sides of the membrane. From the cross-sections of the membranes, it was seen that those short circuits were occasional, localized and always perpendicular to the membrane surface. The appearance of short circuits was more probable in the case of the Py monomer because of its lower viscosity and higher solubility

in water. Such deeper penetration of CP into the membrane was rare (the vast majority of membranes did not have short circuits at all), easily detectable with an ohmmeter, and were avoided when cutting the electropolymerized film into actuator strips by cutting out, and did not influence the properties of the remaining material. The polymerization took place simultaneously in solution (solution become gray) and on the surface of the membrane, assisted most probably by the adsorption of the monomer on the hydrophobic membrane (MPI) and additionally by the monomer diffusing out of the membrane pores (MPI and MPD).

IH SPE membrane was cooled down to  $-30\text{ }^{\circ}\text{C}$  before immersion in chemical synthesis solution. The synthesis was carried out at RT and the previous cooling of the membrane was an attempt to prevent the dilution of SPE due to the diffusion of EMImBF<sub>4</sub> out of the membrane. This process step was proven unnecessary with later experiments.

The oxidant concentration 0.1 M in the synthesis solution was initially chosen based on typical values for monovalent oxidants in published works [206, 207], the monomer concentration was based on published stoichiometric molar ratio 1:2.33 between the monomer and the oxidant, assuming expected doping level 0.33. The molar ratio between SDBS and the monomer was chosen 1:3, assuming the same doping level [207]. After several attempts, double-charged SPS and APS were used as oxidants for PPy synthesis instead of the conventional FeCl<sub>3</sub> [208] in order to prevent the formation of insoluble complexes of iron and DBS<sup>-</sup> [185], but based on the satisfactory results, the molar ratios remained unchanged in order to retain similar rate of the synthesis reaction. For later experiments, APS oxidant was used instead of SPS without any influence on the results. For hydrophilic membranes and PEDOT, synthesis conditions were further optimized. In APS solution, EDOT polymerized too slowly, and therefore, 1.5 M FeCl<sub>3</sub> was used instead.

SDBS had several functions. According to Kudoh [75] and Omastova *et al.* [208], an anionic surfactant increases the chemical polymerization yield, the polymerization rate and the conductivity of the resulting polymer, compared to a polymer doped solely with sulfate anions from the peroxydisulfate oxidants. Upon the presence of both anions in the solution, inclusion of DBS<sup>-</sup> as the dopant is preferred [75]. In addition, the SDBS surfactant improved the wetting of the hydrophobic membrane and offered (in conventional stoichiometric ratio 1:3 with monomer, based on expected doping level) the same doping anion, which was planned for the following EC synthesis.

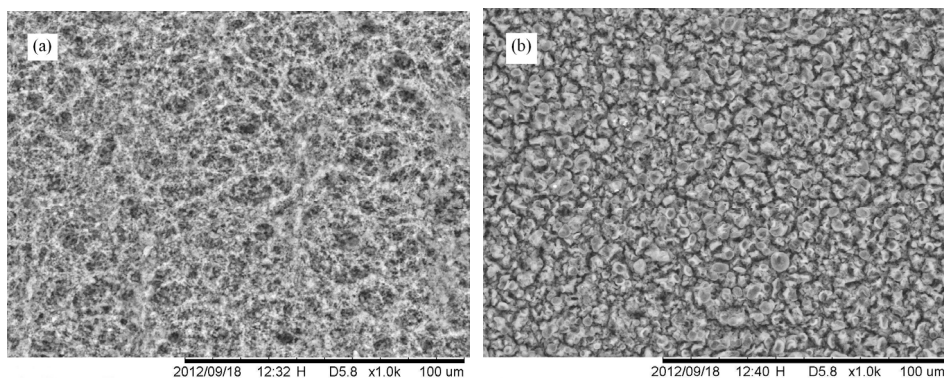


**Figure 3.2.** SEM images of chemically synthesized electrodes on MPD membranes: a) PPy/DBS; b) PEDOT/Cl.

For linear tri-layer actuators, PC solutions were used, because CS decomposes in aqueous oxidant solution and in acidic media. To prevent the decomposition of CS film during the chemical synthesis,  $\text{FeCl}_3$  oxidant solution in PC was used with 4 v.% water to facilitate the wetting of the hydrophilic CS and to facilitate proton transport away from the membrane. However, the depolymerization is a relatively slow process, especially in organic solvents. The following factors in any balance played a role in the chemical synthesis without CS substrate degradation:

1. short duration of synthesis (1 min) and sufficient thickness of CS film;
2. excess of synthesis solution for dilution of  $\text{H}^+$  and diffusion away from the CS film;
3. Continuous decrease of exposed CS film area (the formed PEDOT layer protected CS from further decomposition).

In order to evaluate the interaction between the substrate and the chemically synthesized PEDOT/Cl electrode, FTIR and Raman spectra were examined. The FTIR spectrum of pure PVdF (**Figure 3.3a**) shows characteristic peaks at 1409, 1070, 877, 765 and  $613\text{ cm}^{-1}$ . PEDOT/Cl shows characteristic peaks at 1507, 1084, 960, 835,  $691\text{ cm}^{-1}$ . Most of the PVdF and PEDOT/Cl peaks can be recognized (with some minor shifts) in spectrum of PVdF coated with PEDOT/Cl confirming the presence of both compounds. Characteristic peaks of CS at 3301, 1651, 1559,  $1152\text{ cm}^{-1}$  could also be found on the spectrum of PEDOT/Cl on CS. Nevertheless, the N-amide double peak (1651 and  $1559\text{ cm}^{-1}$ ) is missing and additional peaks at 1615 and  $1514\text{ cm}^{-1}$  have appeared. These peaks were attributed to the  $\text{NH}_3^+$  band indicating composite formation between CS and PEDOT [209].

The characteristic features in the Raman spectrum (**Figure 3.3b**) suggest lower oxidation state of CS|PEDOT, compared with PVdF|PEDOT (*e.g.* shift of the peak from  $1424$  to  $1420\text{ cm}^{-1}$  for CS|PEDOT).

CS's amino group is a relatively strong base and it is protonated in acidic or even in neutral solutions. Apparition of  $-\text{NH}_3^+$  in the FTIR spectrum of the chemically coated CS suggests that  $-\text{NH}_2^+$  participates in the PEDOT polymerization process as a proton scavenger. The positive charge, evolved during the oxidative polymerization is compensated by  $\text{Cl}^-$  counterions from the oxidant, yielding a neutral polymer. Probably the protonated amine groups are also compensated by  $\text{Cl}^-$ , and one may write the "complex" as  $-\text{NH}_2\cdot\text{HCl}$ . Han *et al.* also claims: "...amine groups ... can effectively interact with the PEDOT backbone through hydrogen bonding" [210]. The interaction between CS and PEDOT decreases the oxidation state of the composite (absence of  $1507\text{ cm}^{-1}$  peak in FTIR spectrum and shift of the  $1424\text{ cm}^{-1}$  peak in Raman spectrum) compared to that of PEDOT on PVdF.

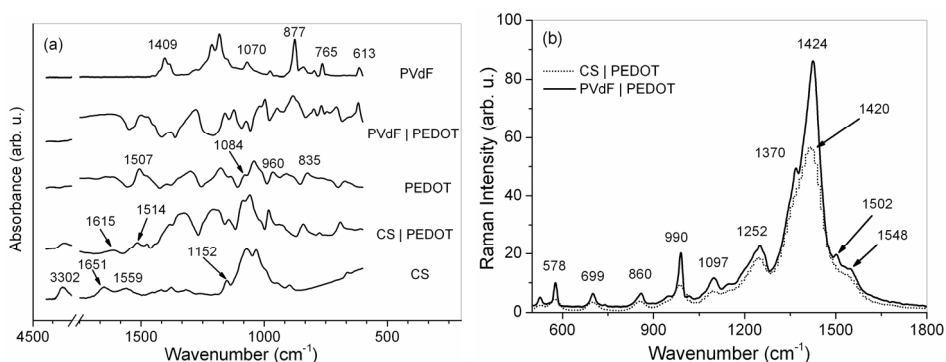


**Figure 3.3.** Chemically synthesized PEDOT on CS and PVdF substrates: a) FTIR spectrum; b) Raman spectrum.

As FTIR and Raman spectra indicated interactions between CS and CP and not between PVdF and CP, one may conclude that two different mechanisms ensure good adhesion – physical grip *vs.* a more complicated chemical adhesion due to composite formation.

### 3.1.3 Electrochemical synthesis

Only a very thin layer of CP was polymerized chemically with most of the CP electrode synthesized EC. The high synthesis temperature of the chemical synthesis and the thin layer of CP yielded high sheet resistance of the EC synthesis substrate. The lowered EC synthesis current reduces the potential drop ( $iR$  drop) between the connected edges and the centre point of the membrane in the EC synthesis cell. From the beginning of the electropolymerization, PPy polymerizes in the oxidized (conductive) form and the conductivity of the membrane surface increases quickly, further lowering the potential difference between the clamped edges and the center of the membrane. The thickness of

the resulting actuator material was measured at different points and no systematic deviations in the thickness were noticed. In addition, in the literature the best mechanical properties, strain and conductivity values have been achieved at low synthesis current densities for more aligned distribution of the polymer chains [109]. At the same time, synthesis current density should be high enough to maintain synthesis potential at level, which keeps pH from dropping too low in the proximity of the electrode and causes formation of soluble trimers and conjugation defects due to acid-catalyzed polymerization ([49, 51], **Figure 1.8c**).

In case of PPy, low synthesis temperatures reduce the number of conjugation defects, cross-links, chain branching, chain termination defects and over-oxidation, resulting in improved mechanical properties (elasticity) and higher conductivity. For both, PPy and PEDOT, lowered temperatures were supposed to result better chain alignment. Therefore, low current densities ( $0.1 \text{ mA cm}^{-2}$ ) and low temperatures were chosen for the EC synthesis. At lowered synthesis temperatures and galvanostatic regime, low diffusion speed causes higher voltage between the anode and the cathode. The voltage increase could be lowered by increased concentrations and lower current density. The galvanostatic (constant current) deposition regime was chosen because the different oxidation potentials of Py and EDOT. In addition, deposition kinetics and total synthesis charge are more controllable and can be equalized to get comparable results for PPy and PEDOT. According to equations (2.8) and (2.9), the molar amount of the polymer is proportional to the synthesis charge and therefore, at fixed current density the total amount of the polymer can be controlled by synthesis time. The chronopotentiometry technique was used to monitor the potential during the EC synthesis. SEM micrographs with EC synthesized working layers are depicted in **Figure 3.4**. The surface morphology was found to be almost independent of the membrane type and the CP used for the chemically synthesized electrode layers. The morphology was qualitatively different for PPy and PEDOT and somewhat more rough for the EC synthesized PPy/DBS, compared to PPy/TFSI. SEM images of cross sections suggested that the physical grip with membrane surface was the main reason for good adhesion on PVdF-based membranes.

### 3.1.3.1 Electrochemical synthesis of dodecylbenzenesulfonate doped conducting polymers

Usually, low-temperature EC synthesis has been used in combination with low melting point polar organic solvents, and for the synthesis in aqueous solutions (often forced by the solubility of the salt of the electrolyte, containing the chosen dopant anion) temperatures above the water melting point has been used. In the current work, the low melting point (in the range that of organic solvents) for the synthesis using water-soluble electrolyte salts (*e.g.* SDBS, sodium polystyrenesulfonate *etc.*) was achieved in the eutectic mix of water and MEG,

having the melting point below  $-50\text{ }^{\circ}\text{C}$ . In addition, MEG is known for its plasticizing properties. The only known attempt to conduct EC synthesis in the mix of water and MEG was done by Diaz *et al.* [56], but not at lowered temperatures and with a different goal to study solvent influence on the mechanical properties of the film. For both PPy/DBS and PEDOT/DBS, to the author's best knowledge, only aqueous synthesis above  $0\text{ }^{\circ}\text{C}$  has been used [160, 161]. DBS<sup>-</sup> as a doping anion was chosen for the elasticity and good actuation properties achieved for PPy actuators [211, 212]. The relatively large and therefore immobile DBS<sup>-</sup> doping anion usually enforces cation motion and was supposed (upon oxidation) to recover the conductivity quickly after the reduction half-cycle. The solubility of the EDOT monomer in water is low. According to Sakmeche *et al.* [65, 213] and Heinze *et al.* [15] surfactants (especially anionic) can increase EDOT solubility in water several times, decrease the oxidation potential ( $0.76 \dots 0.78\text{ V vs. SCE}$  in micellar medium [213]) and increase the deposition rate.  $0.2\text{ M}$  EDOT,  $0.2\text{ M}$  SDBS microemulsion in mix of water and MEG retained clear appearance at temperature  $-25\text{ }^{\circ}\text{C}$ .

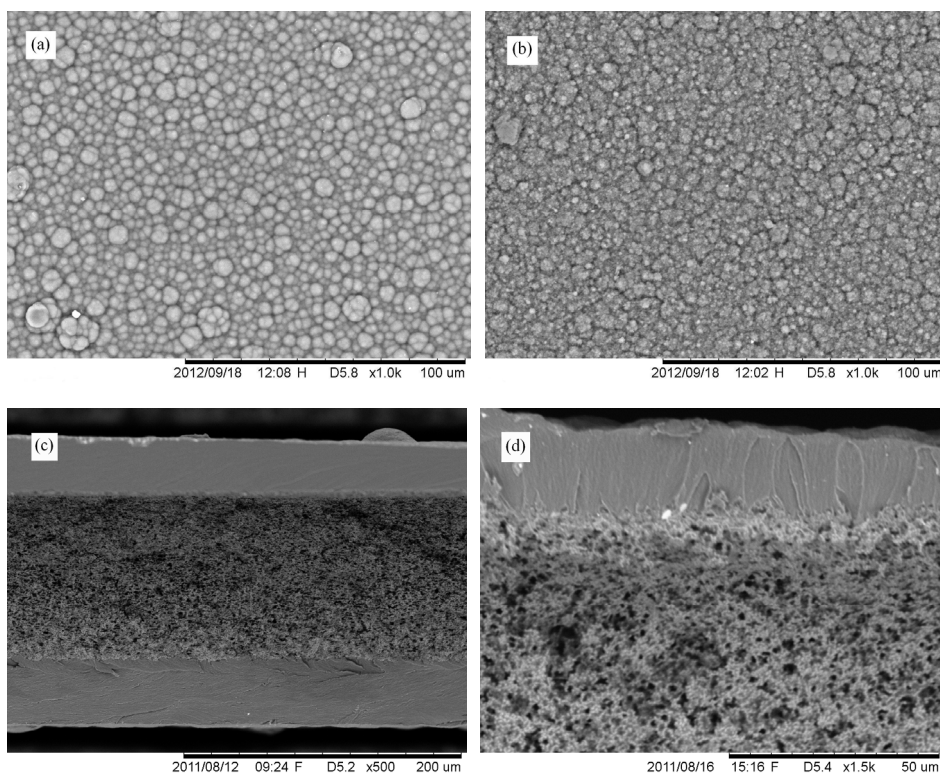


**Figure 3.4.** EC synthesized electrodes and the final structure of the actuators: a) surface morphology of PPy|PPy/TFSI film; b) surface morphology of PEDOT|PEDOT/TFSI film; c) cross-section of PPy|PPy/DBS film on MPI membrane (MPI-immersion); d) interface between IH SPE membrane and PPy|PPy/DBS film (IH-immersion).

### 3.1.3.2 Electrochemical synthesis of bis(trifluoromethanesulfonyl)imide doped conducting polymers

With the exception of the PPy substrate, the synthesis potentials (**Figure 3.5**) are generally higher for the PEDOT EC layer, which can be explained by the higher oxidation potential of EDOT. There was a strong correlation between the synthesis potentials and the effective conductivities (**Table 3.2**) for the same EC synthesized CPs. The shapes, the order of the potential levels and the development of the potential plateau in the chronopotentiograms suggested that the voltage between anode and cathode consists of three components:

1.  $iR$  drop in solution (depends on concentrations and temperature);
2. oxidation potential of the monomer at electrode interface (approximately constant at galvanostatic conditions, low current density and for the same monomer and electrolyte);
3.  $iR$  drop at apparent sheet resistance of already formed polymer (approximately constant and independent from thickness of the film for thick and homogeneous polymer, and depends on sheet resistance of resulting polymer).

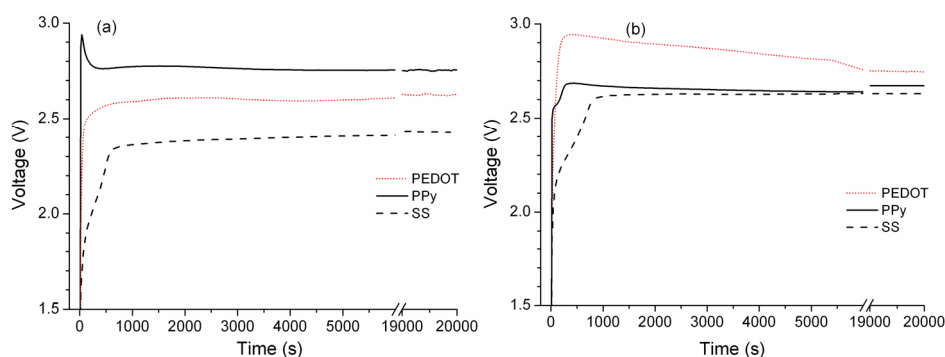


**Figure 3.5.** Chronopotentiograms: a) TFSI-doped PPy; b) PEDOT, synthesis on PEDOT, PPy and SS substrates, respectively.

Considering the influence of the aforementioned three components suggests that the slopes at the beginning of SS substrate synthesis were caused by the decreasing influence of the more conductive substrate to the apparent sheet resistance of the forming polymer. In case of the synthesis of PPy on the PPy chemically synthesized PPy layer, an induction (monomer oxidation and oligomerization) step is clearly visible. Appearance of the peak could be attributed to the hydrophilicity of the substrate, which prevents the formation of an adsorbed Py monomer layer. In principle, all three potential components can be separately quantified, using potential dependence on sheet resistance of the resulting film and potential dependence on current density.

The chemical-EC synthesis method, applied to porous membranes also proved to be beneficial for the EC deposition of large freestanding films. For some synthesis conditions, such as 0.2 M PPy, 0.2 M LiTFSI with 2 v.% H<sub>2</sub>O in PC at low temperatures, large internal strain (*ca.* 10%) evolves during the EC synthesis, curling the resulting film and peeling it off from the traditional metal electrodes or any other smooth substrate with insufficient grip. Locally peeled-off film loses proper contact with the anode, resulting in uneven deposition due to the large curves leading to the uneven distance between the CP film and the cathode inside the narrow (and hence economical) EC synthesis cells. The result is an uneven, rough and fragile film, tending to break on removal. A porous substrate ensures good grip even at high internal stresses. Some limited curling may occur, but without sharp transitions and peeled off areas. Free-standing films can be obtained after dissolving the membrane substrate. The same results can be achieved with membranes sputter coated with gold, but the drawback is the cumbersome technique, and the remaining gold layer, distorting the conductive properties of the freestanding film significantly more than the chemically synthesized electrode layer.

### **3.1.4 Actuator preparation and structure**

A variety of chemical synthesis methods, conditions, different substrates and combinations of CP materials of the chemically and EC synthesized layers were used for actuator preparation.

The active layer of the EC synthesized actuator material is generally anisotropic and useful (and measureable) strain changes along the actuator are accompanied with the change in the thickness of the CP layer. Therefore, the strain difference between the widths of both sides of the actuator, can cause curling along the actuator and increase rigidity working against the bending movement. In order to keep the conditions similar to those reported in literature, actuator width was chosen in accordance with Minato *et al.* [149] not to exceed 4 mm.

The influence of the chemically synthesized electrode layer on the structure was compared for actuators with the TFSI-doped EC layer. SEM images and EDX sulfur mappings of cross-sections of actuators with different polymers for chemically and EC synthesized layers are presented in **Figure 3.6** (adapted from Figure 4 of paper **II**).



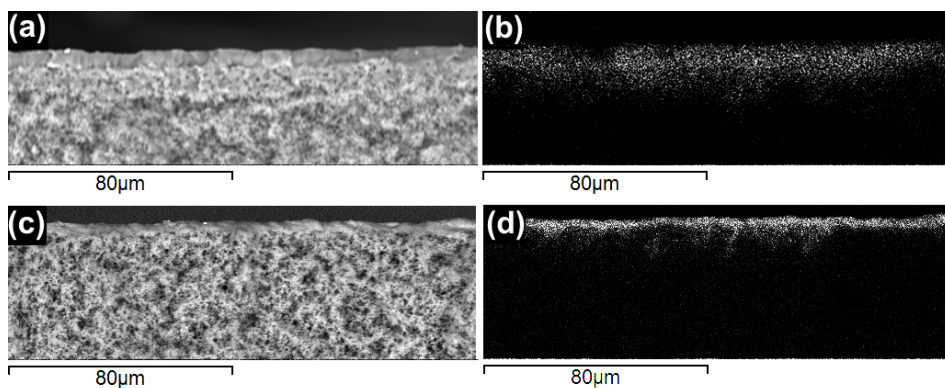


**Figure 3.6.** SEM micrographs (a, c) and EDX sulfur mappings (b, d) of actuators with different CP for chemical and EC layer: a), b) PEDOT|PPy; c), d) PPY|PEDOT (adapted from Figure 4 of paper II).

The rough morphology of the thin chemically deposited electrode layer was inherited from the porous surface of PVdF membrane (**Figure 3.1**). The chemical PPy layer appears to be uniform and denser than the PEDOT chemical layer. Considering the negligible thickness change after the chemical synthesis step one may conclude that the chemically synthesized electrode layer remained mostly inside of the pores of the membrane outer layer. The thickness increase after the EC synthesis (Table 3 in paper II) reveals that in case of the chemically synthesized PEDOT electrode, the electropolymerization occurs mostly in the outer layers of the membrane (total thickness increase 7 ... 8  $\mu\text{m}$ ) and in case of chemically synthesized PPy electrode, mostly on top of the membrane (thickness increase 20 ... 27  $\mu\text{m}$ ). The same conclusions can be drawn from the SEM images and the EDX sulfur mappings of the cross-sections (**Figure 3.6**). The difference in the structure could be attributed to the higher viscosity and lower solubility of EDOT in water. During the chemical polymerization, Py diffuses out of the membrane pores and PPy forms on the membrane from the solution, while EDOT rather polymerizes in the pores of the outer layer of the membrane, blocking the oxidant from the deeper penetration into pores. This reasoning is supported by the observation that in case of chemically polymerized EDOT, short circuits between electrodes were developed less often. The different synthesis depth of the chemically synthesized electrodes influences also the EC synthesis step. Actuators with chemically synthesized PEDOT electrodes were thinner than the ones with PPy electrodes, regardless of the EC synthesized CP. The two different structure-forming pathways, depending on the identity of the CP of the chemically synthesized electrode layer are summarized in **Figure 3.7** (Figure 5 of paper II).

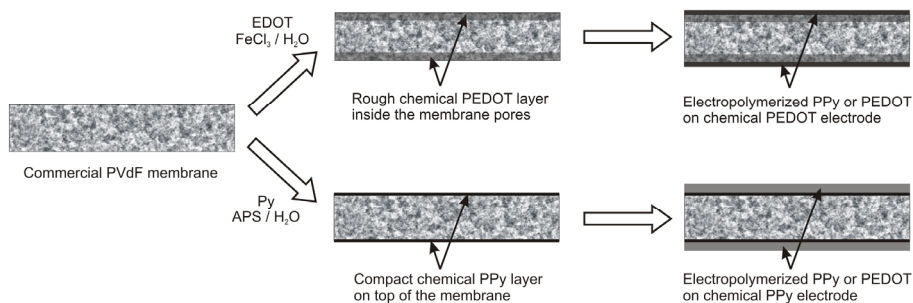


**Figure 3.7.** Structure-forming pathways depending on the choice of monomer for the chemical synthesis of electrode layers (Figure 5 of paper II).

### 3.1.5 Conductivity and doping level

#### 3.1.5.1 Chemically synthesized substrate

By using the aforementioned synthesis methods, it was difficult to measure the conductivity of the chemically synthesized electrode layer, because the thickness and the exact geometry of the deposited layer were unknown due to the porosity and the poor reproducibility of the chemical synthesis in general. In addition, chemical synthesis using different methods and different monomers gave very different morphologies. The chemical polymerization of Py in aqueous peroxydisulfate acid solution was used for first time in 1973 (even before the official discovery of CPs in 1977) with the reported conductivity of  $7 \text{ S cm}^{-1}$  [214]. The conductivity achieved in this work was probably lower than that, due to the elevated synthesis temperature, causing a less ordered structure and more conjugation defects.

**Table 3.1.** Sheet resistances of the chemically synthesized electrodes

Sample (CP)	Sheet resistance ( $\text{k}\Omega/\text{sq.}$ )
MPI-immersion (MPI PPy/DBS)	1.35
MPI-vapor (MPI PPy/DBS)	1.14
IH-immersion (SPE PPy/DBS)	3.6
Sample A (MPD PEDOT/Cl)	$4.0 \pm 0.6$
Sample B (CS PEDOT/Cl)	$165 \pm 15$

As one may notice, the sheet resistance of the sample IH-immersion, prepared at room temperature for 200 s was higher than that of MPI-immersion at  $70 \text{ }^\circ\text{C}$  for the same oxidant and dopant ion. This behavior was most probably caused by the lower monomer concentration and shallow polymerization depth due to

the narrower pores compared to the MPI-immersion sample, where the pores were initially filled with the monomer. The high sheet resistance of Sample B, as compared to Sample A was explained by the formation of a composite between CS and PEDOT, the lower oxidation level and the shorter conjugation length. This conclusion was supported by FTIR and Raman analysis and the comparison of oxidation/reduction charge densities ( $24/38$  and  $40/60$   $\text{mC cm}^{-2}$ , for Sample A and Sample B, respectively), which were higher for Sample B (III).

Despite the inherent disadvantages of the chemical synthesis, the immersion method turned out to be the most reproducible for actuator preparation, providing good grip, leaving pores of the membrane open, ensuring sufficient conductivity for the EC synthesis, and having negligible influence to the actuator's performance, compared to the EC synthesized working layer.

### 3.1.5.2 Conductivity after electrochemical synthesis and doping level

After EC synthesis, the thickness can be estimated, and based on the smooth surface morphology of the EC synthesized layer, (as seen from SEM images), uniformity of the thickness may be assumed; the measured conductivities ( $20 \pm 2$   $\text{S cm}^{-1}$ ) for MPI-immersion, MPI-vapor and IH-immersion samples did not depend on the chemical synthesis method. For Sample A and Sample B, sheet resistances decreased to  $18.4 \pm 0.2$  and  $45.2 \pm 1.5$   $\Omega/\text{sq.}$ , respectively. The higher sheet resistance for Sample B could be explained by the higher synthesis potential during the EC synthesis, causing shorter conjugation length. The thickness for Sample A and Sample B was estimated using a linear approximation that the synthesis charge density of  $4$   $\text{C cm}^{-2}$  yields a  $25$   $\mu\text{m}$  thick PPy/DBS layer [215], and the corresponding calculated conductivities for Sample A and Sample B were  $21.7$  and  $8.8$   $\text{S cm}^{-1}$ . The measured conductivities (except Sample B) around  $20$   $\text{S cm}^{-1}$  were in good agreement with the conductivity of  $19.8$   $\text{S cm}^{-1}$ , measured by Bay *et al.* [60] at slightly different conditions.

For TFSI<sup>-</sup>-doped actuators, the conductivity calculations were based on the effective thickness, and the calculated effective conductivities together with the conductivities of other samples are summarized in **Table 3.2**.

In case of PPy/DBS samples, the conductivity of the chemically synthesized electrode had only a minor influence on the following EC synthesis and to the conductivity of the final material. Even in case of Sample B (compared to Sample A), the initial 40-fold difference in sheet resistance caused only about 2.5-fold difference in the final conductivity. The situation was different when PPy, PEDOT and their combinations were compared. The results were influenced by two factors: the much higher conductivity of PEDOT (compared to PPy) and the difference in the structure, depending on the CP chosen for the chemical synthesis.

**Table 3.2.** Conductivities of the final EC synthesized materials.

Sample (CP)	Composition	Conductivity (S cm <sup>-1</sup> )
MPI-immersion (PPy/DBS)	PVdF PPy PPy/DBS	20 ± 2
MPI-vapor (PPy/DBS)	PVdF PPy PPy/DBS	20 ± 2
IH-immersion (PPy/DBS)	SPE PPy PPy/DBS	20 ± 2
Sample A (PPy/DBS)	MPD PEDOT PPy/DBS	21.7
Sample B (PPy/DBS)	CS PEDOT PPy/DBS	8.8
PEDOT PEDOT/TFSI	MPD PEDOT PEDOT/TFSI	176.7*
PPy PPy/TFSI	MPD  PPy PPy/TFSI	45.0*
PEDOT PPy/TFSI	MPD  PEDOT PPy/TFSI	65.0*
PPy PEDOT/TFSI	MPD  PPy PEDOT/TFSI	290.8*
PEDOT/TFSI-FS**	PEDOT/TFSI	295.9*
PPy/TFSI-FS**	PPy/TFSI	76.7*

\* Effective conductivity based on effective thickness

\*\* Free-standing films, synthesized on SS electrode

Doping levels are rarely comparable between different literature sources, because the analytical doping level depends on the synthesis conditions and the EC doping level also on film thickness, electrolyte and scan rate. Doping levels were calculated for PPy/DBS films, PPy/TFSI and PEDOT/TFSI films. EC doping level, calculated using Eq. (1.12) for IH-immersion actuator from synthesis charge (4 C cm<sup>-2</sup>) and maximum polarization charges (synthesis charge 4 C cm<sup>-2</sup> and polarization charge 289.3 mC cm<sup>-2</sup> at scan rate 60 mV s<sup>-1</sup>) was 0.16. Average doping level of Sample A and Sample B was 0.17 (synthesis charge 4 C cm<sup>-2</sup> and scan rate 5 mV s<sup>-1</sup>). Similar values ( $\approx 0.15$ , at scan rate 2 mV s<sup>-1</sup>) were obtained by Bay *et al.* [60] for 10  $\mu\text{m}$  thick freestanding PPy film electrode using the same method. Expectedly, Bay *et al.* obtained higher EC doping levels for much thinner EC films ( $\approx 0.22$  for EC doping level of 0.2  $\mu\text{m}$  thick film at scan rate 10 mV s<sup>-1</sup>) and by mass change during synthesis using EQCM method ( $\approx 0.29$ ). Doping levels of EC synthesized TFSI-doped freestanding films, estimated by weights of freestanding films using Eq. (2.10) were 0.2 and 0.21 for PEDOT/TFSI-FS and PPy/TFSI-FS, respectively. A similar EC doping level value (0.2 at scan rate 100 mV s<sup>-1</sup>) was measured by Garcia *et al.* for about ten times thinner PPy/TFSI films, synthesized EC at similar current densities (0.1 ... 0.5 mA cm<sup>-2</sup>) in acetonitrile [216].

### 3.1.6 Electrolytes

The electrolytes were chosen based on previously reported good results of other workers in order to compare the results and to broaden the analysis base. EMImBF<sub>4</sub> with the initial concentration 1.8 M (in PC) was included due to the previously published fabrication method. For commercial membranes, the same electrolyte was chosen for adequate comparison between different membranes. PPy/TFSI actuators in LiTFSI in PC electrolyte are known for the good actuation properties due to the large yet mobile anion [128]. Li<sup>+</sup> ions in PC are coordinated as an average by 4.5 PC molecules [217], and thus, despite the larger crystallographic radius, TFSI<sup>-</sup> is the dominant mobile species. For TFSI<sup>-</sup>-doped anion-active actuators, an electrolyte with the same anion is a reasonable choice. Another widely used electrolyte, the RTIL EMImTFSI, known by stability, high ionic conductivity and low viscosity [218], was chosen due to the added benefit of observing the influence of cation size and the absence of a solvation shell on the actuation properties. A RTIL with negligible vapor pressure was also beneficial for conducting long-term experiments where the influence of solvent evaporation had to be taken into account. The same, LiTFSI in PC electrolyte was used for DBS<sup>-</sup>-doped actuators, expecting that DBS<sup>-</sup> does not become mobile due to its large size. Space filling model images of the used doping- and electrolyte ions are depicted in **Figure 3.8**.

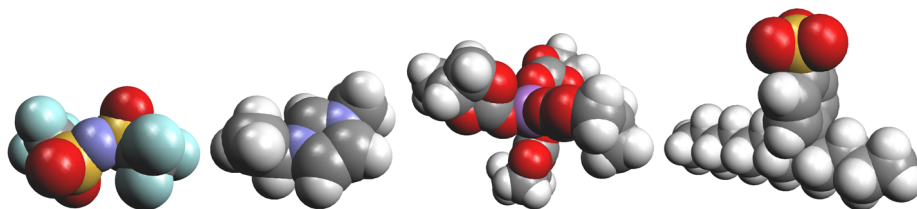


**Figure 3.8.** Images of space-filling models of TFSI<sup>-</sup>, EMIm<sup>+</sup>, Li<sup>+</sup> solvated with four PC molecules, and DBS<sup>-</sup>, respectively.

Electrolyte concentration was chosen to be at least three times higher than the minimum concentration calculated using Eq. (2.4). Such elevated concentrations improve the results for PPy/TFSI actuators, compared with dilute electrolytes (John [219]). Concentrations of 0.1 ... 0.2 M have been often used for PPy/TFSI actuators, synthesized with similar charge density ([157, 195]), but no criterion for minimum concentration has been given.

### 3.1.7 Electrochemical measurements

The most characteristic CVs (in a two-electrode setup and EMImTFSI electrolyte) at two different voltages for PPy|PPy/TFSI and PEDOT|PEDOT/TFSI

actuators are presented in **Figure 3.9**. The figures of the combinations with different CPs for the chemically synthesized layers and for the higher scan rates differed qualitatively very little (except the pseudo capacitance values, which decreased with increasing scan rate) and not shown. At low voltages, the actuators exhibited symmetric EDLC-like behavior. At higher voltages, characteristic redox peaks appeared and for actuators with the EC PPy working layer, irreversible (at given conditions) creep evolves.

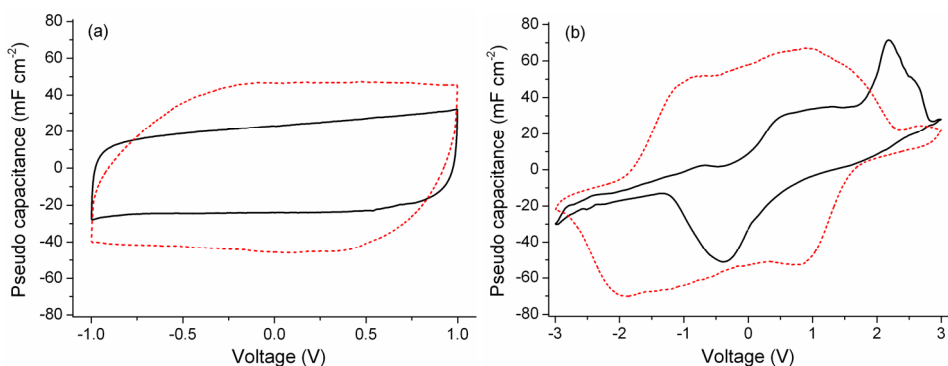


**Figure 3.9.** Results of CV measurements: a) potential range  $\pm 1$  V; b)  $\pm 3$  V (solid black line PPy|PPy and red dashed line PEDOT|PEDOT actuators, respectively, at scan rate  $50 \text{ mV s}^{-1}$ ).

The facts that higher voltages ( $\pm 3$  V) did not cause permanent damage to the actuators, and that the bending creep can be compensated with longer polarization at the opposite voltage suggest that two different structures exist in CPs with different diffusion speed and activation potentials. The more accessible structures exhibit EDLC-like behavior and regions with hindered diffusion show redox peaks, characteristic of Faradaic processes.

From CV experiments at different scan rates (RTIL EMImTFSI electrolyte, concentration 3.89 M) for actuators with different combinations of CP for electrode and working layer, the apparent diffusion coefficients and fractal dimension of the electrolyte-CP interface were calculated from equations (2.5) and (2.7), respectively. The results are summarized in **Table 3.3**.

It can be concluded that interface roughness and mobility of the ions depend mostly on the EC synthesized working layer. The EC PEDOT layer appears to be porous and easily accessible to ions. The EC PPy has lower ionic mobility regardless, whether PPy EC layer is located mostly inside of the membrane (PEDOT|PPy) or on top of the membrane (PPy|PPy). Higher ionic mobility for the PEDOT EC layer also predicts faster response on actuation.

**Table 3.3.** Apparent diffusion coefficients and fractal dimensions of the membrane-CP interface.

Sample (CP)	Apparent diffusion coefficient (cm <sup>2</sup> s <sup>-1</sup> )	Fractal dimension
PEDOT PEDOT/TFSI	1.0 · 10 <sup>-9</sup>	2.98
PPy PPy/TFSI	6.8 · 10 <sup>-10</sup>	2.59
PEDOT PPy/TFSI	5.5 · 10 <sup>-10</sup>	2.61
PPy PEDOT/TFSI	1.6 · 10 <sup>-9</sup>	2.98

It can be concluded that interface roughness and mobility of the ions depend mostly on the EC synthesized working layer. The EC PEDOT layer appears to be porous and easily accessible to ions. The EC PPy has lower ionic mobility regardless, whether PPy EC layer is located mostly inside of the membrane (PEDOT|PPy) or on top of the membrane (PPy|PPy). Higher ionic mobility for the PEDOT EC layer also predicts faster response on actuation.

### 3.1.8 Electro-chemo-mechanical deformation measurements

#### 3.1.8.1 Influence of solvent evaporation and implications to measurement method

Unless a RTIL with negligible vapor pressure is used as the electrolyte, the influence of the electrolyte solvent evaporation must be considered. Frequency response measurements at fixed frequencies are time consuming, and the immersion of the material in the electrolyte in between the measurements at different frequencies causes deviations in the results due to the non-repeatability of the positioning between clamps. In addition, separate measurements at different frequencies constrain the feasible number of measurement points and the resonance frequency identification.

According to relation [220]:

$$\omega = \sqrt{\frac{3 \cdot E \cdot I}{(33/140) \cdot m \cdot L^3}}, \quad (3.1)$$

where  $E \cdot I$  is the structural rigidity,  $m$  is the mass and  $L$  is the length of the beam, the resonance frequency of the bending beam, clamped from one end, depends on the mass and the structural rigidity of the beam. Presumably, both parameters change on solvent evaporation.

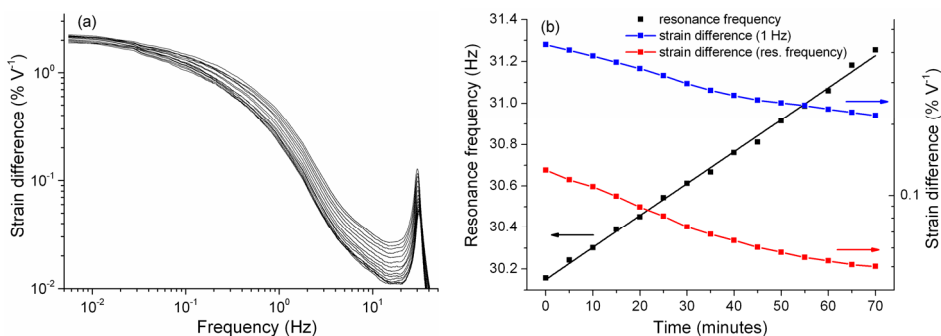


**Figure 3.10.** Effect of electrolyte solvent evaporation: a) frequency response change during drying; b) resonance frequency dependency on measurement time (straight line is linear fit), strain difference change at frequency 1 Hz, and at resonance frequency (PPy/TFSI actuator with 1 M LiTFSI in PC electrolyte).

In order to mitigate the influence of solvent evaporation during the measurements of frequency response, the duration of the measurements was significantly reduced by evaluating the dynamical behavior of the actuator similarly to John *et al.* [219, 221] and Pillai [222]. At low voltages, a linear approximation was applied to the dependence of displacement [219, 221, 223], and blocking force [224] on voltage, allowing the representation and comparison of the measured values in normalized units of  $\% V^{-1}$  and  $mN V^{-1}$ , respectively. The normalized values were obtained from the frequency-wise division of the Fourier transform of the measured response by the Fourier transform of the actuation voltage [219, 221, 222].

PPy and PEDOT actuators are essentially electro-chemo-mechanical ones, working according to equations (1.5), (1.6), (1.18) primarily under charge control through the EC redox reactions. At higher voltages, distinguishable redox peaks appear (**Figure 3.9**), but at low voltages, a CP actuator behaves like an EDLC capacitor (**Figure 3.9a**). According to Madden *et al.*, strain can be considered proportional to the transferred charge at low strain values where creep and back-relaxation are not significant [94], Gaihre *et al.* found that the displacement of TFSI-doped PPy and PEDOT bi-layer actuators increased approximately linearly with voltage up to 1 V in both LiTFSI in PC and EMImTFSI electrolytes [145]. Therefore, under the assumption of proportionality between charge and strain in specific narrow potential ranges, this technique, commonly used for potential-controlled devices, can be used for qualitative and semi-quantitative comparison of CP actuators.

Several types of exciting signals were tried, such as linear sweep sine, logarithmic sweep sine, band-limited white noise, and their combinations, *e.g.* mirrored logarithmic sweep sine and logarithmic sweep sine, modulated with band-limited white noise. Most of the tried signals gave almost identical frequency response graphs, with exception of the linear sweep signal, which had



some random deviations at low frequencies (well observable due to the logarithmic frequency scale) and barely visible beat behavior before and after the resonance frequency. In terms of the coherence value, the best results were achieved with logarithmic signals. Therefore, mirrored logarithmic sweep signals were used and the typical magnitude squared coherence value (**Figure 3.11b**) shows that strain difference is excited by the input signal. Other coherence graphs were very similar, and therefore, not shown.

### 3.1.8.2 Comparison of chemically synthesized electrode layer with sputter coated electrode

Comparison of the actuators with chemically synthesized electrodes with the ones using conventional gold sputter coated electrodes was conducted. Influence of the electrode layer was studied for different PPy and PEDOT combinations and dopant anions (TFSI<sup>-</sup>, DBS<sup>-</sup> and pTS<sup>-</sup>) in 1 M LiTFSI in PC electrolyte. The frequency response of the strain difference is presented in **Figure 3.11** (EC synthesis charge density 2.2 C cm<sup>-2</sup>, current density 0.11 mA cm<sup>-2</sup>).

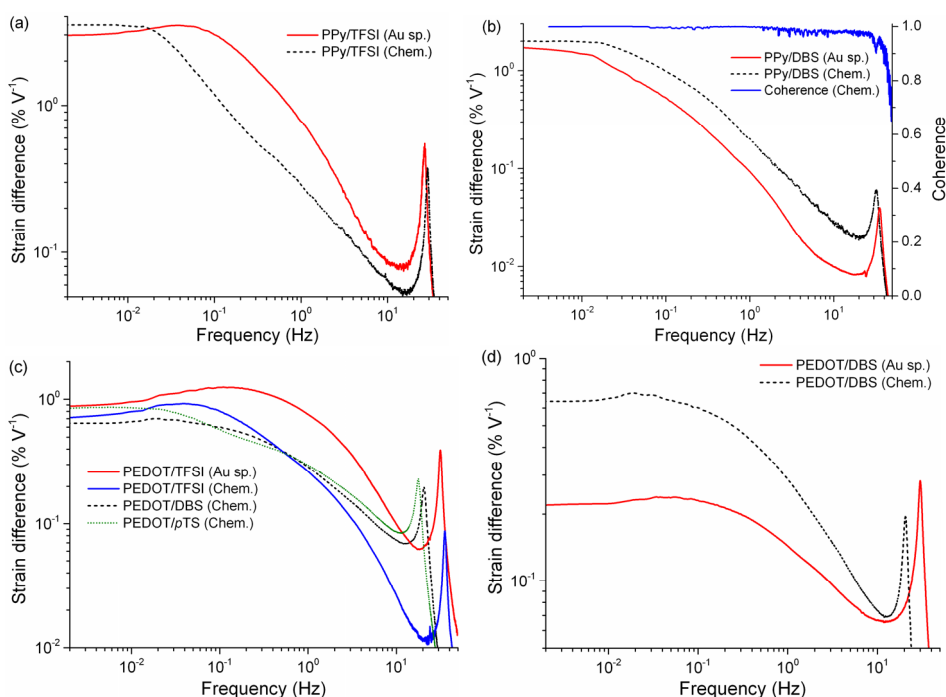


**Figure 3.11.** Frequency response of strain difference depending on electrode layer (sputter coated with 50 nm gold vs. chemically synthesized electrode on MPD membrane): a) PPy/TFSI; b) PPy/DBS and typical coherence function; c) PEDOT/TFSI compared with PEDOT/DBS (chemical) and PEDOT/pTS (chemical); d) PEDOT/DBS.

Comparison of the graphs in **Figure 3.11a, c, d** shows that sputter coated gold electrodes improved the frequency response for PPy and PEDOT in case of the TFSI<sup>-</sup>-doped EC layer. When the EC layer is doped with large (DBS<sup>-</sup>) or medium-sized (*p*TS<sup>-</sup>) anions, the actuators with chemically synthesized electrode layers have higher strain difference (**Figure 3.11b,d**). Despite the large and immobile anions, the actuators with DBS<sup>-</sup> and *p*TS<sup>-</sup>-doped working layers were anion-active. After a few cation-active actuation cycles, the accumulation of cations occurred [34, 196, 225] and the charge compensation mechanism becomes anion active, while the charge of the immobile DBS<sup>-</sup> and *p*TS<sup>-</sup> anions remains compensated by the accumulated cations. While the actuation was in all cases dominated by TFSI<sup>-</sup> motion, the higher performance of actuators with large anions and chemically synthesized under-layer can be explained by their participation in the conductivity recovery after reduction (note also the similar behavior of DBS<sup>-</sup> and *p*TS<sup>-</sup>-doped actuators with chemically synthesized under-layers in **Figure 3.11d**).

### 3.1.8.3 Step response and frequency response of strain difference, strain difference rate and blocking force

Step response and frequency response were compared for all PPy and PEDOT combinations for chemically and EC synthesized layers in two different electrolytes (1 M LiTFSI in PC and the RTIL EMImTFSI). For the same electrolyte, the qualitative behavior was influenced mostly by the EC deposited working layer and the electrolyte. Combinations of two different CPs had only minor differences compared with the responses of actuators with the same CP for both layers. Characteristic results are presented in **Figure 3.12**.

As expected, the best actuation strain differences were achieved for PPy/TFSI actuators with 1 M LiTFSI in PC electrolyte (**Figure 3.12a**). A characteristic feature is the creep, developing at voltages over 0.8 V. PEDOT/TFSI actuators (**Figure 3.12b**) exhibited fast response, overshoot phenomena at lower voltages (absent for PPy|PEDOT/TFSI actuators) and the absence of creep behavior. In PC solution, Li<sup>+</sup> ions are solvated with PC molecules (**Figure 3.8c**) and due to smaller size the TFSI<sup>-</sup> (**Figure 3.8a**) anion becomes the most mobile ion, resulting in anion-active actuation. In case of the RTIL EMImTFSI electrolyte, EMIm<sup>+</sup> (**Figure 3.8a**) cation and TFSI<sup>-</sup> anion have similar sizes and mixed-type ion mobility could be observed. Again, PEDOT/TFSI actuators respond faster and after the initial cation-dominated movement, anion-activity becomes dominating.

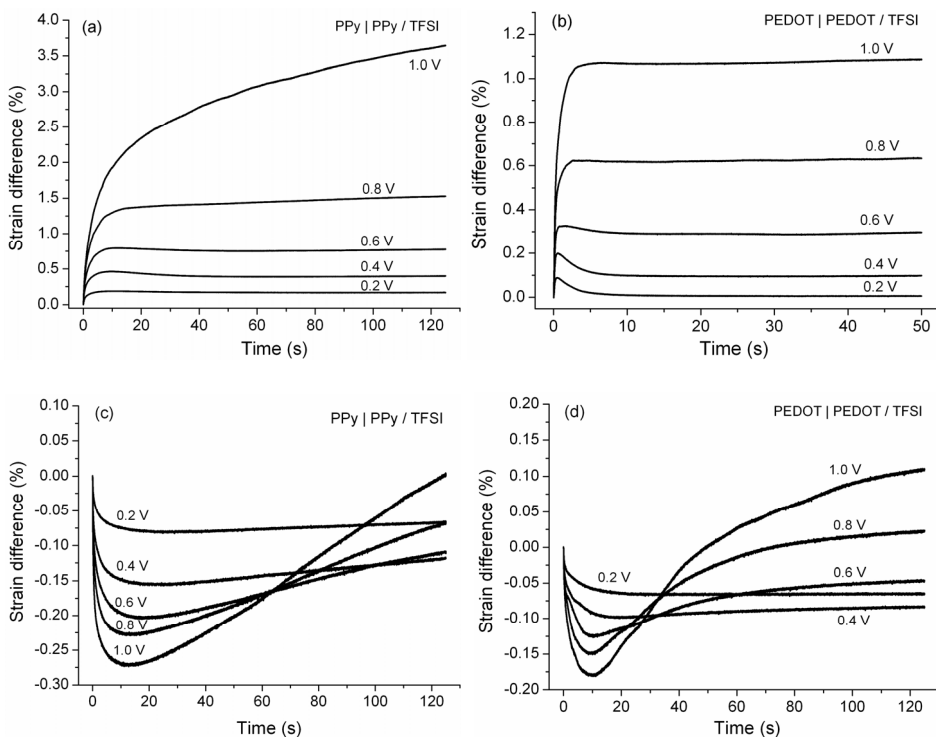


**Figure 3.12.** Step responses of PPy|PPy/TFSI (a, c) and PEDOT|PEDOT/TFSI (b, d) in 1 M LiTFSI in PC (a, b) and in RTIL EMImTFSI (c, d) (adapted from Figure 11 of paper II).

Detailed observation of PPy/TFSI actuators' response (**Figure 3.13**) shows that strain difference follows charge evolution in both voltage ranges, EDLC-like behavior range and Faradaic behavior range and creep behavior is reversible. After the second step, the position corresponding to voltage 0 V recovers close to its initial position. Therefore, actuation at higher voltages can be considered as actuation at a slower rate, the rate is even slower for the relaxation at voltage 0 V. This sharp voltage dependent transition from one actuation mode to another indicates the presence of two different structures or processes in PPy with different ionic mobility, going beyond the assumptions used in the current work, but limiting for PPy voltage ranges, available for comparison. The presence of two different processes with different ionic mobility in the EC polymerized PPy has been suggested by several authors. For example, Pei and Inganäs attributed the slower process (for cation-mobile film, [34]) with weaker dependence on film's thickness to phase relaxation of PPy layers and considered the faster, more thickness-dependent process as diffusion-controlled.

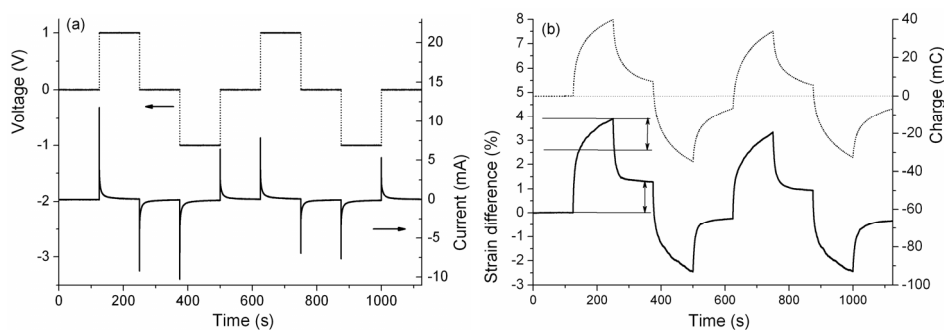


**Figure 3.13.** Step response measurements protocol and example response: a) actuating voltage and current response; b) strain difference and charge responses of PPy/TFSI actuator (adapted from Figure 10 of paper II).

For comparison with other sources, the frequency responses of the strain difference, strain difference rate and blocking force are shown only for the measurements in 1 M LiTFSI in PC electrolyte (**Figure 3.14a–c**).

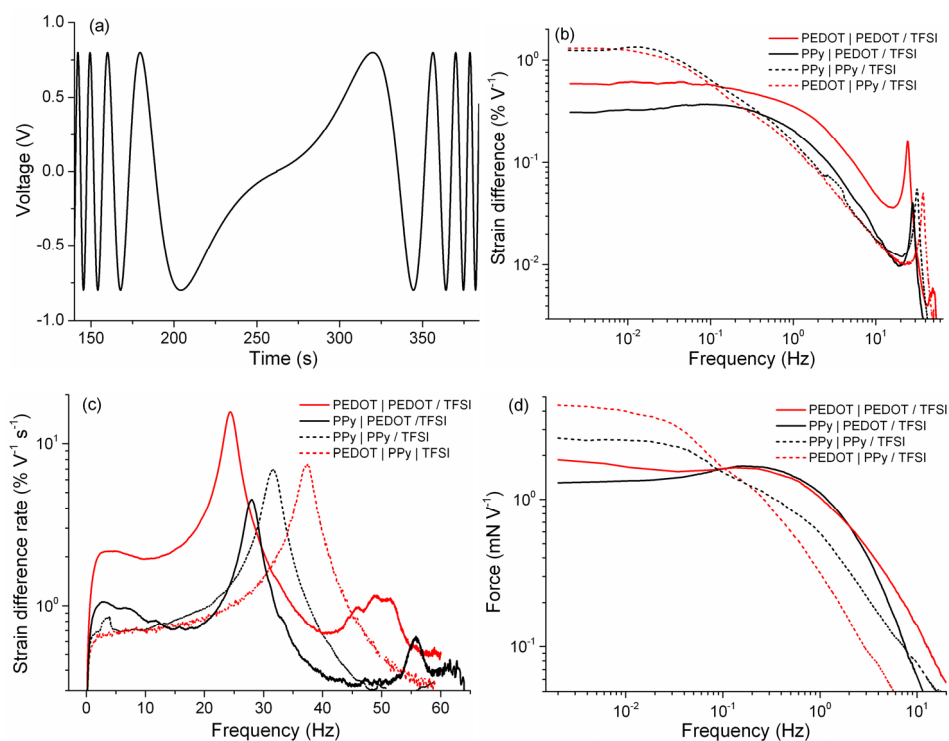


**Figure 3.14.** Results of frequency response measurements: a) middle part (mirrored regarding to polarity and sweep direction at 262 s) of the input signal with total length 524 s; b) strain difference; c) strain difference rate; d) blocking force (Figures b–c adapted from Figure 12 of paper II).

The frequency response of strain difference (**Figure 3.14b**) of the actuators with the PEDOT working layer generally exhibit lower strain difference and higher bandwidth. Despite that, the lack of the creep behavior allows actuating at higher voltages without suffering from creep. The frequency response of the strain difference rate (**Figure 3.14c**) also demonstrated higher strain difference rates and lower flexural rigidity (resonance frequency shift toward lower frequencies) for actuators with PEDOT working layer allowing the observation of the 2<sup>nd</sup> harmonic of the resonance frequency. Except for the absence of resonance behavior, the frequency response of the blocking force (**Figure 3.14d**) qualitatively follows the strain difference graph. A preliminary qualitative implication would be that internal stress, generated by ion flux, mostly determines the bending ability of the actuators. For conclusive analysis, models that are more sophisticated should be used, considering also the charge to strain ratio dependence on the strain difference, actuator's rigidity dependence on strain difference, *etc.*

Strain difference (and therefore the strain difference rate, ignoring values measured at resonance conditions) is more difficult to compare with the results of other workers. Usually just the best values are reported for electrolyte-operated linear actuators. For PPy/DBS and PEDOT/TFSI air-operated tri-layer actuators, no results were found for comparison, the performance for PPy/TFSI actuators is usually presented in terms of tip displacement, and the strain difference rate for similar actuators is rarely reported. In addition, strain difference depends on the applied voltage (or current for current-driven actuators), its shape, actuation speed, electrolyte and the thickness of the active layer. The largest strain difference and strain difference rate values reported in paper **I** were 4.4% for IH-immersion actuators at frequency 0.005 Hz (strain) and 0.17% s<sup>-1</sup> at 1.9 Hz (strain difference rate, MPI-immersion) with 1 M LiTFSI in PC electrolyte at AC  $\pm 3$ V and 2% V<sup>-1</sup> at AC 0.8 V at 0.002 Hz) for PPy/DBS tri-layer actuators. This performance is in the same order with DBS free-standing films of Bay *et al.* [60]. They achieved a maximum of 2.5% reversible linear strain (5.6% with 1-pentanol additive on EC synthesis) in 0.2 M NaCl aqueous electrolyte in potential range 0.2 ... -0.9 ... 0.2 V at steady conditions of strain. The largest blocking force, reported in paper **I** was  $\approx 4$  mN at the measurement distance 5 mm (MPI-immersion in 1 M EMImBF<sub>4</sub> in PC electrolyte). Although the step response of the blocking force was not measured, values obtained for TFSI-doped actuators at low frequency remain in the same order of magnitude as those of a similar actuator system of Wu *et al.* [156] (synthesis charge 4.3 C cm<sup>-2</sup>, actuator length and measurement distance 20 mm, width 2 mm, applied voltage 1 V).

In order to compare the results (especially for air-operated tri-layer PPy/TFSI actuators in PC electrolyte) with those of other workers, *e.g.* [156], who have used only tip displacement for the characterization, and also for experiment planning, simple conversion equations (Appendix 1) were used, based on the model of Sugino *et al.* ([127] and **Figure 1.18**). Using Newton's

method [226] to solve Eq. (8.1) allows the conversion from tip displacement to strain difference using equations (8.5) and (8.6).

The largest strain difference values reported in paper II (also in **Figure 3.12a**) were 3.7% (at step response 1 V after 124 s) and 1.2%  $V^{-1}$  at 0.002 Hz (in **Figure 3.14b**) for PPy|PPy/TFSI actuators. The best strain difference value was 2.1%  $V^{-1} s^{-1}$  for PEDOT|PEDOT/TFSI (at frequency 5 Hz). Comparison with the data reported by Wu *et al.* [156] showed that although the maximum displacement for their very similar actuator ( $L = 40$  mm,  $w = 140$   $\mu$ m,  $D = 33$  mm (half of the peak to peak displacement),  $f = 1$  Hz) was large, the theoretical maximum displacement, assuming uniform curvature is not more than 29 mm. This value corresponds to a strain difference of 0.82%. Strain difference rate, calculated from Eq. (2.30) is then 3.28%  $s^{-1}$ . Better performance at higher frequencies can be explained by the influence of gold sputter coated electrodes in combination with anion-active actuation (see comparison in **Figure 3.11a**).

Comparison of the actuators with literature data shows that strains difference values were comparable. Strain difference is preferred the characterization, instead of maximum tip displacement because:

1. maximum tip displacement value does not coincide with the largest strain difference at large strain difference values;
2. for the same tip displacement value (except maximum displacement value) corresponds more than one strain difference value;
3. at equal consumed charge and the same electrode material, the displacement depends on the total thickness of actuators and is not proportional to the consumed charge at large displacement values, which makes it difficult to compare different CP electrode materials. It is important due to the charge-controlled principle of CP actuation.

### **3.1.9 Stability and mobility of ions**

Although no special experiments were conducted, chemically synthesized electrode layers were stable at least for two years when stored under ambient conditions for both, chemically synthesized PPy and PEDOT. No significant differences in mechanical properties were observed and the conductivity remained sufficient for EC synthesis.

Since there are no metal electrodes involved and the various polymer layers are rather strongly attached to each other, there was no delamination observed, inherent to many other actuators. It is obvious that the complete elimination of the delamination problem cannot be proved in the same way as can be proved the existence of the delamination problem. During actuation experiments, no signs of delamination were noticed under any circumstances, including a large number of actuation cycles (in order of several thousand), aging during several years, or subjection to extreme strains, causing the curling of the actuator by several turns. Quantitative stability testing was complicated, as electrolytes, causing higher strains were based on the PC electrolyte, which evaporated

slowly during the experiments. It can be concluded that chemically synthesized electrodes ensured strong adhesion between the CP and PVdF membrane.

Considering the large size of  $\text{DBS}^-$  anions, cation-active actuation was expected for PPy/ $\text{DBS}^-$  actuators. Nevertheless, in 1 M LiTFSI in PC electrolyte and 1 M EMImBF<sub>4</sub> in PC electrolyte, after 10 ... 20 cation-active cycles, the actuation became anion-active. The reversal of the actuation relative to voltage was attributed to the reduced mobility of  $\text{Li}^+$  due to the solvation with PC molecules, formation of  $\text{Li}^+\text{DBS}^-$  ion pairs or LiDBS salt, which is insoluble in the PC electrolyte. Another reason could be the very different diffusion speed of  $\text{Li}^+$  cations on oxidation, when compared to that of anions, and  $\text{Li}^+$  diffusion on reduction. When the charge of doping  $\text{DBS}^-$  of the reduced CP is compensated by the not very mobile cation, the oxidation charge was compensated by the more mobile anions from the electrolyte. The latter reasoning (excluding the solvation shell) remains relevant also for  $\text{DBS}^-$ -doped CP with 1 M EMImBF<sub>4</sub> electrolyte. After being kept in electrolyte overnight, the actuators behaved again as cation-active for 10 ... 20 cycles and then became anion-mobile. The TFSI-doped actuators in EMImTFSI showed mixed behavior. At high frequencies cation-activity dominated, followed by mixed-type activity, where the movement of both ion types compensated each other, and the strain difference became low, finally anion-activity became dominant at low frequencies. The switching from one mobility type to another is clearly observable from the step responses depicted in **Figure 3.12c,d**. The actuators with 1 M EMImBF<sub>4</sub> in PC electrolyte showed noticeable creep, which was attributed to the uneven accumulation of cations inside the CP (starting already from the first cycle).

All TFSI-doped CP combinations showed only anion-active behavior in 1 M LiTFSI in PC electrolyte.

For electrolyte-operated linear tri-layer PEDOT|PPy/DBS (Sample A on PVdF membrane and Sample B on CS film) actuators, actuated in 0.1 TBACF<sub>3</sub>SO<sub>3</sub> in PC, the transition from one type of activity to another was also observed. Sample A (PVdF|PEDOT) transformed from anion-active to cation-active (**Figure 3.15**) at low scan rate, the transition from cation-active to anion-active took place at high frequencies, introduced by potential steps (**Figure 3.16a**).

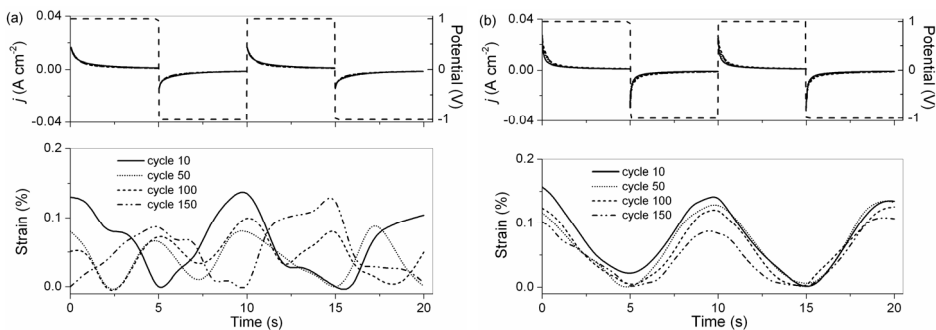


**Figure 3.16.** Response of current density ( $j$ ) and strain to square wave potential (0.1 Hz,  $\pm 1.0$  V, in 0.1 M TBACF<sub>3</sub>SO<sub>3</sub> in PC electrolyte) recorded at cycles 10, 50, 100, and 150: a) Sample A; b) Sample B (adapted from Figure 5 of paper III).

The transition period for Sample A lasted about 150 square wave cycles in the potential range  $E = 1 \dots -1 \dots 1$  V vs. Ag/AgCl (3 M KCl) (**Figure 3.16a**). The actuation was restored to the initial cation dominated character after resting overnight. CV measurements at 10 and 50 mV s<sup>-1</sup> exhibited only cation dominated transport after 8 cycles. After 4 ... 8 cycles at the scan rate of 5 mV s<sup>-1</sup>, sample A become cation-active, while Sample B was cation-active from the very beginning (**Figure 3.15**, **Figure 3.16b**). Since the EC polymerization conditions and the CP for the chemically synthesized electrodes were identical, the different behavior of Sample A and Sample B was attributed to the less stretchable substrate of Sample B, preventing the accumulation of cations inside the CP. Similar behavior, where ion mobility type depends on applied stress has been observed by Kaneto, *et al.* [227]. Cation accumulation inside the electrode has been observed in many cases, but is still not a well explained phenomenon yet and cannot be covered within the scope of this work. Accumulation of cations in PPy films with less mobile anions has been studied by several authors, typically the recovery of the exchanged charge after resting overnight has been observed. The recovery is most probably related to the diffusion of the accumulated cations out of the film and various relaxation phenomena. An alternative explanation has been proposed by Yamato *et al.* [228]. They cycled PPy/TFSI in BMPTFSI in PC solution and observed a transition to anionic behavior, which they explained by the lubricating effect of PC, which allows doping and dedoping by the large TFSI<sup>-</sup> anion. However, it was not clear from the paper if the moving TFSI<sup>-</sup> anions originate from the electrolyte or were the dopant during the EC synthesis.



## 3.2 Polypyrrole hydrogels and the derived aerogels

The chemical polymerization on various surfaces can be considered as interfacial or hard template synthesis, since the structure and appearance of the resulting CP is determined by the substrate. The appearance of the product of the chemical synthesis in micellar media (soft template synthesis) is determined by the properties of the micellar solution. Usually, the result is in form of powder or non-uniform aggregated clusters, but with carefully tuned conditions, also self-assembly of stable 3D structures is possible. The chemical synthesis of PPy hydrogels and the derived aerogels represent another type of chemical synthesis as well as another type of synthesis result.

### 3.2.1 Sodium dodecylbenzenesulfonate colloidal solution formation

Colloidal solution formation was tested separately with 1 M SDBS solution and the oxidants SPS or APS at different concentrations (without Py). The results are summarized in **Table 3.4**.

**Table 3.4.** Oxidants and concentrations used for colloidal solution formation evaluation.

Oxidant and concentration	Result
0.5 M APS	Clear solution
0.1 M APS *	Stable opalescent colloidal solution
0.15 M APS	Visible sedimentation of micelles
0.1 M SPS **	Clear solution
0.15 M SPS	Stable opalescent colloidal solution
0.1 M SPS, 0.1 M NaCl	Stable opalescent colloidal solution
0.2 M SPS	Visible sedimentation of micelles

\* pH was measured to be 6.9

\*\* Initial pH was 7.6, but it was lowered gradually to 6.5 by adding H<sub>2</sub>SO<sub>4</sub>

While blending 0.1 M SDBS with APS at different concentrations, there was a narrow concentration range around 0.1 M APS, where a stable opalescent colloidal solution was formed. At lower concentrations, no colloidal solution was formed, and at higher concentrations, visible sedimentation of micelles occurred. The suitable range appeared to depend on the chosen salt(s), their concentrations and to be independent of pH.

The presence of an optimal concentration range can explain the observation of DeArmitt *et al.* that by replacing the ammonium cation in SDBS and APS solution for sodium (using the same concentration of SPS instead of APS) prevented the formation of pre-polymerization micelles and colloidal particles [185]. Similarly, in the current work no colloidal solution was formed using

SDBS and SPS as 0.1 M solution (the colloidal solution forming concentrations for SDBS and APS). Only after increasing the SPS concentration to 0.15 M, a stable colloidal solution was formed, *i.e.* only a slightly higher concentration was needed for an opaque colloidal solution to be formed in case of the Na<sup>+</sup> cation. In addition, a stable colloidal solution was achieved by adding a salt with a different anion, NaCl (total composition: 0.1 M SDBS, 0.1 M SPS, 0.1 M NaCl). At concentrations 0.1 M SDBS and 0.2 M SPS, sedimentation occurred again.

### 3.2.2 Hydrogel formation

The concentrations of the components were varied in order to study the influence of the concentrations on the characteristics of the resulting hydrogels and for finding reliable boundary conditions for the hydrogel synthesis. The final concentrations of the compounds are summarized in **Table 3.5**. The key parameter was found to be the concentration of SDBS. At low SDBS concentrations (below 0.1 M), very liquid gels were formed (visually indistinguishable from dispersion, but remaining intact when immersed in water). High SDBS concentrations (over 0.1 M) yielded stable aqueous dispersions. The optimal SDBS concentration for gel formation was found to be around 0.1 M (all concentrations given in respect to the final volume of hydrogel) with equal oxidizer and Py concentrations of 0.05 ... 0.4 M (with oxidizer:Py molar ratio 1:1). In addition, stoichiometric (considering the oxidant amount needed for doping) molar ratios between Py and oxidant were suitable. The vast majority of the experiments were carried out by preparing first SDBS and Py monomer solution and finally adding the APS solution. Experiments with reversed mixing order (solution of APS with SDBS mixed with Py monomer solution (*e.g.* using solution, described in the second row of the **Table 3.4**) *vs.* solution of Py monomer with SDBS mixed with APS solution) had no influence on hydrogel formation.

Firmness of the gel was tuned by varying the concentrations of Py and APS (Py-APS) equally in the range of 0.05 ... 0.4 M. Successful formation of hydrogel was confirmed by tilting in air (more solid samples), tilting in water (softer samples) and by stability against decomposition in water. Appearances of the resulting hydrogels are depicted in **Figure 3.17b–c**.

As can be seen from equations (1.7), (1.8) and **Figure 1.9**, a large amount (2H<sup>+</sup> per Py unit) of protons is released during Py polymerization. Therefore, the progress of gelation can be monitored by pH measurements. It can be seen from **Figure 3.17a** that at concentration 0.1 M Py-APS, the polymerization was almost complete after 1 h (no further significant evolution of H<sup>+</sup> ions from the  $\alpha$ -positions of the polymerizing Py units).

**Table 3.5.** Prepared hydrogel samples (all concentrations given in respect to the final volume of the hydrogel).

Sample designation	SDBS concentration (M)	Py concentration (M)	Oxidant and concentration (M)	Result description
–	0.1	0.05	APS, 0.05	Soft gel
0.1 M Py–APS	0.1	0.1	APS, 0.1	Normal gelation ( <b>Figure 3.17a</b> )
0.2 M Py–APS	0.1	0.2	APS, 0.2	Normal gelation ( <b>Figure 3.17b</b> )
0.3 M Py–APS	0.1	0.3	APS, 0.3	Firm gel instantly ( <b>Figure 3.17c</b> )
0.4 M Py–APS	0.1	0.4	APS, 0.4	Slightly crumbling firm gel instantly
–	0.2	0.2	APS, 0.2	No gelation
–	0.05	0.1	APS, 0.1	Very soft, almost liquid gel
–	0.1	0.3	SPS, 0.3	Normal gelation
–	0.1	0.3	APS, 0.3	More elastic gel instantly*

\* polymerized in 1.0 M HCl solution (more elastic in comparison with 0.3 M Py-APS)

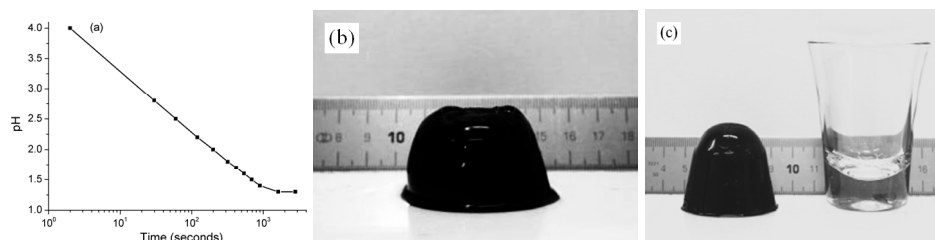


**Figure 3.17.** PPy hydrogel: a) pH change during 0.1 M Py-APS hydrogel gelation: b) 0.1 M SDBS, 0.2 M Py-APS; c) 0.1 M SDBS, 0.3 M Py-APS.

The narrow range of suitable SDBS concentrations is perhaps the main reason, why this simple method had not been discovered before. DeArmitt *et al.* [185] used similar concentrations, leading to gel formation in the current work (0.14 M SDBS, 0.17 M APS, 0.14 M Py and 0.09 SDBS M, 0.17 M APS and 0.14 M Py), but obtained only dispersions. They also tried adding APS as the last component, but only fine PPy precipitate was obtained. Besides the

unsuitable SDBS concentration, also the processing method may prevent hydrogel formation, such as vigorous stirring during polymerization or drop wise addition of the Py monomer. Stirring prevents the formation and self-assembly of the hydrogel.

Observations support the concept of micelle guided growth [185] and cluster-to-cluster aggregation from surfactant solutions having concentration close to that needed for colloidal solution formation. Micellar structures, formed from the surfactant can be considered as soft templates.

### **3.2.3 Polypyrrole aerogel and carbonized aerogel preparation**

A characteristic of hydrogels is the collapse on drying due to capillary forces. Low-density aerogels can be prepared by supercritical CO<sub>2</sub> extraction, as there are no capillary forces in the supercritical state.



**Figure 3.18.** Aerogel from 0.1 M Py-APS hydrogel.

Carbonization of the PPy aerogel was carried out for a relatively long time and at mild conditions: 350 °C for 12 h (comparing to literature reports about the carbonization of PPy powder, where temperatures 600 ... 700 °C for 1 h were used [190]) in order to preserve the physical structure of the sparse 0.1 M Py-APS aerogel. Thermogravimetry data in the literature indicate that the decomposition of nanostructured PPy/DBS, polymerized using an emulsion template method in presence of APS oxidant, accelerates already from about 300 °C [25]. Later experiments showed that carbonized aerogels retained their appearance on carbonizing at 1000 °C for 2 h and became more conductive, compared to ones, carbonized at mild conditions.

## 3.2.4 Electrochemical properties

### 3.2.4.1 Electrochemical impedance spectroscopy measurements

EIS measurements were conducted for a 0.3 M Py-APS hydrogel electrode in 0.2 M NaBF<sub>4</sub> electrolyte. The results are depicted in **Figure 3.19**.

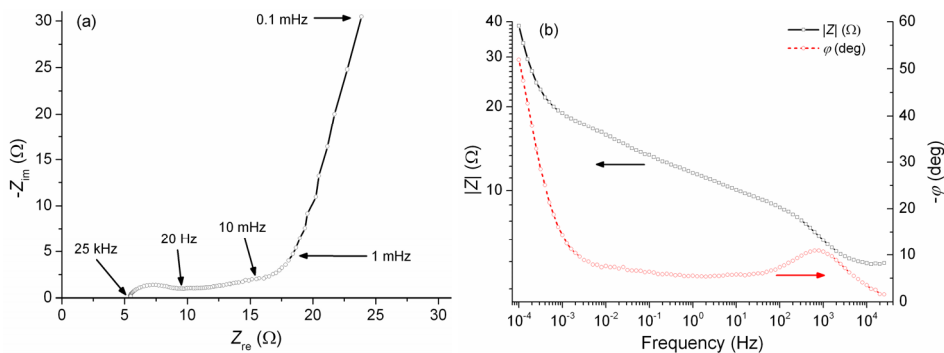


**Figure 3.19.** The results of EIS measurements of the 0.3 M Py-APS hydrogel electrode in 0.2 M NaBF<sub>4</sub> electrolyte: a) Nyquist plot; b) Bode  $|Z|$  and phase plots.

The series resistance value (5.4 Ω) of the electrolyte and electrode was obtained from the high frequency region 1 ... 25 kHz, where the weak dependence of the impedance on the frequency and the diminishing phase shift indicate purely ohmic behavior (the beginning of the semicircle in **Figure 3.19a**, and plateau of  $|Z|$  at high frequencies in **Figure 3.19b**). In range of 20 Hz ... 10 mHz, the Bode phase plot has a broad minimum, describing transition from charge transfer region to the semi-infinite cylindrical diffusion at the polymer surface [229]. At frequencies below 1 mHz, the nearly linear Nyquist plot describes the dominating capacitive behavior. The steep increase of  $|Z|$  in **Figure 3.19b** and the phase angle below 21° indicate mixed kinetics according to the finite diffusion model [230] with finite reflective boundaries, characteristic of thin CP films [176, 229].

### 3.2.4.2 Energy storage properties

Specific capacitances of 0.3 M Py-APS hydrogel electrodes, calculated according to equations (2.22), (2.23) and (2.24) were 159.1, 154.8 and 150.0 F g<sup>-1</sup>, respectively. The comparison with the maximum theoretical doping-division-dependent specific capacitance (195.6 F g<sup>-1</sup>), calculated from Eq. (2.25) indicates that *ca.* 80% of the material is accessible for energy storage. Capacitances, normalized to the outer surface area of the electrode were 3.3, 3.2 and 3.1 F cm<sup>-2</sup>, respectively. The specific capacitance values were smaller than were those reported previously (for example Kim *et al.*, PPy/pTS, 420 F g<sup>-1</sup> [199]).

However, the published high specific capacitance values have been usually achieved for very thin CP layers (in [199] *ca.* 450 nm, with a mass loading of *ca.* 0.1 mg cm<sup>-2</sup> and surface specific capacitance of 0.04 F cm<sup>-2</sup>, as calculated from synthesis charge using equations (2.8) and (2.9)) *vs.* the commercial level mass loading of *ca.* 20 mg cm<sup>-2</sup> for the 0.3 M Py-APS hydrogel.

The maximum gravimetric energy density was calculated from the maximum gravimetric specific capacitance using Eq. (2.26). The maximum gravimetric energy density of 0.3 M Py-APS hydrogel electrode was 34.5 W h kg<sup>-1</sup> (14.6 W h kg<sup>-1</sup> at scan rate 0.25 mV s<sup>-1</sup>). These values were again lower than those reported by Kim *et al.* for thin layers (*ca.* 100 W h kg<sup>-1</sup> at scan rate 10 mV s<sup>-1</sup>, [199]). The results of the comparison were more favorable for energy density and power density, normalized to the surface area of the electrode (calculated using equations analogous to (2.22) ... (2.27)). The maximum measured energy density and power density for 0.3 M Py-APS hydrogel were 0.691 mW h cm<sup>-2</sup> and 0.5 mW cm<sup>-2</sup> *vs.* 9.6 μW h cm<sup>-2</sup> and 0.27 mW cm<sup>-2</sup>, respectively.

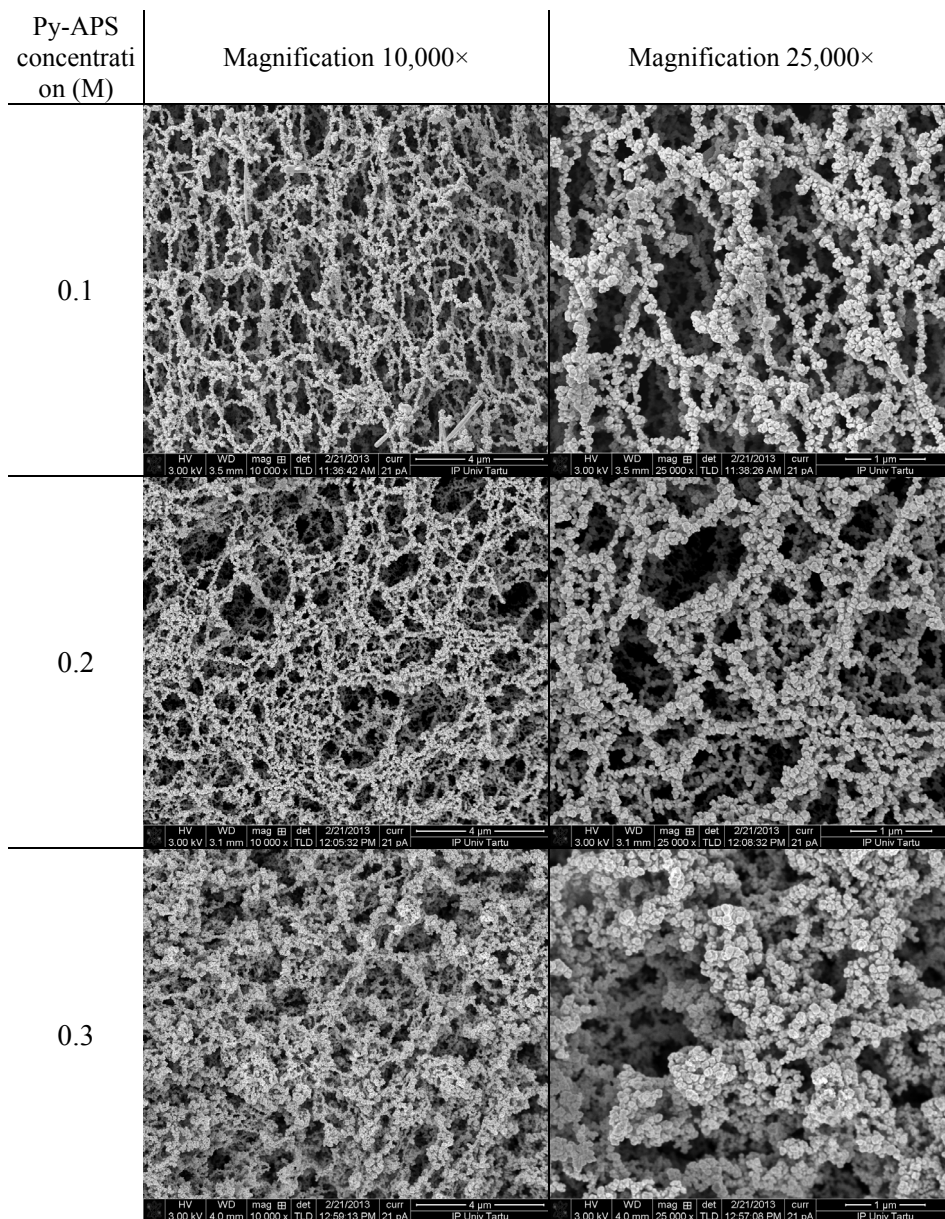
### 3.2.5 Stability evaluation

The stability of the hydrogel electrodes was tested during long-term continuous CV experiments. During several months, the hydrogel retained its initial appearance and electroactivity. Stability regarding pH was tested in pH range 1 ... 14 and no signs of decomposition were observed. Long-term treatment with a variety of organic solvents (MP, hexanol, EtOH, MEG, 3-methylphenol, MeOH, n-pentanol, PC) showed stability in all solvents tested. On immersion in water, aerogel become hydrogel again.

### 3.2.6 Structure, morphology and doping level

SEM micrographs of aerogels, prepared using different Py-APS concentrations are presented in **Figure 3.20**.

PPy aerogels exhibit granular structures, similar to the ones reported by Xu *et al.* [189]. Aerogels, prepared from hydrogels of lower Py-APS concentrations differed remarkably from the ones made from hydrogels of higher Py-APS concentrations. Aerogels, prepared from 0.1 ... 0.2 M Py-APS appear to be composed from chains of connected PPy nodules, while at Py-APS concentrations 0.3 ... 0.4 M, the structure consists of denser clusters and larger voids.



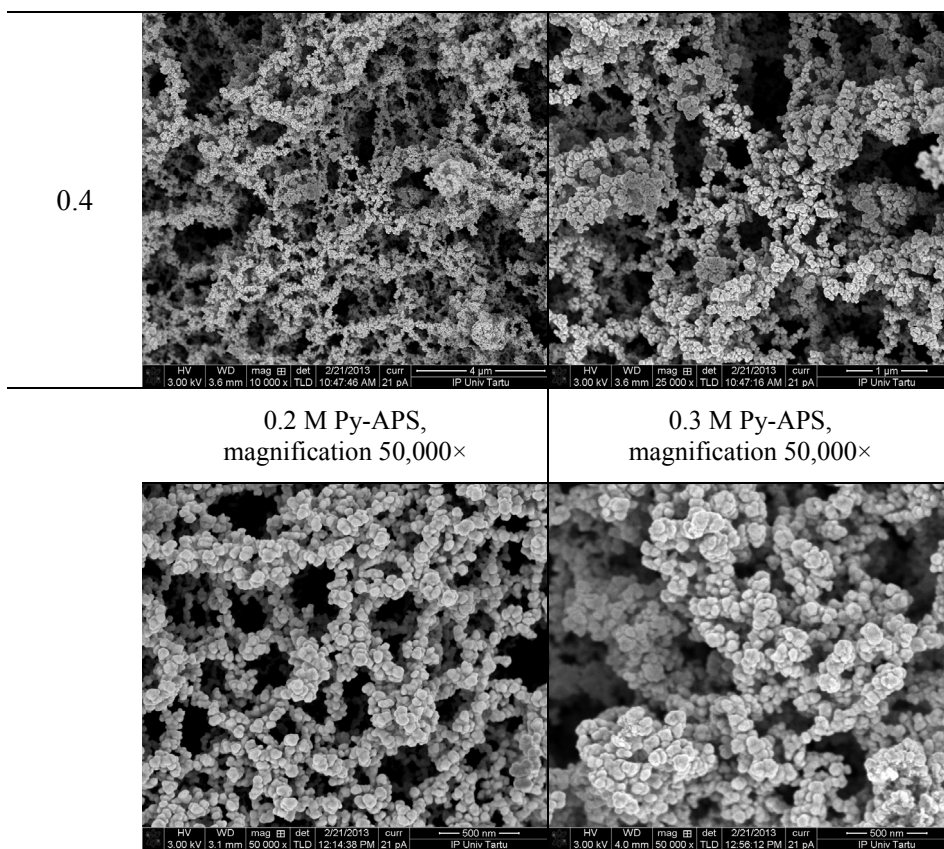


**Figure 3.20.** SEM micrographs of aerogels (sputter coated with Au), prepared with different Py-APS concentrations.

The combination of the EC active CP and the hydrogel structure allowed structure characterization using EC methods. The results of the fractal dimension measurements are presented in ESI of paper IV. Fractal dimensions, calculated from CV experiments with 0.2 M Py-APS and 0.3 M Py APS hydrogels revealed the transition from diffusion limited cluster-cluster aggregation ( $d_f = 1.7$ ) to reaction limited cluster-cluster aggregation ( $d_f = 2.1$ ). The transition can be explained by gelation speed, which increased with increasing concentrations of Py-APS, and decreasing pH. According to the small-angle X-ray scattering experiments of Knoblich and Gerber [231], the fractal dimension of SiO<sub>2</sub> hydrogel depends on the surface charge and the Coulomb repulsion between the aggregating particles, and depends on both, pH and gelation time. They observed almost stable  $d_f$  values in broad pH and gelation time ranges and a sharp transition of the  $d_f$  value from 1.7 to 2.2 at the lowest gelation times, but also a higher  $d_f$  value at low pH values. According to computer simulations,



$d_f = 1.7$  is characteristic of diffusion limited cluster-cluster aggregation and values  $d_f = 2.2 \dots 2.3$  refer to reaction limited cluster-cluster aggregation [231]. In case of PPy hydrogels both, pH and gelation time depend on Py-APS concentrations. According to Jullien [232] fractal dimension depends also on concentration of particles and nature of aggregation (Brownian, linear with and without impact parameter or chemical model). Fractal dimension over 2 indicates chemical nature of aggregation.

Doping levels (**Table 3.6, Figure 3.21**) for the aerogels, extracted from hydrogels with different concentrations were calculated using equations (2.11), (2.15) and (2.16) and the atomic ratios from EDX measurements (ESI of paper IV).

**Table 3.6.** Doping levels of aerogels depending on concentration.

Py-APS concentration (M)	Doping level		
	$d_{DBS}$	$d_{SO_4}$	$d_{sum}$
0.1	0.285	0.031	0.316
0.2	0.278	0.062	0.340
0.3	0.238	0.073	0.311
0.4	0.204	0.090	0.294
0.3*	0.303	0	0.303

\* Blue, soluble PPy extracted from Ac, used for washing

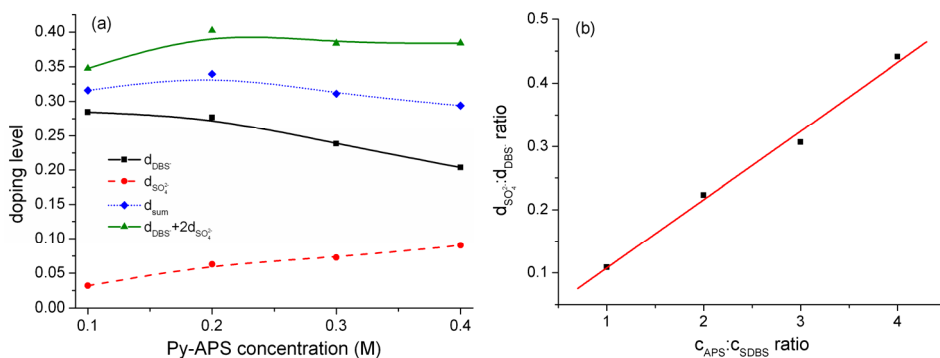


**Figure 3.21.** Doping level of aerogels depending on Py-APS concentration: a) total doping level and the contribution from sulfate and  $DBS^-$  anions (adapted from Figure 2 of paper IV); b) dependence of the molar ratio of dopants on the relative concentrations of APS and SDBS, the straight line is the linear fit.

The results indicate that the total analytical doping level (**Table 3.6** last column, **Figure 3.21a**) was almost constant, but with increasing Py-APS concentration (and thereby SDBS:APS molar ratio) the doping by sulfate anions increases and

the doping by  $\text{DBS}^-$  decreases. The almost linear dependence of the ratio of sulfate and  $\text{DBS}^-$  doping levels on the relative concentration of APS and SDBS (**Figure 3.21a**) indicates that the doping of the hydrogel proceeds under kinetic control. Slight decrease of the total doping level at the expense of  $\text{DBS}^-$  at higher Py-APS concentrations can be explained by the higher solubility of  $\text{DBS}^-$ -doped PPy oligomers in organic solvents. Higher synthesis temperature, diffusion-controlled synthesis regime and hindered diffusion in hydrogels of higher Py-APS concentrations promoted the polymerization of shorter chains and formation of a less densely packed structure. Last row of **Table 3.6** indicates that during solvent exchange the extracted fragments were almost exclusively  $\text{DBS}^-$ -doped.

### 3.2.7 Density, conductivity and low temperature $\text{N}_2$ sorption measurements

The results of the density and conductivity measurements are summarized in **Table 3.7** and depicted in **Figure 3.22**.

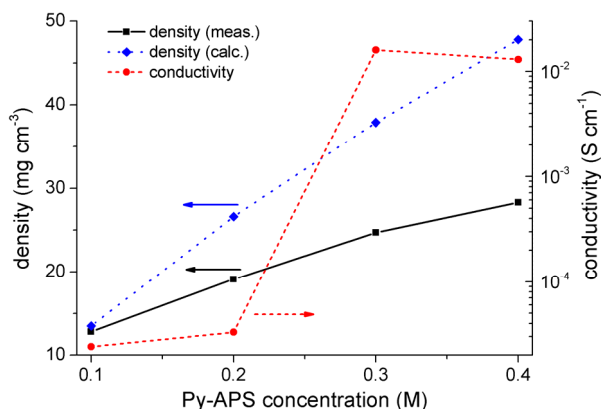


**Figure 3.22.** Conductivities and semi-theoretical and measured densities of the aerogels, depending on Py-APS concentration (from Figure 2 of paper IV).

#### 3.2.7.1 Density measurements

Several methods were used for aerogel density measurements. Due to the softness of the aerogels, the dry powder pycnometry technique did not give reproducible results (35... 39 mg cm<sup>-3</sup> for 0.4 M Py-APS aerogel).

Aerogels, extracted using Ac as solvent (unlike extraction, using EtOH or MeOH), did not shrink visibly on extraction. Thus, densities of the aerogels were estimated on basis of volume of the extraction basket and the measured weight of the aerogel. Semi-theoretical densities were calculated using the measured analytical doping levels (**Table 3.6**) in Eq. (2.31). The results are presented in **Table 3.7**.

**Table 3.7.** Semi-theoretical, and measured densities of the aerogels and polymerization yield.

Py-APS concentration (M)	Calculated density ( $\text{mg cm}^{-3}$ )	Measured density ( $\text{mg cm}^{-3}$ )	Yield (%)	Conductivity ( $\text{S cm}^{-1}$ )
0.1	13.3	12.8	96.3	$2.4 \cdot 10^{-5}$
0.2	25.8	19.1	74.0	$3.3 \cdot 10^{-5}$
0.3	36.3	24.7	68.1	$1.6 \cdot 10^{-2}$
0.4	45.3	28.3	62.5	$1.3 \cdot 10^{-2}$

The expected aerogel densities were somewhat higher than the measured values. The calculated density was semi-theoretical due to the measured analytical doping levels used in the calculations and was based on the assumption that the polymerization yield depends on the available oxidant only (due to the oxidant deficiency condition). Discrepancy, increasing with concentration, could be justified by the incomplete polymerization, hindered by diffusion in denser hydrogels and causing the formation of a less contiguous network. The difference can also be attributed to the solubility of the unreacted Py and non-contiguous, detached low molecular weight oligomers in water, assisted by the residues of surfactant, present after gelation, and possibly to the small amount of unreacted oxidant.

Another reason for the density discrepancy could have been the very low pH, characteristic of chemical polymerization, where protons, originating from the  $\alpha$ -positions of polymerizing units cannot be reduced in the same way as it occurs on the cathode during anodic polymerization in an one-compartment EC cell. Usually, low pH has a good effect on polymerization [51], but according to Otero and Rodríguez [49] (for EC polymerization) low pH also causes lower conductivity due to the formation of non-conjugated trimers by acid-catalyzed coupling. These trimers react further to form a PPy with conjugation defects and either participate in film formation or diffuse freely to the solution, thus not participating in the formation of the hydrogel structure.

Water, used for washing of the hydrogels, became yellowish on the first washing cycles and remained clear for later cycles. After exchanging water for Ac, MeOH or EtOH, the washing solvent obtained blue color. EDX measurements of the dried washing solvent confirmed that the color originated from  $\text{DBS}^-$ -doped PPy fragments (**Table 3.6**, last row). Thus, the mismatch between the measured and calculated densities and its dependence on concentration was interpreted as a measure of the overall gelation efficiency (polymerization yield, **Table 3.7**).

The mass of the initial 0.1 M Py-APS aerogel was found to drop by 29% upon carbonization.

### 3.2.7.2 Conductivities of the aerogels

With the increasing contribution of  $\text{SO}_4^{2-}$  in the analytical doping level, the conductivity was expected to grow faster due to the double charge of sulfate. The increasing oxidation state cannot fully explain the sharp transition of the conductivities (more than two orders of magnitude, **Table 3.7** last column, **Figure 3.22**), between Py-APS concentrations 0.2 ... 0.3 M. The sharp transition is mainly attributed to the exceeded percolation threshold (considering also the higher doping level of 0.2 M Py-APS aerogel and the higher synthesis temperature of 0.3 M Py-APS aerogel). Conductivities of the denser aerogels were similar to those measured by DeArmitt *et al.* (ca.  $0.01 \text{ S cm}^{-1}$  for PPy/DBS cast films and compressed pellets [185]).

### 3.2.7.3 Low temperature $\text{N}_2$ sorption measurements

Low-temperature  $\text{N}_2$  sorption measurements were conducted for 0.1 M Py-APS, 0.3 M Py-APS and carbonized 0.1 M Py-APS aerogels. Samples were chosen based on the most significant qualitative differences in morphology. Porosity data, based on the DFT method are depicted in **Figure 3.23**.

In general, the peaks in the differential pore volume (**Figure 3.23a**) and the differential surface area graph (**Figure 3.23b**) follow the same pattern. The most significant qualitative change is the peak shift between 1 and 2 nm, attributed to changes in inter-chain distances due to different proportion between the two doping anions. The total BET surface area, the specific total volume of pores and the specific micropore volume are summarized in **Table 3.8**.

Upon carbonization, the surface area vs. pore width graph (**Figure 3.23c,d**) became similar to that of resorcinol-formaldehyde-derived carbon aerogels [233].

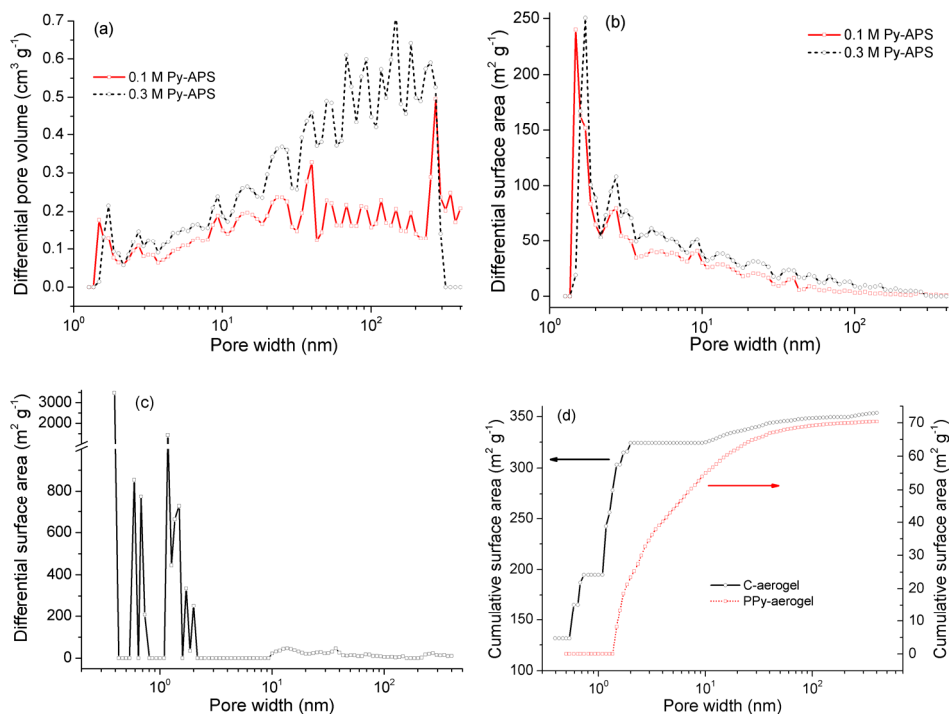


**Figure 3.23.** N<sub>2</sub> sorption measurements of 0.1 M Py-APS, 0.3 M Py-APS and carbonized aerogels: a) differential pore volume (0.1 and 0.3 M Py-APS); b) differential surface area (0.1 and 0.3 M Py-APS); c) differential surface area (0.1 M Py-APS derived carbonized aerogel); d) cumulative surface area PPy (squares) and carbon (circles) aerogels (0.1 M Py-APS) (From Figure 3 of paper IV)\*.

\* the cumulative surface area is presented for convenient comparison with literature source [233] only, and the total specific surface area is presented as a BET specific surface area in **Table 3.8**.

**Table 3.8.** Specific surface area and pore distribution of aerogels.

Aerogel sample	BET specific surface area (m <sup>2</sup> g <sup>-1</sup> )	Specific total volume of pores** (cm <sup>3</sup> g <sup>-1</sup> )	Specific micropore volume (cm <sup>3</sup> g <sup>-1</sup> )
0.1 M Py-APS	134.4	0.41	$7.4 \cdot 10^{-3}$
0.3 M Py-APS	167.1	0.73	$2.7 \cdot 10^{-3}$
0.1 M Py-APS*	425.8	1.18	$1.85 \cdot 10^{-1}$

\* carbonized aerogel

\*\* pore size  $p < 400$  nm

### 3.2.8 Control of the doping balance and the electrochemical modification of hydrogels

The kinetic control of PPy doping suggests that the doping structure can be controlled to some extent by the composition of the synthesis solution. Synthesis in 1 M HCl solution (0.3 M Py-APS, 0.1 M SDBS) showed that additional anions from the synthesis solution could participate in doping. The resulting total analytical doping level remained approximately the same and the resulting hydrogel was additionally doped with  $\text{Cl}^-$  mostly in expense of  $\text{SO}_4^{2-}$ .

The EC modification of the doping structure (redoping) was conducted by EC cycling in an electrolyte, containing the target anions.

Results of the synthesis-time modification and EC modification are summarized in **Table 3.9**. Doping levels were calculated based on the atomic ratios published in the ESI of paper **IV**.

**Table 3.9.** Doping levels of hydrogels after synthesis-time and post-synthesis modification.

Py-APS concentration(M)	Cycling/synthesis solution	Doping level			
		$d_{\text{DBS}}$	$d_{\text{SO}_4}$	$d$ (anion)	$d_{\text{sum}}$
0.3*	1.0 M HCl	0.224	0.022	0.046 ( $\text{Cl}^-$ )	0.292
0.3	0.2 M $\text{NaBF}_4$	0.199	0.081	0.053 ( $\text{BF}_4^-$ )	0.333
0.3	0.2 M $\text{LiClO}_4$	0.057	0.079	0.208 ( $\text{ClO}_4^-$ )	0.344
0.2	1 M $\text{H}_2\text{SO}_4$	0.145	0.192	N/A	0.337

\* Synthesis-time modification (not EC, **Table 3.5** last row)

Generally, the total analytical doping level remained approximately constant. Comparison with **Table 3.6** suggests that during the synthesis, the additional anion preferably replaced the sulfate anions (relatively to the unmodified value), and preferably, despite their large size (**Figure 3.8c**)  $\text{DBS}^-$  anions were replaced by EC cycling. The more difficult exchange of sulfate anions was attributed to their double charge and high charge density.

The possibility of introducing a dopant of choice on synthesis or after synthesis by redoping, gives an advantage compared with several other CP hydrogels for applications, where such flexibility is important (e.g. controlled drug release devices).

The modification of the conducting hydrogels by EC synthesis has been demonstrated by Ghosh and Inganäs ([177, 179]). In the current work, PPy was EC deposited inside of a 0.15 M Py-APS hydrogel. The EC deposited PPy comprised *ca.* 0.5 mol% of hydrogel's total amount of PPy repeating units. Nevertheless, due to the increased charge transfer rate both, the pseudo capacitance and the reduction charge (0.78 and 15.84  $\text{mC cm}^{-2}$ , before and after EC synthesis, respectively at scan rate 10  $\text{mV s}^{-1}$ ) increased more than 20 times

(**Figure 3.24a**). In addition, the EC deposition caused changes in internal structure of the hydrogel. Fractal dimension increased from  $d_f = 1.43$  to  $d_f = 2.14$  (**Figure 3.24b**). The initially low specific capacitance ( $2.7 \text{ F g}^{-1}$ ), energy density ( $0.6 \text{ W h kg}^{-1}$ ) and power density ( $0.4 \text{ W kg}^{-1}$ ) increased to  $9.2 \text{ F g}^{-1}$ ,  $2 \text{ W h kg}^{-1}$ , and  $1.4 \text{ W kg}^{-1}$ , respectively. The significant increase of specific capacitance and energy density indicates that EC deposition increased part of the material, accessible for energy storage and additional deposition created new electrical connections, increasing electronic accessibility of material. Nevertheless, the specific capacitance remains much lower than theoretical doping division dependent capacitance of  $177 \text{ F g}^{-1}$  (calculated from Eq. (2.25) using doping level values, interpolated for 0.15 M Py-APS hydrogel).

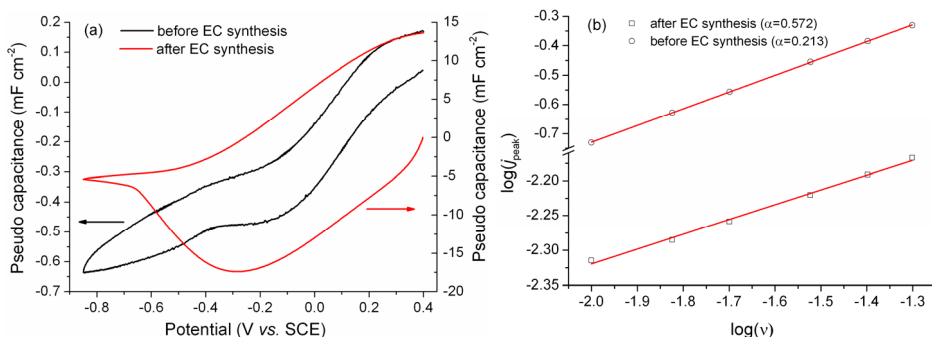


**Figure 3.24.** CV measurements before and after EC synthesis inside of the hydrogel: a) cyclic voltammograms (at scan rate  $10 \text{ mV s}^{-1}$  in  $0.2 \text{ M LiClO}_4$  in MEG electrolyte); b)  $\log(j_{\text{peak}})$  ( $\text{mA cm}^{-2}$ ) vs.  $\log(v)$  ( $\text{V s}^{-1}$ ) graph.

## 4 CONCLUSIONS, FUTURE WORK AND SUMMARY

The electrochemical modifications of the chemically synthesized CP electrodes were studied in context of their application in two distinctively different application areas and for the two most popular CPs – PPy, PEDOT, and their combinations. For both applications, the chemically synthesized CP was in the role of an electrochemically active electrode instead of the conventional usage as powders, dispersions or modification of some other underlying material. The two application areas were chosen based on their diametrically different requirements regarding to ion-CP mechanical interaction in order to show the versatility of the approach. The actuator type application assumes strong interaction between the mobile ions and the CP material and good electromechanical coupling, whereas the application as hydrogel electrodes assumes high permeability to ions. Highlights:

- Novel chemical-EC synthesis method was developed and applied for the preparation of air-operated tri-layer, metal-free, and assembly-free bending actuators.
- Chemical-EC synthesis method was applied for the preparation of a new type of electrolyte-operated tri-layer linear actuators.
- A new, simple and affordable method was developed for PPy hydrogel preparation. PPy hydrogels were used as electrodes and as precursors for PPy aerogels and carbonized aerogels.

### 4.1 Conclusions

#### ***4.1.1 Combined chemical-electrochemical synthesis method***

##### 4.1.1.1 What was done

Several chemical synthesis methods were compared and optimized for the chemical synthesis on porous PVdF membrane, SPE membrane and CS film. Two different CPs were used separately and in combination for the chemical deposition and the EC synthesis. The chemically synthesized CP coatings were used as electrodes for the following EC synthesis. The chemically and EC synthesized layers were characterized by means of four-point probe conductivity measurements, CV, SEM and EDX. Low temperature semi-aqueous synthesis method was used for electrolyte salts, insoluble in organic solvents. The combined synthesis method was used for the chemically synthesized hydrogel electrode.



#### 4.1.1.2 Novel results

CP electrodes were chemically synthesized for the following EC synthesis on initially non-conducting surfaces. The chemical synthesis of PPy and PEDOT, and the following EC synthesis were successfully conducted on the following substrates:

- 1) IH PVdF-HFP based SPE membrane;
- 2) commercial MPI porous membrane (hydrophobic, pore size 0.45  $\mu\text{m}$ );
- 3) commercial MPD porous membrane (hydrophilic, pore size 0.1  $\mu\text{m}$ );
- 4) non-porous CS film (hydrophilic).

Low temperature EC synthesis of PPy and PEDOT using solely water-soluble electrolyte salts was conducted at temperatures below  $-25\text{ }^{\circ}\text{C}$  (non-limiting temperature value) in eutectic semi-aqueous electrolyte in mix of  $\text{H}_2\text{O}:\text{MEG}$  (50:50 v/v.%). At the same temperature, using the same electrolyte salts semi-aqueous synthesis of PEDOT was conducted at EDOT concentration 0.2 M.

#### 4.1.1.3 Other conclusions from the characterization

Conclusions:

- 1) different synthesis conditions are optimal for different CPs on different substrates;
- 2) the method gives reproducible results;
- 3) chemically synthesized PPy and PEDOT are conductive enough at anodic potentials and therefore suitable for the following anodic deposition;
- 4) the poor conductivity of the chemically synthesized electrode has no influence on the EC synthesized material due to the quick increase of the conductivity during the EC deposition;
- 5) CP, chosen for the chemically synthesized electrode layer influences on the spatial distribution of the EC synthesized CP;
- 6) the properties of the resulting material are determined almost entirely by the EC synthesized layer;
- 7) while on porous and SPE membranes the adhesion is due to physical grip, CS forms a composite with PEDOT;
- 8) low temperature semi-aqueous synthesis has the same influence on the resulting material, as organic solvents;
- 9) the conductivity of chemically synthesized hydrogels can be improved by the following EC synthesis inside the hydrogel.

## **4.1.2 Metal-free conducting polymer actuators with electrochemically synthesized working layers**

### **4.1.2.1 What was done**

The chemical-EC synthesis method was applied for the production of PPy and PEDOT bending and linear tri-layer actuators. The actuation properties were characterized for two (PPy and PEDOT) CPs, for two dopant anions and for different combinations of the CPs for the chemical and EC layers. The structure and the actuation performance were characterized in terms of the frequency response of strain difference, strain difference rate and blocking force. The constructed actuators were characterized in different electrolytes in order to compare the advantages and the disadvantages of the different synthesis conditions. The actuators were characterized using EC, ECMD, SEM and EDX measurements. The ion-activity type was characterized by actuation properties.

### **4.1.2.2 Benefits and disadvantages of metal-free conducting polymer actuators**

Air operated, bending type tri-layer CP actuators with porous or SPE membrane were prepared. The benefits of the actuators, compared to analogous actuators:

- 1) simple preparation procedure;
- 2) metal and assembly free design;
- 3) stable and delamination proof;
- 4) several routes for the chemical step (with structure control option);
- 5) the method is suitable for layered PEDOT actuators (besides the traditional PPy or PEDOT IPN actuators);
- 6) the working layer can be synthesized at sub-zero temperatures using water-soluble electrolyte salts;
- 7) the method results in a less heterogeneous structure and the actuators are easier to model and control;
- 8) the method avoids the usage of vacuum techniques and noble metals, and can be implemented as roll-to-roll process, highly desirable for industrial production;
- 9) the method offers improved performance of PPy/DBS actuators (compared with the actuators with the EC deposited working layers deposited on Au sputter coated electrodes);
- 10) the method allows chemical deposition on SPE membranes.

The disadvantage is a slightly poorer performance with PPy/TFSI and PEDOT/TFSI (latter introduced in this work). All other conditions (such as reproducibility and stability, *etc.*) are at least equal.

### 4.1.2.3 Other conclusions from the characterization

Conclusions:

- 1) using the RTIL EMImTFSI as an electrolyte results in mixed type ion movement for PPy/TFSI and PEDOT/TFSI actuators; at higher frequencies the cation movement dominates, while the anion movement dominates at low frequencies; in order to achieve acceptable performance with RTILs, anions and cations must be of more different dimensions;
- 2) using 1 M EMImBF<sub>4</sub> and 1 M LiTFSI in PC as the electrolytes resulted in mixed or mostly anion dominated actuation for DBS<sup>-</sup>-doped actuators despite the large size of the doping anions, and under certain conditions the transition from one mobility type to another occurred;
- 3) the final ion mobility for actuators with CP electrodes doped with immobile anions was found to depend on the solvent and the sizes of anion and cation of the chosen electrolyte;
- 4) PPy actuators generally had larger strain difference, PEDOT offered higher strain difference rate;
- 5) at voltages over 0.8 V, actuators with EC PPy working layer developed reversible creep; no creep was observed for actuators with EC PEDOT layer up to voltage 1 V;
- 6) the performance of the actuators was found to be influenced mainly by the EC synthesized working layer;
- 7) the actuators proved to be delamination-proof, stable and reproducible;
- 8) acceptable displacement values, strain difference values over 3.5% V<sup>-1</sup> and strain difference rates over 2% V<sup>-1</sup> s<sup>-1</sup> were achieved.

### 4.1.3 Electrolyte-operated tri-layer linear actuators

#### 4.1.3.1 What was done

Electrolyte-operated CP tri-layer metal-free linear actuators were prepared on two distinctively different substrates (commercial MPD PVdF membrane and CS). The chemical synthesis conditions were optimized for both substrates and the resulting actuators were compared side-by-side. The adhesion mechanism was investigated using FTIR and Raman spectroscopy. The morphology was characterized using SEM. The ECMD properties of the actuators were characterized in TBACF<sub>3</sub>SO<sub>3</sub> in PC electrolyte.

#### 4.1.3.2 Benefits and disadvantages of metal-free conducting polymer actuators

Beneficial actuator properties, compared to single layer freestanding actuators:

- 1) stable actuation in terms (of lack) of creep and mechanical durability;

- 2) no bending creep and related issues, inherent to asymmetrical materials, deposited on an electrode
- 3) linear creep can be suppressed and ion mobility type is controllable by the mechanical properties of the passive layer;
- 4) inner passive layer can have better/different mechanical properties, compared with the CP part, not participating in actuation;
- 5) actuator is inherently symmetric;
- 6) the properties of the CP layer and the passive layers can be chosen according to the expected actuation speed and force output;
- 7) the preparation method ensures precise control over the mechanical, EC and ECMD properties.

#### 4.1.3.3 Other conclusions

Conclusions:

- 1) the dominant mobile ion species depended on the substrate and the actuation speed;
- 2) the adhesion mechanism was different for porous PVdF membrane and CS (physical grip *vs.* composite formation).

### **4.1.4 Polypyrrole hydrogels and derived aerogels**

#### 4.1.4.1 What was done

Pristine PPy hydrogels were synthesized chemically, the limits of the synthesis conditions and the optimal synthesis conditions were determined. Hydrogels were characterized by conductivity, fractal dimension, using CV, EIS, SEM, EDX, BET, *etc.* PPy aerogels were prepared from hydrogels of different concentrations. The structure and the synthesis mechanism were studied using SEM. The density, the doping level and the conductivity of the aerogels were characterized. Carbonized aerogels were prepared from PPy aerogels. The characteristic properties of the electrodes and the prepared sample devices were studied by EC, electro-chemo-mechanical deformation, EDX and SEM methods. The influence of the synthesis medium on the doping level was studied. Hydrogels were modified by redoping and EC deposition inside of the hydrogel electrode.

#### 4.1.4.2 Key properties

- 1) the most critical parameter in hydrogel formation is the concentration of the SDBS surfactant and hydrogel formation occurs only in a narrow range of SDBS concentrations;
- 2) the mechanism of the chemical synthesis and the synthesis rate was found to depend on the concentrations of the monomer and the oxidant;

- 3) the carbonization of pristine PPy aerogels can be an alternative way to prepare large surface area nanostructured carbon materials;
- 4) the improved diffusion speed and large surface area facilitate several applications – from energy storage to controlled drug delivery;
- 5) using the most classical and extensively studied components – (poly)pyrrole, ammonium persulfate, and sodium dodecylbenzenesulfonate for traditional chemical synthesis;
- 6) sparse polymer gel networks obtained, not achievable by EC methods;
- 7) the developed synthesis method allows partial control over the density, the mechanical as well as the physical and chemical structure of the hydrogel;
- 8) hydrogel electrodes can be modified by ion exchange and by the EC synthesis inside the hydrogel;
- 9) a competitive solution to the power density limitation of CPs in energy storage applications and rather simple solution to CP diffusion speed limitations in general is provided.

#### 4.1.4.3 Conclusions

- 1) carbonization of pristine polypyrrole aerogels is found to be alternative way to prepare carbonized aerogels;
- 2) PPy aerogels can be carbonized without loss of integrity and the continuous nature of the gel;
- 3) the densities of the aerogels were as low as  $12.8 \text{ mg cm}^{-3}$ , the BET surface area up to  $167.1 \text{ m}^2 \text{ g}^{-1}$  ( $425.8 \text{ m}^2 \text{ g}^{-1}$  for carbonized aerogels), and the conductivity  $1.6 \cdot 10^{-2} \text{ S cm}^{-1}$ ;
- 4) the charge storage ability of the hydrogel was measured as  $154.8 \text{ F g}^{-1}$  at the commercial level mass loading of *ca.*  $20 \text{ mg cm}^{-2}$ ;
- 5) the charge storage ability depends strongly on concentration of hydrogel and *ca.* 80% of the material is accessible at higher concentrations (*e.g.* 0.3 M Py-APS) of hydrogels.

## 4.2 Future work

### 4.2.1 Combined chemical-electrochemical synthesis method

In addition to actuators, the method could be utilized for other applications wherever the EC synthesized electrodes are required on initially non-conducting surfaces.

### 4.2.2 Air-operated metal-free bending actuators

The most acute and equally important problems in the way toward commercial applications are the encapsulation, the scaling up or bundling to macroscopic

devices and increasing the energy conversion efficiency for usage in autonomous devices. These issues were not addressed in the current work, but use of the described preparation methods simplifies actuator preparation, and therefore, contributes to the commercialization efforts.

### 4.2.3 Hydrogels

CP hydrogels and aerogels have great potential in almost every CP application where large surface area is required. Other possible applications span from high sensitivity sensors, controllable drug delivery devices and *in vivo* electrodes to electrode materials for MFCs and full-polymer energy storage devices.

Existing evidence and literature sources support the assumption that PPy electrodes are chemically biocompatible, EC active and modifiable. Due to large surface area, CP electrodes have lower EC impedance, compared with metal electrodes. Hydrogels are known to be mechanically compatible with soft tissues. The combination of CPs and hydrogels makes them promising candidates for *in vivo* electrodes and controlled drug delivery devices.

Most likely, suitable combinations of conditions exist for hydrogel formation from other CP monomers besides Py, from other surfactants besides SDBS and from oxidants other than APS. It is expected that the search for such conditions may follow due to the simplicity of the method, the affordability of materials, the flexibility in usage and the great potential of hydrogel electrodes in real energy storage applications, where the performance of actual bulk material is paramount. In case of success, CP hydrogels could contribute to the lowering of environmental impact of energy storage devices and find use in components of alternative energy systems both in role of buffer energy storage and energy production (MFC).

## 4.3 Summary

Chemically synthesized conductive polymer (CP) electrodes were prepared for the following electrochemical modification by electrodeposition or electrochemical (re)doping. The principal goal of the research was to develop techniques and tentatively optimize the synthesis conditions to meet the needs of CP application areas with distinctively different expectations for the physical structure and ionic mobility of the CP electrodes. The conditions for the chemical and electrochemical synthesis were optimized for two CP application types: artificial muscles and high specific surface area electrodes. The presented techniques of chemical synthesis of the CP hydrogel electrodes and the novel combined chemical-electrochemical synthesis technique of CP on non-conductive substrates offer several advantages over traditional electrodes and preparation methods. The prepared materials and devices, based on widespread CPs polypyrrole and poly(3,4-ethylenedioxythiophene) (PPy and PEDOT), were characterized using primarily electrochemical methods.

It was shown that metal-free actuators, fabricated using the combination of chemical and electrochemical synthesis method effectively solved the delamination problem and facilitate the commercial production by avoiding the usage of precious metals, toxic organic solvents and vacuum techniques. The results of the electro-chemo-mechanical characterization indicate that the actuation performance of the prepared actuators compares well with the ones achieved using alternative techniques. In addition, the developed method was used for the preparation of a new type of liquid-operated tri-layer linear actuators.

Large specific surface area pristine PPy hydrogel electrodes were prepared by the oxidative chemical polymerization using affordable environment-friendly compounds and a simple one-step synthesis method. Large specific surface area PPy hydrogels could be used to relieve the power density limitations of CP-related energy storage devices, for controlled drug delivery devices, sensors, *etc.* Moreover, using PPy hydrogel as a precursor, derived PPy aerogels and carbonized aerogels were prepared, further widening the number of possible applications.

## 4.4 Summary in Estonian

### Keemiliselt sünteesitud juhtivpolümeersete elektroodide elektrokeemia ja uued rakendused

Keemilise sünteesi meetodil valmistati juhtivpolümeerseid (JP) elektroodid, mida on võimalik elektrokeemiliselt modifitseerida ümberdopeerimise või elektrokeemilise sünteesi meetodil. Uurimustöö peamine eesmärk oli välja arendada ja esialgselt optimeerida sünteesimeetodid sobivaks rakendusvaldkondadele, millel on kvalitatiivselt erinevad nõudmised JP elektroodide struktuurile ja ioonjuhtivusele. Keemilise ja elektrokeemilise sünteesi tingimused optimeeriti kahe kasutusala jaoks: tehislühased ja suure eripindalaga JP elektroodid. Töös kirjeldatavad JP elektroodid on valmistatud hüdrogeelide keemilise sünteesi ja mittejuhtivale pinnale sobiva kombineeritud keemilis-elektrokeemilise sünteesi meetoditel. Sellistel elektroodidel on mitmeid eeliseid võrreldes tavapäraste elektroodidega ning nende valmistamise meetoditega. Laialt kasutatavatel JP-del, polüpürroolil ja PEDOT-il põhinevaid materjale ja neist valmistatud elektroode karakteriseeriti peamiselt elektrokeemiliste meetoditega.

Näidati, et kombineeritud keemilis-elektrokeemilisel meetodil valmistatud metallivabad aktuaatorid lahendavad efektiivselt delamineerumisprobleemi ja vastavad kommertseesmärgil tootmise eelistustele, vältides väärismetallide, toksiliste orgaaniliste lahustite ja vaakumtehnoloogiate kasutamist. Teostati elektro-kemo-mehaaniline karakteriseerimine, mille tulemused näitasid, et valmistatud aktuaatorid on aktuatsiooniomadustelt võrreldavad alternatiivsetel meetoditel valmistatud aktuaatoritega. Täiendavalt kasutati väljaarendatud meetodit uut tüüpi, elektrolüüdi keskkonnas töötavate kolmekihiliste lineaarsete aktuaatorite valmistamiseks.

Oksüdatiivse keemilise sünteesi meetodil valmistati suure eripindalaga polüpürrool-hüdrogeel elektroodid, kasutades laialt levinud keskkonnasõbralikke ühendeid ja lihtsat ühe-etapilist sünteesimeetodit. Suure eripindalaga polüpürrool-hüdrogeelid sobivad võimsustiheduse piirangute leevendamiseks JP-e kasutavates energiasalvestites, kasutamiseks kontrollitavaks ravimi manustamiseks, andurites jm. Kasutades polüpürrool-hüdrogeeli lähtematerjalina, valmistati polüpürrool-aerogeelid ja karboniseeritud aerogeelid, mis laiendavad veelgi uudse materjali kasutusvõimalusi.



## **5 ACKNOWLEDGEMENTS**

This work has been partially supported by graduate school “Functional materials and technologies” receiving funding from the European Social Fund under project 1.2.0401.09-0079 in Estonia.

I would like to thank my supervisor, Dr. Tarmo Tamm for valuable support, fruitful discussions and help in preparing manuscripts.

I acknowledge all co-authors of the published papers. In addition, I would like to thank the people from the IMS Lab for the development of a well-equipped and supporting research environment during the years of my study.

## 6 REFERENCES

1. European Cooperation in Science and Technology – COST – Secretariat, “Memorandum of Understanding for the implementation of a European Concerted Research Action designated as COST Action MP1003: European Scientific Network for Artificial Muscles (ESNAM),” available from: [http://w3.cost.eu/fileadmin/domain\\_files/MPNS/Action\\_MP1003/mou/MP1003-e.pdf](http://w3.cost.eu/fileadmin/domain_files/MPNS/Action_MP1003/mou/MP1003-e.pdf) Brussels (2010).
2. European Cooperation in Science and Technology – COST – Secretariat, “Memorandum of Understanding for the implementation of a European Concerted Research Action designated as COST Action MP1004: Hybrid Energy Storage Devices and Systems for Mobile and Stationary Applications,” available from: [http://w3.cost.eu/fileadmin/domain\\_files/MPNS/Action\\_MP1004/mou/MP1004-e.pdf](http://w3.cost.eu/fileadmin/domain_files/MPNS/Action_MP1004/mou/MP1004-e.pdf) Brussels (2010).
3. Otero, T.F.; Martinez, J.G., “Artificial Muscles: A Tool To Quantify Exchanged Solvent during Biomimetic Reactions,” *Chemistry of Materials* 24(21), 4093–4099 (2012).
4. Valero, L.; Otero, T.F.; Martinez, J.G., “Exchanged cations and water during reactions in polypyrrole macroions from artificial muscles,” *ChemPhysChem* 15(2), 293–301 (2014).
5. Letheby, H., “XXIX. – On the production of a blue substance by the electrolysis of sulphate of aniline,” *Journal of the Chemical Society* 15, 161–163 (1862).
6. Dennstedt, M.; Zimmermann, J., “Ueber die durch Einwirkung von Salzsäure auf die Pyrrole entstehenden Basen,” *Berichte der deutschen chemischen Gesellschaft* 21(1), 1478–1481 (1888).
7. Angeli, A.; Alessandri, L., “The electrochemistry of conducting polymers,” *Gazzetta Chimica Italiana* 46, 279–285 (1916).
8. Bolto, B.A.; McNeill, R.; Weiss, D.E., “Electronic Conduction in Polymers. III. Electronic Properties of Polypyrrole,” *Australian Journal of Chemistry* 16(6), 1090–1103 (1963).
9. Okamoto, Y.; Brenner, W., “Chapter 7: Polymers”, in “Organic Semiconductors”, 125–158, Editor, Reinhold Pub. Corp.: New York, USA (1964).
10. Dall’Olio, A.; Dascola, G.; Varacca, V.; Bocchi, V., “Electronic paramagnetic resonance and conductivity of a black electrolytic oxypyrrole,” *Comptes Rendus Hebdomadaires Des Seances De L Academie Des Sciences Serie C* 267(6), 433–435 (1968).
11. Shirakawa, H.; Louis, E.J.; MacDiarmid, A.G.; Chiang, C.K.; Heeger, A.J., “Synthesis of electrically conducting organic polymers: halogen derivatives of polyacetylene, (CH)<sub>x</sub>,” *Journal of the Chemical Society, Chemical Communications* (16), 578–580 (1977).
12. Shirakawa, H.; MacDiarmid, A.G.; Heeger, A.J., “The Nobel Prize in Chemistry 2000,” web page, cited: 03.05.2014, available from: [http://www.nobelprize.org/nobel\\_prizes/chemistry/laureates/2000/](http://www.nobelprize.org/nobel_prizes/chemistry/laureates/2000/) Nobel Media AB (2013).
13. Kanazawa, K.K.; Diaz, A.F.; Gill, W.D.; Grant, P.M.; Street, G.B.; Gardini, G.P., “Polypyrrole – an Electrochemically Synthesized Conducting Organic Polymer,” *Synthetic Metals* 1(3), 329–336 (1980).

14. Diaz, A.F.; Kanazawa, K.K.; Gardini, G.P., "Electrochemical polymerization of pyrrole," *Journal of the Chemical Society, Chemical Communications* (14), 635–636 (1979).
15. Heinze, J.; Frontana-Urbe, B.A.; Ludwigs, S., "Electrochemistry of conducting polymers – persistent models and new concepts," *Chemical Reviews* 110(8), 4724–4771 (2010).
16. Skotheim, T.A.; Elsenbaumer, R.L.; Reynolds, J.R., "Handbook of conducting Polymers. Second Edition," (1120 p.), CRC Press: New York, USA (1998).
17. Chen, G.Z.; Shaffer, M.S.P.; Coleby, D.; Dixon, G.; Zhou, W.Z.; Fray, D.J.; Windle, A.H., "Carbon nanotube and polypyrrole composites: Coating and doping," *Advanced Materials* 12(7), 522–526 (2000).
18. Wallace, G.G.; Teasdale, P.R.; Spinks, G.M.; Kane-Maguire, L.A.P., "Conductive electroactive polymers: intelligent polymer systems," (263 p.), CRC press: USA (2008).
19. Aradilla, D.; Estrany, F.; Casellas, F.; Iribarren, J.I.; Aleman, C., "All-polythiophene rechargeable batteries," *Organic Electronics* 15(1), 40–46 (2014).
20. Smela, E., "Conjugated polymer actuators for biomedical applications," *Advanced Materials* 15(6), 481–494 (2003).
21. Winther-Jensen, B.; Breiby, D.W.; West, K., "Base inhibited oxidative polymerization of 3,4-ethylenedioxythiophene with iron(III)tosylate," *Synthetic Metals* 152(1–3), 1–4 (2005).
22. Bredas, J.L.; Street, G.B., "Polarons, Bipolarons, and Solitons in Conducting Polymers," *Accounts of Chemical Research* 18(10), 309–315 (1985).
23. Chung, T.C.; Kaufman, J.H.; Heeger, A.J.; Wudl, F., "Charge Storage in Doped Poly(Thiophene) – Optical and Electrochemical Studies," *Physical Review B* 30(2), 702–710 (1984).
24. Nardes, A.M.; Kemerink, M.; Janssen, R.A.J.; Bastiaansen, J.A.M.; Kiggen, N.M.M.; Langeveld, B.M.W.; van Breemen, A.J.J.M.; de Kok, M.M., "Microscopic understanding of the anisotropic conductivity of PEDOT : PSS thin films," *Advanced Materials* 19(9), 1196–1200 (2007).
25. Basavaraja, C.; Kim, N.R.; Jo, E.A.; Pierson, R.; Huh, D.S.; Venkataraman, A., "Transport Properties of Polypyrrole Films Doped with Sulphonic Acids," *Bulletin of the Korean Chemical Society* 30(11), 2701–2706 (2009).
26. Zuppiroli, L.; Bussac, M.N.; Paschen, S.; Chauvet, O.; Forro, L., "Hopping in disordered conducting polymers," *Physical Review B* 50(8), 5196–5203 (1994).
27. Aleshin, A.N.; Williams, S.R.; Heeger, A.J., "Transport properties of poly(3,4-ethylenedioxythiophene)/poly(styrenesulfonate)," *Synthetic Metals* 94(2), 173–177 (1998).
28. Baughman, R.H.; Hsu, S.L.; Pez, G.P.; Signorelli, A.J., "The structures of cis-polyacetylene and highly conducting derivatives," *The Journal of Chemical Physics* 68(12), 5405–5409 (1978).
29. Hsu, S.L.; Signorelli, A.J.; Pez, G.P.; Baughman, R.H., "Highly conducting iodine derivatives of polyacetylene: Raman, XPS and x-ray diffraction studies," *The Journal of Chemical Physics* 69(1), 106–111 (1978).
30. François, B.; Mermilliod, N.; Zuppiroli, L., "Swelling of polyacetylene when doped by iodine or sodium," *Synthetic Metals* 4(2), 131–138 (1981).
31. Baughman, R.H.; Shacklette, L.W.; Elsenbaumer, R.L.; Plichta, E.; Becht, C., "Conducting Polymer Electromechanical Actuators", in "Conjugated Polymeric

- Materials: Opportunities in Electronics, Optoelectronics, and Molecular Electronics”, 624, Editors J.L. Brédas and R.R. Chance, Springer: Netherlands (1990).
32. Burgmayer, P.; Murray, R.W., “An Ion Gate Membrane – Electrochemical Control of Ion Permeability through a Membrane with an Embedded Electrode,” *Journal of the American Chemical Society* 104(22), 6139–6140 (1982).
  33. Otero, T.F.; Angulo, E.; Rodríguez, J.; Santamaría, C., “Electrochemomechanical properties from a bilayer: polypyrrole / non-conducting and flexible material – artificial muscle,” *Journal of Electroanalytical Chemistry* 341(1–2), 369–375 (1992).
  34. Pei, Q.B.; Inganas, O., “Electrochemical Applications of the Bending Beam Method. 1. Mass-Transport and Volume Changes in Polypyrrole during Redox,” *The Journal of Physical Chemistry* 96(25), 10507–10514 (1992).
  35. Pei, Q.B.; Inganas, O., “Electrochemical applications of the beam bending method; a novel way to study ion transport in electroactive polymers,” *Solid State Ionics* 60, 161–166 (1993).
  36. Kaneko, M.; Fukui, M.; Takashima, W.; Kaneto, K., “Electrolyte and strain dependences of chemomechanical deformation of polyaniline film,” *Synthetic Metals* 84(1–3), 795–796 (1997).
  37. Otero, T.F.; Sansinena, J.M., “Bilayer dimensions and movement in artificial muscles,” *Bioelectrochemistry and Bioenergetics* 42(2), 117–122 (1997).
  38. Plieth, W.; Bund, A.; Rammelt, U.; Neudeck, S.; Duc, L.M., “The role of ion and solvent transport during the redox process of conducting polymers,” *Electrochimica Acta* 51(11), 2366–2372 (2006).
  39. Bay, L.; Jacobsen, T.; Skaarup, S.; West, K., “Mechanism of actuation in conducting polymers: Osmotic expansion,” *The Journal of Physical Chemistry B* 105(36), 8492–8497 (2001).
  40. Heywang, G.; Jonas, F., “Poly (alkylenedioxythiophene)s – new, very stable conducting polymers,” *Advanced Materials* 4(2), 116–118 (1992).
  41. Schmidt, C.E.; Shastri, V.R.; Vacanti, J.P.; Langer, R., “Stimulation of neurite outgrowth using an electrically conducting polymer,” *Proceedings of the National Academy of Sciences of the USA* 94(17), 8948–8953 (1997).
  42. Debiecme-Chouvy, C., “A very thin overoxidized polypyrrole membrane as coating for fast time response and selective H<sub>2</sub>O<sub>2</sub> amperometric sensor,” *Biosensors and Bioelectronics* 25(11), 2454–2457 (2010).
  43. Li, J.; Lin, X.Q., “Electrodeposition of gold nanoclusters on overoxidized polypyrrole film modified glassy carbon electrode and its application for the simultaneous determination of epinephrine and uric acid under coexistence of ascorbic acid,” *Analytica Chimica Acta* 596(2), 222–230 (2007).
  44. Debiecme-Chouvy, C., “One-step electrochemical synthesis of a very thin overoxidized polypyrrole film,” *Electrochemical and Solid State Letters* 10(12), E24–E26 (2007).
  45. Nguyen T. Le, H.; Garcia, B.; Deslouis, C.; Le Xuan, Q., “Corrosion protection and conducting polymers: polypyrrole films on iron,” *Electrochimica Acta* 46(26–27), 4259–4272 (2001).
  46. Schlenoff, J.B.; Xu, H., “Evolution of Physical and Electrochemical Properties of Polypyrrole during Extended Oxidation,” *Journal of the Electrochemical Society* 139(9), 2397–2401 (1992).

47. Beck, F.; Barsch, U.; Michaelis, R., "Corrosion of Conducting Polymers in Aqueous-Media," *Journal of Electroanalytical Chemistry* 351(1–2), 169–184 (1993).
48. Xiao, Y.H.; Cui, X.Y.; Hancock, J.M.; Bouguettaya, M.B.; Reynolds, J.R.; Martin, D.C., "Electrochemical polymerization of poly(hydroxymethylated-3,4-ethylenedioxythiophene) (PEDOT-MeOH) on multichannel neural probes," *Sensors and Actuators B: Chemical* 99(2–3), 437–443 (2004).
49. Otero, T.F.; Rodriguez, J., "Parallel Kinetic-Studies of the Electrogeneration of Conducting Polymers – Mixed Materials, Composition and Properties Control," *Electrochimica Acta* 39(2), 245–253 (1994).
50. Malinauskas, A., "Chemical deposition of conducting polymers," *Polymer* 42(9), 3957–3972 (2001).
51. Sadki, S.; Schottland, P.; Brodie, N.; Sabouraud, G., "The mechanisms of pyrrole electropolymerization," *Chemical Society Reviews* 29(5), 283–293 (2000).
52. Lock, J.P.; Im, S.G.; Gleason, K.K., "Oxidative chemical vapor deposition of electrically conducting poly(3,4-ethylenedioxythiophene) films," *Macromolecules* 39(16), 5326–5329 (2006).
53. Otero, T.F.; Rodriguez, J., "Polythiophene Electrogeneration on a Rotating-Disk Electrode – the Influence of Water on Polymerization and Polymer Properties," *Journal of Electroanalytical Chemistry* 310(1–2), 219–237 (1991).
54. Marandi, M.; Kallip, S.; Matisen, L.; Tamm, J.; Sammelselg, V., "Formation of nanometric polypyrrole films on Au (111): A STM, SEM and XPS study," *Synthetic Metals* 162(1–2), 162–170 (2012).
55. Salmon, M.; Diaz, A.F.; Logan, A.J.; Krounbi, M.; Bargon, J., "Chemical Modification of Conducting Polypyrrole Films," *Molecular Crystals and Liquid Crystals* 83(1–4), 1297–1308 (1982).
56. Diaz, A.F.; Hall, B., "Mechanical-Properties of Electrochemically Prepared Polypyrrole Films," *IBM Journal of Research and Development* 27(4), 342–347 (1983).
57. Zama, T.; Hara, S.; Takashima, W.; Kaneto, K., "Comparison of conducting polymer actuators based on polypyrrole doped with  $\text{BF}_4^-$ ,  $\text{PF}_6^-$ ,  $\text{CF}_3\text{SO}_3^-$ , and  $\text{ClO}_4^-$ ," *Bulletin of the Chemical Society of Japan* 78(3), 506–511 (2005).
58. Zhang, X.; Zhang, J.; Song, W.; Liu, Z., "Controllable synthesis of conducting polypyrrole nanostructures," *The Journal of Physical Chemistry B* 110(3), 1158–1165 (2006).
59. Lawal, A.T.; Wallace, G.G., "Vapour phase polymerisation of conducting and non-conducting polymers: a review," *Talanta* 119, 133–143 (2014).
60. Bay, L.; West, K.; Skaarup, S., "Pentanol as co-surfactant in polypyrrole actuators," *Polymer* 43(12), 3527–3532 (2002).
61. Zheng, W.; Razal, J.M.; Spinks, G.M.; Truong, V.T.; Whitten, P.G.; Wallace, G.G., "The role of unbound oligomers in the nucleation and growth of electrodeposited polypyrrole and method for preparing high strength, high conductivity films," *Langmuir* 28(29), 10891–10897 (2012).
62. Yamaura, M.; Hagiwara, T.; Iwata, K., "Enhancement of electrical conductivity of polypyrrole film by stretching: Counter ion effect," *Synthetic Metals* 26(3), 209–224 (1988).
63. Stankovic, R.; Pavlovic, O.; Vojnovic, M.; Jovanovic, S., "The Effects of Preparation Conditions on the Properties of Electrochemically Synthesized Thick-Films of Polypyrrole," *European Polymer Journal* 30(3), 385–393 (1994).

64. Kaynak, A., "Effect of synthesis parameters on the surface morphology of conducting polypyrrole films," *Materials Research Bulletin* 32(3), 271–285 (1997).
65. Sakmeche, N.; Aaron, J.J.; Aeiyaeh, S.; Lacaze, P.C., "Usefulness of aqueous anionic micellar media for electrodeposition of poly-(3,4-ethylenedioxythiophene) films on iron, mild steel and aluminium," *Electrochimica Acta* 45(12), 1921–1931 (2000).
66. Tsakova, V.; Winkels, S.; Schultze, J.W., "Anodic polymerization of 3,4-ethylenedioxythiophene from aqueous microemulsions," *Electrochimica Acta* 46(5), 759–768 (2001).
67. Cohen, Y.S.; Levi, M.D.; Aurbach, D., "Micromorphological dynamics of polypyrrole films in propylene carbonate solutions studied by in situ AFM and EQCM," *Langmuir* 19(23), 9804–9811 (2003).
68. Yang, R.; Evans, D.F.; Christensen, L.; Hendrickson, W.A., "Scanning tunneling microscopy (STM) evidence of semicrystalline and helical conducting polymer structures," *The Journal of Physical Chemistry* 94(15), 6117–6122 (1990).
69. Caple, G.; Wheeler, B.L.; Swift, R.; Porter, T.L.; Jeffers, S., "Scanning Tunneling Microscopy of Polythiophene, Poly(3-Methylthiophene), and Poly(3-Bromothiophene)," *The Journal of Physical Chemistry* 94(15), 5639–5641 (1990).
70. Hwang, B.J.; Santhanam, R.; Lin, Y.L., "Evaluation of structure, nucleation and growth mechanism of electropolymerized polypyrrole on highly oriented pyrolytic graphite electrode," *Electroanalysis* 15(2), 115–120 (2003).
71. Hwang, B.J.; Santhanam, R.; Lin, Y.L., "Nucleation and growth mechanism of electroformation of polypyrrole on a heat-treated gold/highly oriented pyrolytic graphite," *Electrochimica Acta* 46(18), 2843–2853 (2001).
72. Randriamahazaka, H.; Noel, V.; Chevrot, C., "Nucleation and growth of poly(3,4-ethylenedioxythiophene) in acetonitrile on platinum under potentiostatic conditions," *Journal of Electroanalytical Chemistry* 472, 103–111 (1999).
73. Pigani, L.; Heras, A.; Colina, Á.; Seeber, R.; López-Palacios, J., "Electropolymerisation of 3,4-ethylenedioxythiophene in aqueous solutions," *Electrochemistry Communications* 6(11), 1192–1198 (2004).
74. Snook, G.A.; Kao, P.; Best, A.S., "Conducting-polymer-based supercapacitor devices and electrodes," *Journal of Power Sources* 196(1), 1–12 (2011).
75. Kudoh, Y., "Properties of polypyrrole prepared by chemical polymerization using aqueous solution containing  $\text{Fe}_2(\text{SO}_4)_3$  and anionic surfactant," *Synthetic Metals* 79(1), 17–22 (1996).
76. Raudsepp, T. "Influence of dopant anions on the electrochemical properties of polypyrrole films," Ph.D. dissertation, University of Tartu, Tartu 2010, 112 p.
77. Bar-Cohen, Y., "Electroactive Polymer (EAP) Actuators as Artificial Muscles: Reality, Potential, and Challenges, Second Edition," Vol. PM136 (816 p.), SPIE Press: Washington, USA (2004).
78. Carpi, F.; De Rossi, D.; Kornbluh, R.; Pelrine, R.; Sommer-Larsen, P., "Dielectric Elastomers as Electromechanical Transducers: Fundamentals, Materials, Devices, Models and Applications of an Emerging Electroactive Polymer Technology," First edition (344 p.), Elsevier: Amsterdam, Netherlands (2011).
79. Guiseppi-Elie, A., "An implantable biochip to influence patient outcomes following trauma-induced hemorrhage," *Anal Bioanal Chem* 399(1), 403–419 (2011).

80. Petricca, L.; Ohlckers, P.; Che, X., "The Future of Energy Storage Systems", in "Energy Storage – Technologies and Applications", 113–130, Editor A. Zobaa, InTech (2013).
81. Leclerc, M.; Najari, A., "Organic thermoelectrics: green energy from a blue polymer," *Nature Materials* 10(6), 409–410 (2011).
82. Pan, L.; Yu, G.; Zhai, D.; Lee, H.R.; Zhao, W.; Liu, N.; Wang, H.; Tee, B.C.; Shi, Y.; Cui, Y.; Bao, Z., "Hierarchical nanostructured conducting polymer hydrogel with high electrochemical activity," *Proceedings of the National Academy of Sciences of the USA* 109(24), 9287–9292 (2012).
83. Otero, T.F.; Martinez, J.G.; Arias-Pardilla, J., "Biomimetic electrochemistry from conducting polymers. A review Artificial muscles, smart membranes, smart drug delivery and computer/neuron interfaces," *Electrochimica Acta* 84, 112–128 (2012).
84. Fabre-Francke, I.; Aubert, P.H.; Alfonsi, S.; Vidal, F.; Sauques, L.; Chevrot, C., "Electropolymerization of 3,4-ethylenedioxythiophene within an insulating nitrile butadiene rubber network: Application to electroreflective surfaces and devices," *Solar Energy Materials and Solar Cells* 99, 109–115 (2012).
85. Burroughes, J.H.; Bradley, D.D.C.; Brown, A.R.; Marks, R.N.; Mackay, K.; Friend, R.H.; Burns, P.L.; Holmes, A.B., "Light-Emitting-Diodes Based on Conjugated Polymers," *Nature* 347(6293), 539–541 (1990).
86. Siringhaus, H.; Tessler, N.; Friend, R.H., "Integrated optoelectronic devices based on conjugated polymers," *Science* 280(5370), 1741–1744 (1998).
87. Kotov, N.A.; Winter, J.O.; Clements, I.P.; Jan, E.; Timko, B.P.; Campidelli, S.; Pathak, S.; Mazzatenta, A.; Lieber, C.M.; Prato, M.; Bellamkonda, R.V.; Silva, G.A.; Kam, N.W.S.; Patolsky, F.; Ballerini, L., "Nanomaterials for Neural Interfaces," *Advanced Materials* 21(40), 3970–4004 (2009).
88. Xu, L.; Chen, W.; Mulchandani, A.; Yan, Y., "Reversible conversion of conducting polymer films from superhydrophobic to superhydrophilic," *Angewandte Chemie International Edition* 44(37), 6009–6012 (2005).
89. Alici, G.; Huynh, N.N., "Predicting force output of trilayer polymer actuators," *Sensors and Actuators A: Physical* 132(2), 616–625 (2006).
90. Ding, J.; Liu, L.; Spinks, G.M.; Zhou, D.Z.; Wallace, G.G.; Gillespie, J., "High performance conducting polymer actuators utilising a tubular geometry and helical wire interconnects," *Synthetic Metals* 138(3), 391–398 (2003).
91. Otero, T.F.; Sansiena, J.M., "Soft and wet conducting polymers for artificial muscles," *Advanced Materials* 10(6), 491–494 (1998).
92. Vidal, F.; Plesse, C.; Teyssie, D.; Chevrot, C., "Long-life air working conducting semi-IPN/ionic liquid based actuator," *Synthetic Metals* 142(1–3), 287–291 (2004).
93. Federico, C.; Elisabeth, S., "Biomedical Applications of Electroactive Polymer Actuators," (496 p.), Wiley: Chippenham, United Kingdom (2009).
94. Madden, J.D.W.; Vandesteeg, N.A.; Anquetil, P.A.; Madden, P.G.A.; Takshi, A.; Pytel, R.Z.; Lafontaine, S.R.; Wieringa, P.A.; Hunter, I.W., "Artificial muscle technology: Physical principles and naval prospects," *IEEE Journal of Oceanic Engineering* 29(3), 706–728 (2004).
95. Mirfakhrai, T.; Madden, J.D.W.; Baughman, R.H., "Polymer artificial muscles," *Materials Today* 10(4), 30–38 (2007).
96. Kim, J.K.; Tadokoro, S., "Electroactive Polymers for Robotic Applications," *Artificial Muscles and Sensors* (291 p.), Springer: London, United Kingdom (2007).

97. Khaldi, A.; Plesse, C.; Soyer, C.; Troadec, D.; Vidal, F.; Cattan, E.; Chevrot, C.; Teysié, D. "Micro-beam actuator based on conducting interpenetrating polymer networks: From patterning process to actuation in open air," in 16th International Solid-State Sensors, Actuators and Microsystems Conference (Transducers), Beijing, China: IEEE (2011).
98. Alici, G.; Devaud, V.; Renaud, P.; Spinks, G., "Conducting polymer micro-actuators operating in air," *Journal of Micromechanics and Microengineering* 19(2), 1–9 (2009).
99. Bar-Cohen, Y.; Zhang, Q., "Electroactive Polymer Actuators and Sensors," *MRS Bulletin* 33(03), 173–181 (2011).
100. Baughman, R.H., "Conducting polymer artificial muscles," *Synthetic Metals* 78(3), 339–353 (1996).
101. Herod, T.E.; Schlenoff, J.B., "Doping-induced strain in polyaniline: stretcho-electrochemistry," *Chemistry of Materials* 5(7), 951–955 (1993).
102. Madden, J.D.; Madden, P.G.; Hunter, I.W. "Conducting polymer actuators as engineering materials," in *Proceeding of SPIE Smart Structures and Materials 2002: Electroactive Polymer Actuators and Devices*: SPIE Press, Bellingham, WA (2002).
103. Spinks, G.M.; Liu, L.; Wallace, G.G.; Zhou, D.Z., "Strain response from polypyrrole actuators under load," *Advanced Functional Materials* 12(6–7), 437–440 (2002).
104. Kaneto, K.; Kaneko, M.; Min, Y.; MacDiarmid, A.G., "'Artificial muscle': Electromechanical actuators using polyaniline films," *Synthetic Metals* 71(1–3), 2211–2212 (1995).
105. Lee, K.K.C.; Munce, N.R.; Shoa, T.; Charron, L.G.; Wright, G.A.; Madden, J.D.; Yang, V.X.D., "Fabrication and characterization of laser-micromachined polypyrrole-based artificial muscle actuated catheters," *Sensors and Actuators A: Physical* 153(2), 230–236 (2009).
106. Madden, J. D. "Conducting polymer actuators," Ph.D. dissertation, Massachusetts Institute of Technology, Cambridge 2000, 355 p.
107. Madden, J.D.; Cush, R.A.; Kanigan, T.S.; Brennan, C.J.; Hunter, I.W., "Encapsulated polypyrrole actuators," *Synthetic Metals* 105(1), 61–64 (1999).
108. Madden, J.D.; Cush, R.A.; Kanigan, T.S.; Hunter, I.W., "Fast contracting polypyrrole actuators," *Synthetic Metals* 113(1–2), 185–192 (2000).
109. Chu, S.Y.; Peng, H.; Kilmartin, P.A.; Bowmaker, G.A.; Cooney, R.P.; Travas-Sejdic, J., "Effect of deposition current density on the linear actuation behaviour of PPy(CF<sub>3</sub>SO<sub>3</sub>) films," *Current Applied Physics* 8(3–4), 324–327 (2008).
110. Smee, A., "Principles of the Human Mind, Deduced from Physical Laws: Together with a Lecture on Electro-biology, Or, the Voltaic Mechanism of Man," (64 p.), Fowler and Wells: New York, USA (1850).
111. Brochu, P.; Pei, Q., "Advances in dielectric elastomers for actuators and artificial muscles," *Macromolecular Rapid Communications* 31(1), 10–36 (2010).
112. De Rossi, D.; Della Santa, A.; Mazzoldi, A., "Dressware: wearable hardware," *Materials Science and Engineering: C* 7(1), 31–35 (1999).
113. Kruusamäe, K. "Deformation-dependent electrode impedance of ionic electro-mechanically active polymers," Ph.D. dissertation, University of Tartu, Tartu 2012, 128 p.



114. Akbari, S.; Shea, H.R., "An array of 100  $\mu\text{m}$  $\times$ 100  $\mu\text{m}$  dielectric elastomer actuators with 80% strain for tissue engineering applications," *Sensors and Actuators A: Physical* 186, 236–241 (2012).
115. Lehmann, W.; Skupin, H.; Tolksdorf, C.; Gebhard, E.; Zentel, R.; Kruger, P.; Losche, M.; Kremer, F., "Giant lateral electrostriction in ferroelectric liquid-crystalline elastomers," *Nature* 410(6827), 447–450 (2001).
116. Pelrine, R.; Kornbluh, R.; Pei, Q.B.; Joseph, J., "High-speed electrically actuated elastomers with strain greater than 100%," *Science* 287(5454), 836–839 (2000).
117. Zhang, Q.M.; Bharti, V.V.; Zhao, X., "Giant electrostriction and relaxor ferroelectric behavior in electron-irradiated poly(vinylidene fluoride-trifluoroethylene) copolymer," *Science* 280(5372), 2101–2104 (1998).
118. Nalwa, H.S., "Ferroelectric polymers: chemistry, physics, and applications," Vol. 28 (912 p.), CRC Press: New York, USA (1995).
119. Aliev, A.E.; Oh, J.; Kozlov, M.E.; Kuznetsov, A.A.; Fang, S.; Fonseca, A.F.; Ovalle, R.; Lima, M.D.; Haque, M.H.; Gartstein, Y.N.; Zhang, M.; Zakhidov, A.A.; Baughman, R.H., "Giant-stroke, superelastic carbon nanotube aerogel muscles," *Science* 323(5921), 1575–1578 (2009).
120. Asaka, K.; Oguro, K.; Nishimura, Y.; Mizuhata, M.; Takanaka, H., "Bending of polyelectrolyte membrane-platinum composites by electric stimuli. I: Response characteristics to various waveforms," *Polymer Journal* 27(4), 436–440 (1995).
121. Tanaka, T.; Nishio, I.; Sun, S.T.; Ueno-Nishio, S., "Collapse of gels in an electric field," *Science* 218, 467–469 (1982).
122. Baughman, R.H.; Cui, C.; Zakhidov, A.A.; Iqbal, Z.; Barisci, J.N.; Spinks, G.M.; Wallace, G.G.; Mazzoldi, A.; De Rossi, D.; Rinzler, A.G.; Jaschinski, O.; Roth, S.; Kertesz, M., "Carbon nanotube actuators," *Science* 284(5418), 1340–1344 (1999).
123. "Actuators – Danfoss," web page, cited: 03.05.2014, available from: <http://www.polypower.com/products/Actuators/ Danfoss Polypower A/S>.
124. Sarban, R. "Dynamic characterization, modeling, and control of PolyPower tubular DE actuators," in *EuroEAP 2011: First international conference on Electro-mechanically Active Polymer (EAP) transducers & artificial muscles*, Pisa (2011).
125. Otero, T.F.; Grande, H.; Rodriguez, J., "A New Model for Electrochemical Oxidation of Polypyrrole under Conformational Relaxation Control," *Journal of Electroanalytical Chemistry* 394(1–2), 211–216 (1995).
126. Lu, W.; Fadeev, A.G.; Qi, B.; Smela, E.; Mattes, B.R.; Ding, J.; Spinks, G.M.; Mazurkiewicz, J.; Zhou, D.; Wallace, G.G.; MacFarlane, D.R.; Forsyth, S.A.; Forsyth, M., "Use of ionic liquids for pi-conjugated polymer electrochemical devices," *Science* 297(5583), 983–987 (2002).
127. Sugino, T.; Kiyohara, K.; Takeuchi, I.; Mukai, K.; Asaka, K., "Actuator properties of the complexes composed by carbon nanotube and ionic liquid: The effects of additives," *Sensors and Actuators B: Chemical* 141(1), 179–186 (2009).
128. Hara, S.; Zama, T.; Takashima, W.; Kaneto, K., "Free-standing gel-like polypyrrole actuators doped with bis(perfluoroalkylsulfonyl)imide exhibiting extremely large strain," *Smart Materials & Structures* 14(6), 1501–1510 (2005).
129. Spinks, G.M.; Mottaghitalab, V.; Bahrami-Samani, M.; Whitten, P.G.; Wallace, G.G., "Carbon-Nanotube-Reinforced Polyaniline Fibers for High-Strength Artificial Muscles," *Advanced Materials* 18(5), 637–640 (2006).
130. Novák, P.; Müller, K.; Santhanam, K.S.V.; Haas, O., "Electrochemically active polymers for rechargeable batteries," *Chemical Reviews* 97(1), 207–282 (1997).

131. Sultana, I.; Rahman, M.M.; Li, S.; Wang, J.Z.; Wang, C.Y.; Wallace, G.G.; Liu, H.K., "Electrodeposited polypyrrole (PPy)/para (toluene sulfonic acid) (pTS) free-standing film for lithium secondary battery application," *Electrochimica Acta* 60, 201–205 (2012).
132. Levi, M.D.; Gofer, Y.; Aurbach, D., "A synopsis of recent attempts toward construction of rechargeable batteries utilizing conducting polymer cathodes and anodes," *Polymers for Advanced Technologies* 13(10–12), 697–713 (2002).
133. Wang, H.L.; Holt, C.M.B.; Li, Z.; Tan, X.H.; Amirkhiz, B.S.; Xu, Z.W.; Olsen, B.C.; Stephenson, T.; Mitlin, D., "Graphene-nickel cobaltite nanocomposite asymmetrical supercapacitor with commercial level mass loading," *Nano Research* 5(9), 605–617 (2012).
134. Wang, Y.C.; Tao, S.Y.; An, Y.L.; Wu, S.; Meng, C.G., "Bio-inspired high performance electrochemical supercapacitors based on conducting polymer modified coral-like monolithic carbon," *Journal of Materials Chemistry A* 1(31), 8876–8887 (2013).
135. Che, J.F.; Chen, P.; Chan-Park, M.B., "High-strength carbon nanotube buckypaper composites as applied to free-standing electrodes for supercapacitors," *Journal of Materials Chemistry A* 1(12), 4057–4066 (2013).
136. Pieta, P.; Obratsov, I.; D'Souza, F.; Kutner, W., "Composites of Conducting Polymers and Various Carbon Nanostructures for Electrochemical Supercapacitors," *ECS Journal of Solid State Science and Technology* 2(10), M3120–M3134 (2013).
137. Ragone, D.V., "Review of battery systems for electrically powered vehicles," SAE Technical Paper N<sup>o</sup> 680453, C.-M. Univ. (1968).
138. Pell, W.G.; Conway, B.E., "Quantitative modeling of factors determining Ragone plots for batteries and electrochemical capacitors," *Journal of Power Sources* 63(2), 255–266 (1996).
139. Ryan, E.M.; Breslin, C.B.; Moulton, S.E.; Wallace, G.G., "The effect of dopant  $pK_a$  and the solubility of corresponding acid on the electropolymerisation of pyrrole," *Electrochimica Acta* 92, 276–284 (2013).
140. Dreve, S.; Kacso, I.; Bratu, I.; Indrea, E., "Chitosan-based delivery systems for diclofenac delivery: preparation and characterization," *Journal of Physics: Conference Series* 182, 1–4 (2009).
141. Esrafilzadeh, D.; Razal, J.M.; Moulton, S.E.; Stewart, E.M.; Wallace, G.G., "Multifunctional conducting fibres with electrically controlled release of ciprofloxacin," *Journal of Controlled Release* 169(3), 313–320 (2013).
142. Smits, F.M., "Measurement of Sheet Resistivities with the Four-Point Probe," *Bell System Technical Journal* 37(3), 711–718 (1958).
143. De Levie, R., "The influence of surface roughness of solid electrodes on electrochemical measurements," *Electrochimica Acta* 10(2), 113–130 (1965).
144. Mukai, K.; Asaka, K.; Kiyohara, K.; Sugino, T.; Takeuchi, I.; Fukushima, T.; Aida, T., "High performance fully plastic actuator based on ionic-liquid-based bucky gel," *Electrochimica Acta* 53(17), 5555–5562 (2008).
145. Gaihre, B.; Ashraf, S.; Spinks, G.M.; Innis, P.C.; Wallace, G.G., "Comparative displacement study of bilayer actuators comprising of conducting polymers, fabricated from polypyrrole, poly(3,4-ethylenedioxythiophene) or poly(3,4-propylenedioxythiophene)," *Sensors and Actuators A: Physical* 193, 48–53 (2013).

146. Liang, W.B.; Lei, J.T.; Martin, C.R., "Effect of Synthesis Temperature on the Structure, Doping Level and Charge-Transport Properties of Polypyrrole," *Synthetic Metals* 52(2), 227–239 (1992).
147. Bay, L.; West, K.; Vlachopoulos, N.; Skaarup, S. "Potential profile in a conducting polymer strip," in SPIE's 8th Annual International Symposium on Smart Structures and Materials: International Society for Optics and Photonics (2001).
148. Careem, M.A.; Vidanapathirana, K.P.; Skaarup, S.; West, K., "Dependence of force produced by polypyrrole-based artificial muscles on ionic species involved," *Solid State Ionics* 175(1–4), 725–728 (2004).
149. Minato, R.; Alici, G.; McGovern, S.; Spinks, G. "Tri-layer conducting polymer actuators with variable dimensions," in The 14th International Symposium on: Smart Structures and Materials & Nondestructive Evaluation and Health Monitoring: International Society for Optics and Photonics (2007).
150. Smela, E.; Inganas, O.; Pei, Q.B.; Lundstrom, I., "Electrochemical Muscles – Micromachining Fingers and Corkscrews," *Advanced Materials* 5(9), 630–632 (1993).
151. Smela, E.; Kallenbach, M.; Holdenried, J., "Electrochemically driven polypyrrole bilayers for moving and positioning bulk micromachined silicon plates," *Journal of Microelectromechanical Systems* 8(4), 373–383 (1999).
152. Pyo, M.; Bohn, C.C.; Smela, E.; Reynolds, J.R.; Brennan, A.B., "Direct strain measurement of polypyrrole actuators controlled by the polymer/gold interface," *Chemistry of Materials* 15(4), 916–922 (2003).
153. Liu, Y.; Gan, Q.; Baig, S.; Smela, E., "Improving PPy adhesion by surface roughening," *The Journal of Physical Chemistry C* 111(30), 11329–11338 (2007).
154. Zhang, W.; Yang, F.K.; Pan, Z.; Zhang, J.; Zhao, B., "Bio-inspired dopamine functionalization of polypyrrole for improved adhesion and conductivity," *Macromolecular Rapid Communications* 35(3), 350–354 (2014).
155. Smela, E.; Inganas, O.; Lundstrom, I., "Conducting polymers as artificial muscles: challenges and possibilities," *Journal of Micromechanics and Microengineering* 3(4), 203–205 (1993).
156. Wu, Y.; Alici, G.; Spinks, G.M.; Wallace, G.G., "Fast trilayer polypyrrole bending actuators for high speed applications," *Synthetic Metals* 156(16–17), 1017–1022 (2006).
157. Wang, J.W.; Botelho, S.J.; Naguib, H.E.; Bazylak, A., "Development of a Novel Active Polypyrrole Trilayer Membrane," *ACS Sustainable Chemistry & Engineering* 1(2), 226–231 (2013).
158. Chen, X.W.; Xing, K.Z.; Inganas, O., "Electrochemically induced volume changes in poly(3,4-ethylenedioxythiophene)," *Chemistry of Materials* 8(10), 2439–2443 (1996).
159. Vidal, F.; Plesse, C.; Popp, J.F.; Chevrot, C.; Teyssie, D., "Feasibility of conducting semi-IPN based on PEO network and poly(3,4-ethylenedioxythiophene) in actuator design," *Journal of Applied Polymer Science* 90, 3569–3577 (2003).
160. Zainudeen, U.L.; Careem, M.A.; Skaarup, S., "PEDOT and PPy conducting polymer bilayer and trilayer actuators," *Sensors and Actuators B: Chemical* 134(2), 467–470 (2008).
161. Zainudeen, U.L.; Careem, M.A.; Skaarup, S. "Ionic motion in PEDOT and PPy conducting polymer bilayers," in *Solid State Ionics. Advanced Materials for Emerging Technologies*, (2006).

162. Omastova, M.; Micusik, M., "Polypyrrole coating of inorganic and organic materials by chemical oxidative polymerisation," *Chemical Papers* 66(5), 392–414 (2012).
163. Diaz, A.F.; Logan, J.A., "Electroactive Polyaniline Films," *Journal of Electroanalytical Chemistry* 111(1), 111–114 (1980).
164. Takeuchi, I.; Asaka, K.; Kiyohara, K.; Sugino, T.; Terasawa, N.; Mukai, K.; Fukushima, T.; Aida, T., "Electromechanical behavior of fully plastic actuators based on bucky gel containing various internal ionic liquids," *Electrochimica Acta* 54(6), 1762–1768 (2009).
165. Fukushima, T.; Asaka, K.; Kosaka, A.; Aida, T., "Fully Plastic Actuator through Layer-by-Layer Casting with Ionic-Liquid-Based Bucky Gel," *Angewandte Chemie International Edition* 44(16), 2410–2413 (2005).
166. Wang, K.; Wu, H.; Meng, Y.; Wei, Z., "Conducting polymer nanowire arrays for high performance supercapacitors," *Small* 10(1), 14–31 (2014).
167. Wang, H.; Zhang, L.; Tan, X.; Holt, C.M.B.; Zahiri, B.; Olsen, B.C.; Mitlin, D., "Supercapacitive Properties of Hydrothermally Synthesized  $\text{Co}_3\text{O}_4$  Nanostructures," *The Journal of Physical Chemistry C* 115(35), 17599–17605 (2011).
168. Kadyk, T.; Eikerling, M. "Moving Reaction Fronts in Supercapacitors With Pseudocapacitance," in *Meeting Abstracts: The Electrochemical Society* (2013).
169. Siddhanta, S.K.; Gangopadhyay, R., "Conducting polymer gel: formation of a novel semi-IPN from polyaniline and crosslinked poly (2-acrylamido-2-methyl propanesulphonicacid)," *Polymer* 46(9), 2993–3000 (2005).
170. Tang, Q.W.; Wu, J.H.; Sun, H.; Fan, S.J.; Hu, D.; Lin, J.M., "Superabsorbent conducting hydrogel from poly(acrylamide-aniline) with thermo-sensitivity and release properties," *Carbohydrate Polymers* 73(3), 473–481 (2008).
171. Guo, B.L.; Finne-Wistrand, A.; Albertsson, A.C., "Degradable and Electroactive Hydrogels with Tunable Electrical Conductivity and Swelling Behavior," *Chemistry of Materials* 23(5), 1254–1262 (2011).
172. Pépin-Donat, B.; Viallat, A.; Blachot, J.F.; Lombard, C., "Electromechanical Polymer Gels Combining Rubber Elasticity with Electronic Conduction," *Advanced Materials* 18(11), 1401–1405 (2006).
173. Chen, L.; Kim, B.; Nishino, M.; Gong, J.P.; Osada, Y., "Environmental responses of polythiophene hydrogels," *Macromolecules* 33(4), 1232–1236 (2000).
174. Tsai, T.S.; Pillay, V.; Choonara, Y.E.; du Toit, L.C.; Modi, G.; Naidoo, D.; Kumar, P., "A Polyvinyl Alcohol-Polyaniline Based Electro-Conductive Hydrogel for Controlled Stimuli-Actuable Release of Indomethacin," *Polymers* 3(1), 150–172 (2011).
175. Lin, J.; Tang, Q.; Wu, J.; Li, Q., "A multifunctional hydrogel with high-conductivity, pH-responsive, and release properties from polyacrylate/polypyrrole," *Journal of Applied Polymer Science* 116, 1376–1383 (2009).
176. Du, R.; Zhang, X.T., "Alkoxysulfonate-Functionalized Poly(3,4-ethylenedioxythiophene) Hydrogels," *Acta Physico-Chimica Sinica* 28(10), 2305–2314 (2012).
177. Ghosh, S.; Inganas, O., "Conducting polymer hydrogels as 3D electrodes: Applications for supercapacitors," *Advanced Materials* 11(14), 1214–1218 (1999).
178. Ghosh, S.; Inganas, O., "Nano-structured conducting polymer network based on PEDOT-PSS," *Synthetic Metals* 121(1–3), 1321–1322 (2001).

179. Ghosh, S.; Inganäs, O., “Electrochemical Characterization of Poly (3, 4-ethylene dioxithiophene) Based Conducting Hydrogel Networks,” *Journal of the Electrochemical Society* 147(5), 1872–1877 (2000).
180. Kim, B.C.; Spinks, G.; Too, C.O.; Wallace, G.G.; Bae, Y.H., “Preparation and characterisation of processable conducting polymer-hydrogel composites,” *Reactive and Functional Polymers* 44(1), 31–40 (2000).
181. Harreld, J.; Wong, H.P.; Dave, B.C.; Dunn, B.; Nazar, L.F., “Synthesis and properties of polypyrrole-vanadium oxide hybrid aerogels,” *Journal of Non-Crystalline Solids* 225, 319–324 (1998).
182. Bai, H.; Sheng, K.X.; Zhang, P.F.; Li, C.; Shi, G.Q., “Graphene oxide/conducting polymer composite hydrogels,” *Journal of Materials Chemistry* 21(46), 18653–18658 (2011).
183. Wei, D.L.; Lin, X.; Li, L.; Shang, S.M.; Yuen, M.C.W.; Yan, G.P.; Yu, X.H., “Controlled growth of polypyrrole hydrogels,” *Soft Matter* 9(10), 2832–2836 (2013).
184. Du, R.; Xu, Y.; Luo, Y.; Zhang, X.; Zhang, J., “Synthesis of conducting polymer hydrogels with 2D building blocks and their potential-dependent gel-sol transitions,” *Chemical Communications* 47(22), 6287–6289 (2011).
185. Dearmitt, C.; Armes, S.P., “Colloidal Dispersions of Surfactant-Stabilized Polypyrrole Particles,” *Langmuir* 9(3), 652–654 (1993).
186. Pekala, R.W.; Kong, F.M. “Resorcinol-formaldehyde aerogels and their carbonized derivatives,” in *Abstracts of Papers of the American Chemical Society: American Chemical Society* (1989).
187. An, H.F.; Wang, Y.; Wang, X.Y.; Zheng, L.P.; Wang, X.Y.; Yi, L.H.; Bai, L.; Zhang, X.Y., “Polypyrrole/carbon aerogel composite materials for supercapacitor,” *Journal of Power Sources* 195(19), 6964–6969 (2010).
188. Wong, H.P.; Dave, B.C.; Leroux, F.; Harreld, J.; Dunn, B.; Nazar, L.F., “Synthesis and characterization of polypyrrole vanadium pentoxide nanocomposite aerogels,” *Journal of Materials Chemistry* 8(4), 1019–1027 (1998).
189. Xu, Y.Z.; Sui, Z.Y.; Xu, B.; Duan, H.; Zhang, X.T., “Emulsion template synthesis of all conducting polymer aerogels with superb adsorption capacity and enhanced electrochemical capacitance,” *Journal of Materials Chemistry* 22(17), 8579–8584 (2012).
190. Wei, L.; Sevilla, M.; Fuertes, A.B.; Mokaya, R.; Yushin, G., “Polypyrrole-Derived Activated Carbons for High-Performance Electrical Double-Layer Capacitors with Ionic Liquid Electrolyte,” *Advanced Functional Materials* 22(4), 827–834 (2012).
191. Qi, K.; Qiu, Y.; Chen, Z.; Guo, X., “Corrosion of conductive polypyrrole: Effects of possibly formed galvanic cells,” *Corrosion Science* 80, 318–330 (2014).
192. Pérez-Caballero, F.; Peikolainen, A.-L.; Uibu, M.; Kuusik, R.; Volobujeva, O.; Koel, M., “Preparation of carbon aerogels from 5-methylresorcinol-formaldehyde gels,” *Microporous and Mesoporous Materials* 108(1), 230–236 (2008).
193. Kiefer, R.B.; Bowmaker, G.A.; Kilmartin, P.A.; Travas-Sejdic, J., “Effect of polymerization potential on the actuation of free standing poly-3,4-ethylenedioxythiophene films in a propylene carbonate electrolyte,” *Electrochimica Acta* 55(3), 681–688 (2010).
194. Travas-Sejdic, J.; Tamm, T.; Kilmartin, P.A.; Temmer, R.; Aabloo, A.; Kiefer, R. “PEDOT/TBACF<sub>3</sub>SO<sub>3</sub> bending actuators based on a PEDOT-PEDOT sandwich

- complex,” in *Electroactive Polymer Actuators and Devices (EAPAD) 2013*, San Diego, California, USA (2013).
195. Gaihre, B.; Alici, G.; Spinks, G.M.; Cairney, J.M., “Effect of electrolyte storage layer on performance of PPy-PVDF-PPy microactuators,” *Sensors and Actuators B: Chemical* 155(2), 810–816 (2011).
  196. Dziewoński, P.M.; Grzeszczuk, M., “Impact of the electrochemical porosity and chemical composition on the lithium ion exchange behavior of polypyrroles (ClO<sub>4</sub><sup>-</sup>, TOS<sup>-</sup>, TFSI<sup>-</sup>) prepared electrochemically in propylene carbonate. Comparative EQCM, EIS and CV studies,” *The Journal of Physical Chemistry B* 114(21), 7158–7171 (2010).
  197. Cao, J.H.; Zhu, B.K.; Xu, Y.Y., “Structure and ionic conductivity of porous polymer electrolytes based on PVDF-HFP copolymer membranes,” *Journal of Membrane Science* 281(1–2), 446–453 (2006).
  198. Isidorsson, J.; Stromme, M.; Gahlin, R.; Niklasson, G.A.; Granqvist, C.G., “Ion transport in porous Sn oxide films: Cyclic voltammograms interpreted in terms of a fractal dimension,” *Solid State Communications* 99(2), 109–111 (1996).
  199. Kim, B.C.; Too, C.O.; Kwon, J.S.; Bo, J.M.; Wallace, G.G., “A flexible capacitor based on conducting polymer electrodes,” *Synthetic Metals* 161(11–12), 1130–1132 (2011).
  200. Ryu, K.S.; Lee, Y.G.; Kim, K.M.; Park, Y.J.; Hong, Y.S.; Wu, X.L.; Kang, M.G.; Park, N.G.; Song, R.Y.; Ko, J.M., “Electrochemical capacitor with chemically polymerized conducting polymer based on activated carbon as hybrid electrodes,” *Synthetic Metals* 153(1–3), 89–92 (2005).
  201. Brunauer, S.; Emmett, P.H.; Teller, E., “Adsorption of gases in multimolecular layers,” *Journal of the American Chemical Society* 60(2), 309–319 (1938).
  202. Lastoskie, C.; Gubbins, K.E.; Quirke, N., “Pore-Size Distribution Analysis of Microporous Carbons – a Density-Functional Theory Approach,” *The Journal of Physical Chemistry* 97(18), 4786–4796 (1993).
  203. Nishida, T.; Nishikawa, K.; Fukunaka, Y., “Diffusivity Measurement of LiPF<sub>6</sub>, LiTFSI, LiBF<sub>4</sub> in PC,” *ECS Transactions* 6(18), 1–14 (2008).
  204. Tokuda, H.; Hayamizu, K.; Ishii, K.; Susan, M.A.; Watanabe, M., “Physico-chemical properties and structures of room temperature ionic liquids. 2. Variation of alkyl chain length in imidazolium cation,” *The Journal of Physical Chemistry B* 109(13), 6103–6110 (2005).
  205. Leceta, I.; Guerrero, P.; de la Caba, K., “Functional properties of chitosan-based films,” *Carbohydrate Polymers* 93(1), 339–346 (2013).
  206. Machida, S.; Miyata, S.; Techagumpuch, A., “Chemical Synthesis of Highly Electrically Conductive Polypyrrole,” *Synthetic Metals* 31(3), 311–318 (1989).
  207. Thieblemont, J.C.; Planche, M.F.; Petrescu, C.; Bouvier, J.M.; Bidan, G., “Stability of Chemically Synthesized Polypyrrole Films,” *Synthetic Metals* 59(1), 81–96 (1993).
  208. Omastova, M.; Trchova, M.; Kovarova, J.; Stejskal, J., “Synthesis and structural study of polypyrroles prepared in the presence of surfactants,” *Synthetic Metals* 138(3), 447–455 (2003).
  209. Ritthidej, G.C.; Phaechamud, T.; Koizumi, T., “Moist heat treatment on physico-chemical change of chitosan salt films,” *International Journal of Pharmaceutics* 232(1–2), 11–22 (2002).

210. Han, Y.H.; Travas-Sejdic, J.; Wright, B.; Yim, J.H., "Simultaneous Vapor-Phase Polymerization of PEDOT and a Siloxane into Organic/Inorganic Hybrid Thin Films," *Macromolecular Chemistry and Physics* 212(5), 521–530 (2011).
211. Oh, E.J.; Jang, K.S.; Park, S.Y.; Han, S.S.; Suh, J.S., "Electrochemical synthesis and characterization of stretchable polypyrrole films," *Molecular Crystals and Liquid Crystals* 371(1), 243–246 (2001).
212. Maw, S.; Smela, E.; Yoshida, K.; Sommer-Larsen, P.; Stein, R.B., "The effects of varying deposition current density on bending behaviour in PPy(DBS)-actuated bending beams," *Sensors and Actuators A: Physical* 89(3), 175–184 (2001).
213. Sakmeche, N.; Aeiyaeh, S.; Aaron, J.J.; Jouini, M.; Lacroix, J.C.; Lacaze, P.C., "Improvement of the electrosynthesis and physicochemical properties of poly(3,4-ethylenedioxythiophene) using a sodium dodecyl sulfate micellar aqueous medium," *Langmuir* 15(7), 2566–2574 (1999).
214. Hautiere-Cristofini, F.; Kuffer, D.; Yu, L.T., "Preparation and Study of Properties, Exchange and Continuous Current Conductivity of Pyrrole Oxidation-products," *C. R. Acad. Sci. Paris, Ser. C* 277(24), 1323–1326 (1973).
215. Benslimane, M.; Gravesen, P.; West, K.; Bay, L.; Skaarup, S. "Conducting polymer materials and their mechanical properties for actuation: the case of polypyrrole," in *Proc 7th Int Conf New Actuators*, Bremen, Germany, (2000).
216. Garcia, B.; Belanger, D., "Electrochemical preparation and characterization of polypyrrole doped with bis(trifluoromethanesulfone)imide anions," *Synthetic Metals* 98(2), 135–141 (1998).
217. Kameda, Y.; Umebayashi, Y.; Takeuchi, M.; Wahab, M.A.; Fukuda, S.; Ishiguro, S.; Sasaki, M.; Amo, Y.; Usuki, T., "Solvation structure of Li<sup>+</sup> in concentrated LiPF<sub>6</sub>-propylene carbonate solutions," *The Journal of Physical Chemistry B* 111(22), 6104–6109 (2007).
218. Bonhote, P.; Dias, A.P.; Papageorgiou, N.; Kalyanasundaram, K.; Gratzel, M., "Hydrophobic, Highly Conductive Ambient-Temperature Molten Salts," *Inorganic Chemistry* 35(5), 1168–1178 (1996).
219. John, S.W. "Modelling and control of conducting polymer actuators," Ph.D. dissertation, University of Wollongong, Wollongong 2008, 141 p.
220. Steidel, R.F., "An introduction to mechanical vibrations. Third Edition.," (464 p.), Wiley (1989).
221. John, S.W.; Alici, G.; Cook, C. "Frequency response of polypyrrole trilayer actuator displacement," in *The 15th International Symposium on: Smart Structures and Materials & Nondestructive Evaluation and Health Monitoring: International Society for Optics and Photonics* (2008).
222. Pillai, P.V. "Development and characterization of conducting polymer actuators," Ph.D. dissertation, Massachusetts Institute of Technology, Cambridge 2011, 127 p.
223. Alici, G.; Huynh, N.N., "Performance quantification of conducting polymer actuators for real applications: A microgripping system," *IEEE – ASME Transactions on Mechatronics* 12(1), 73–84 (2007).
224. Tadesse, Y.; Grange, R.W.; Priya, S., "Synthesis and cyclic force characterization of helical polypyrrole actuators for artificial facial muscles," *Smart Materials & Structures* 18(8), 1–17 (2009).
225. Wang, J.; Xu, Y.; Wang, J.; Zhu, J.; Bai, Y.; Xiong, L., "Study on capacitance evolving mechanism of polypyrrole during prolonged cycling," *The Journal of Physical Chemistry B* 118(5), 1353–1362 (2014).

226. Bronshtein, I.N.; Semendyayev, K.A.; Musiol, G.; Muehlig, H., "Handbook of mathematics, 5th ed.," 5th ed. Vol. 3 (1208 p.), Springer: New York, USA (2007).
227. Sonoda, Y.; Takashima, W.; Kaneto, K., "Characteristics of soft actuators based on polypyrrole films," *Synthetic Metals* 119(1-3), 267-268 (2001).
228. Yamato, K.; Tominaga, K.; Takashima, W.; Kaneto, K., "Stability of electrochemomechanical strains in polypyrrole films using ionic liquids," *Synthetic Metals* 159(9-10), 839-842 (2009).
229. Lasia, A., "Electrochemical impedance spectroscopy and its applications", in "Modern aspects of electrochemistry", 143-248, Editor, Kluwer Academic/Plenum Publishers: New York (1999).
230. Ho, C.; Raistrick, I.D.; Huggins, R.A., "Application of A-C Techniques to the Study of Lithium Diffusion in Tungsten Trioxide Thin Films," *Journal of the Electrochemical Society* 127(2), 343-350 (1980).
231. Knoblich, B.; Gerber, T., "Aggregation in SiO<sub>2</sub> sols from sodium silicate solutions," *Journal of Non-Crystalline Solids* 283(1), 109-113 (2001).
232. Jullien, R. "Les phénomènes d'agrégation et les agrégats fractals," in *Annales des télécommunications*: Springer (1986).
233. Yang, K.L.; Ying, T.Y.; Yiacoumi, S.; Tsouris, C.; Vittoratos, E.S., "Electro-sorption of ions from aqueous solutions by carbon aerogel: An electrical double-layer model," *Langmuir* 17(6), 1961-1969 (2001).



## **7 PUBLICATIONS**

## 8 APPENDICES

### 8.1 Experiment planning for the ECMD characterization of tri-layer bending actuators

#### 8.1.1 Bending actuator model for strain difference calculation

Following the equations based on the more specific **Figure 8.1**, it is possible to calculate the trajectory of every chosen point along the actuator at different strain difference values as well as the transformation of the actuator tip coordinates to strain difference and to model the actuator's shape at the chosen strain difference values. The same assumptions were used (uniform curvature, constant actuator length and curvature being proportional to strain difference).

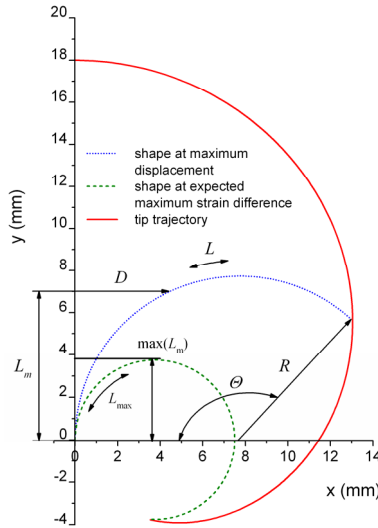


**Figure 8.1.** Bending actuator shape and tip movement depending on strain difference (actuator width not shown, the free length of the actuator,  $L$  is 18 mm).

#### 8.1.2 Conversion from tip displacement to strain difference

Knowing only the length, the thickness and the peak displacement value of the actuator, the following equations were used (derived from **Figure 8.1**):

$$\frac{D}{l} = \frac{[1 - \cos(\Theta)]}{\Theta}, \quad (8.1)$$

where  $l$  is the free length of the actuator. After substitution on the left side, Eq. (8.1) can be solved numerically for  $\Theta$ , using the Newton's method:

$$u = \frac{D}{l}, \quad 0 \leq \Theta \leq \pi, \quad \text{with the initial value and iteration, respectively:} \quad (8.2)$$

$$\Theta_0 = 2 \cdot u, \quad (8.3)$$

$$\Theta_{n+1} = \Theta_n - \frac{\cos(\Theta_n) + u \cdot \Theta_n - 1}{-\sin(\Theta_n) + u}. \quad (8.4)$$

Additionally, from **Figure 8.1** and using Eq. (1.23),

$$R = \frac{l}{\Theta}, \quad (8.5)$$

$$\varepsilon \cong \frac{w}{R}. \quad (8.6)$$

Naming coordinates of any given point along the actuator as  $x, y$  (**Figure 8.1**):

$$\cos(\Theta) = \frac{R - x}{R}, \quad (8.7)$$

$$\sin(\Theta) = y. \quad (8.8)$$

Solving equations (8.7) and (8.8) for  $x$  and  $y$ , respectively, yields:

$$x = R \cdot [1 - \cos(\Theta)], \quad (8.9)$$

$$y = R \cdot \sin(\Theta). \quad (8.10)$$

### **8.1.3 Trajectory of chosen point along actuator depending on maximum strain difference**

By fixing the length  $l$  of the actuator (or by choosing any point on distance  $l$  along the actuator) and varying  $\Theta$ :  $0 \leq \Theta \leq \Theta_{\max}$ , where

$$\Theta_{\max} = \frac{l}{R_{\max}} \cong \frac{l \cdot \varepsilon_{\max}}{w}, \quad (8.11)$$

and calculating  $R$  for every  $\Theta$  value from Eq. (8.5), then equations (8.9) and (8.10) give the trajectory of the actuator tip (or any chosen point on distance  $l$  from clamped end and along the actuator) during bending (**Figure 8.1**).

#### 8.1.4 Actuator's shape at chosen strain difference

By fixing  $\varepsilon$  and varying  $\Theta$ :  $0 \leq \Theta \leq \Theta_{max}$ , where

$$\Theta_{max} = \frac{l}{R} \cong \frac{l \cdot \varepsilon}{w}, \text{ and using} \quad (8.12)$$

$$R \cong \frac{w}{\varepsilon}, \quad (8.13)$$

from Eq. (8.6), then equations (8.9) and (8.10) give the shape of the actuator at strain difference  $\varepsilon$  (**Figure 8.1**).

# CURRICULUM VITAE

**Name:** Rauno Temmer  
**Born:** 1970, Tartu, Estonia  
**Citizenship:** Estonian  
**E-mail:** rauno.temmer@ut.ee

## Education:

2010 onwards University of Tartu, Faculty of Science and Technology,  
doctoral studies in Engineering and Technology  
1996 ... 1999 University of Tartu, M.Sc. in physics, 1999  
1988 ... 1993 University of Tartu, B.Sc. in physics, 1993  
1977 ... 1988 14<sup>th</sup> Secondary School of Tartu

## Employment:

2005 ... 2009 Estonian Informatics Centre (public sector, ICT, area  
manager)  
2005 Hansabank (project manager)  
1998 ... 2003 Estonian Traffic Insurance Fund (public sector, CIO)  
1997 ... 1998 Estonian Consumers` Co-operatives, CIO  
1994 ... 1997 University of Tartu, IT manager of physics department

## International research experience:

1. Research Training Program (03/2012 ... 07/2012, University of Wollongong, Australia);
2. Scientific program between the University of Tartu and the University of Cergy-Pontoise – Egide Program – PHC Parrot 2011 (Ph.D. student, 11/2011 ... 12/2011, France).

## Publications:

– *1.1. Scholarly articles indexed by Thomson Reuters Web of Science:*

1. Kiefer, R.; Aydemir, N.; Torop, J.; Tamm, T.; **Temmer, R.**; Travas-Sejdic, J.; Must, I.; Kaasik, F.; Aabloo, A., “Carbide-derived carbon as active interlayer of polypyrrole tri-layer linear actuator,” *Sensors and Actuators B: Chemical* (2014 (*Forthcoming*)).
2. Kilmartin, P.A.; Travas-Sejdic, J.; **Temmer, R.**; Tamm, T.; Aabloo, A.; Kiefer, R., “PEDOT-PSS/MWCNT coatings on PET for conducting polymer actuators,” *International Journal of Nanotechnology* 11(5–8), 477–485 (2014).
3. Kiefer, R.; **Temmer, R.**; Aydemir, N.; Travas-Sejdic, J.; Aabloo, A.; Tamm, T., “Electrochemistry of interlayer supported polypyrrole tri-layer linear actuators,” *Electrochimica Acta* 122, 322–328 (2014).
4. **Temmer, R.**; Kiefer, R.; Aabloo, A.; Tamm, T., “Direct chemical synthesis of pristine polypyrrole hydrogels and their derived aerogels for high power

- density energy storage applications,” *Journal of Materials Chemistry A* 1(48), 15216–15219 (2013).
5. **Temmer, R.**; Maziz, A.; Plesse, C.; Aabloo, A.; Vidal, F.; Tamm, T., “In search of better electroactive polymer actuator materials: PPy versus PEDOT versus PEDOT-PPy composites,” *Smart Materials and Structures* 22(10), 104006 (2013).
  6. Kiefer, R.; **Temmer, R.**; Tamm, T.; Travas-Sejdic, J.; Kilmartin, P.A.; Aabloo, A., “Conducting polymer actuators formed on MWCNT and PEDOT-PSS conductive coatings,” *Synthetic Metals* 171, 69–75 (2013).
  7. Lee, R.-J.; **Temmer, R.**; Tamm, T.; Aabloo, A.; Kiefer, R., “Renewable antioxidant properties of suspensible chitosan-polypyrrole composites,” *Reactive and Functional Polymers* 73(8), 1072–1077 (2013).
  8. Lee, R.-J.; Tamm, T.; **Temmer, R.**; Aabloo, A.; Kiefer, R., “Two formation mechanisms and renewable antioxidant properties of suspensible chitosan-PPy and chitosan-PPy-BTDA composites,” *Synthetic Metals* 164, 6–11 (2013).
  9. **Temmer, R.**; Must, I.; Kaasik, F.; Aabloo, A.; Tamm, T., “Combined chemical and electrochemical synthesis methods for metal-free polypyrrole actuators,” *Sensors and Actuators B: Chemical* 166, 411–418 (2012).
- *3.1. Articles in collections indexed by the Thomson Reuters Conference Proceedings Citation Index:*
1. Travas-Sejdic, J.; Tamm, T.; Kilmartin, P.A.; **Temmer, R.**; Aabloo, A.; Kiefer, R. “PEDOT/TBACF<sub>3</sub>SO<sub>3</sub> bending actuators based on a PEDOT-PEDOT sandwich complex,” in *Electroactive Polymer Actuators and Devices (EAPAD) 2013*, San Diego, California, USA (2013).
  2. Kaasik, F.; Must, I.; Lust, E.; Jürgens, M.; Presser, V.; Punning, A.; **Temmer, R.**; Kiefer, R.; Aabloo, A. “In situ measurements with CPC micro-actuators using SEM,” in *Proceedings SPIE, Electroactive Polymer Actuators and Devices (EAPAD) 2014*, San Diego, California, USA (2014).

# ELULOOKIRJELDUS

**Nimi:** Rauno Temmer  
**Sünniaeg ja koht:** 1970, Tartu, Eesti  
**Kodakondsus:** Eesti  
**E-post:** rauno.temmer@ut.ee

## Hariduskäik:

alates 2010 Tartu Ülikool, loodus- ja tehnoloogiateaduskond, tehnika ja tehnoloogia doktorantuur  
1996 ... 1999 Tartu Ülikool, füüsika- ja keemiateaduskond, füüsika teadusmagister  
1988 ... 1993 Tartu Ülikool, füüsika- ja keemiateaduskond, bakalaureusekraad füüsikas  
1977 ... 1988 Tartu 14. Keskkool

## Teenistuskäik:

2005 ... 2009 Riigi Infosüsteemide Arenduskeskus (valdkonnajuht)  
2005 Hansapank (projektijuht)  
1998 ... 2003 Eesti Liikluskindlustuse Fond (infoosakonna juhataja, arendusdirektor)  
1997 ... 1998 Eesti Tarbijateühistute Keskühistu (peainfoloog)  
1994 ... 1997 Tartu Ülikool, füüsikaosakonna IT juht

## Rahvusvahelise teadustöö kogemus:

1. Uurimistöö õppeprogramm (03/2012 ... 07/2012, Wollongongi Ülikool, Austraalia);
2. Tartu Ülikooli ja Cergy-Pontoise Ülikooli vaheline teadusliku koostöö programm – Egide-Parrot 2011 (Ph.D. üliõpilane, 11/2011 ... 12/2011, Prantsusmaa).

## Publikatsioonid:

- *1.1. Teadusartiklid, mis on kajastatud Thomson Reuters Web of Science andmebaasis:*
1. Kiefer, R.; Aydemir, N.; Torop, J.; Tamm, T.; **Temmer, R.**; Travas-Sejdic, J.; Must, I.; Kaasik, F.; Aabloo, A., “Carbide-derived carbon as active interlayer of polypyrrole tri-layer linear actuator,” *Sensors and Actuators B: Chemical* (2014 (*Forthcoming*)).
  2. Kilmartin, P.A.; Travas-Sejdic, J.; **Temmer, R.**; Tamm, T.; Aabloo, A.; Kiefer, R., “PEDOT-PSS/MWCNT coatings on PET for conducting polymer actuators,” *International Journal of Nanotechnology* 11(5–8), 477–485 (2014).

3. Kiefer, R.; **Temmer, R.**; Aydemir, N.; Travas-Sejdic, J.; Aabloo, A.; Tamm, T., "Electrochemistry of interlayer supported polypyrrole tri-layer linear actuators," *Electrochimica Acta* 122, 322–328 (2014).
  4. **Temmer, R.**; Kiefer, R.; Aabloo, A.; Tamm, T., "Direct chemical synthesis of pristine polypyrrole hydrogels and their derived aerogels for high power density energy storage applications," *Journal of Materials Chemistry A* 1(48), 15216–15219 (2013).
  5. **Temmer, R.**; Maziz, A.; Plesse, C.; Aabloo, A.; Vidal, F.; Tamm, T., "In search of better electroactive polymer actuator materials: PPy versus PEDOT versus PEDOT-PPy composites," *Smart Materials and Structures* 22(10), 104006 (2013).
  6. Kiefer, R.; **Temmer, R.**; Tamm, T.; Travas-Sejdic, J.; Kilmartin, P.A.; Aabloo, A., "Conducting polymer actuators formed on MWCNT and PEDOT-PSS conductive coatings," *Synthetic Metals* 171, 69–75 (2013).
  7. Lee, R.-J.; **Temmer, R.**; Tamm, T.; Aabloo, A.; Kiefer, R., "Renewable antioxidant properties of suspensible chitosan-polypyrrole composites," *Reactive and Functional Polymers* 73(8), 1072–1077 (2013).
  8. Lee, R.-J.; Tamm, T.; **Temmer, R.**; Aabloo, A.; Kiefer, R., "Two formation mechanisms and renewable antioxidant properties of suspensible chitosan-PPy and chitosan-PPy-BTDA composites," *Synthetic Metals* 164, 6–11 (2013).
  9. **Temmer, R.**; Must, I.; Kaasik, F.; Aabloo, A.; Tamm, T., "Combined chemical and electrochemical synthesis methods for metal-free polypyrrole actuators," *Sensors and Actuators B: Chemical* 166, 411–418 (2012).
- *3.1. Artiklid Thomson Reuters Conference Proceedings Citation Index poolt refereeritud kogumikus:*
1. Travas-Sejdic, J.; Tamm, T.; Kilmartin, P.A.; **Temmer, R.**; Aabloo, A.; Kiefer, R. "PEDOT/TBACF<sub>3</sub>SO<sub>3</sub> bending actuators based on a PEDOT-PEDOT sandwich complex," in *Electroactive Polymer Actuators and Devices (EAPAD) 2013*, San Diego, California, USA (2013).
  2. Kaasik, F.; Must, I.; Lust, E.; Jürgens, M.; Presser, V.; Punning, A.; **Temmer, R.**; Kiefer, R.; Aabloo, A. "In situ measurements with CPC micro-actuators using SEM," in *Proceedings SPIE, Electroactive Polymer Actuators and Devices (EAPAD) 2014*, San Diego, California, USA (2014).



# DISSERTATIONES TECHNOLOGIAE UNIVERSITATIS TARTUENSIS

1. **Imre Mäger.** Characterization of cell-penetrating peptides: Assessment of cellular internalization kinetics, mechanisms and bioactivity. Tartu 2011, 132 p.
2. **Taavi Lehto.** Delivery of nucleic acids by cell-penetrating peptides: application in modulation of gene expression. Tartu 2011, 155 p.
3. **Hannes Luidalepp.** Studies on the antibiotic susceptibility of *Escherichia coli*. Tartu 2012, 111 p.
4. **Vahur Zadin.** Modelling the 3D-microbattery. Tartu 2012, 149 p.
5. **Janno Torop.** Carbide-derived carbon-based electromechanical actuators. Tartu 2012, 113 p.
6. **Julia Suhorutšenko.** Cell-penetrating peptides: cytotoxicity, immunogenicity and application for tumor targeting. Tartu 2012, 139 p.
7. **Viktoryia Shyp.** G nucleotide regulation of translational GTPases and the stringent response factor RelA. Tartu 2012, 105 p.
8. **Mardo Kõivomägi.** Studies on the substrate specificity and multisite phosphorylation mechanisms of cyclin-dependent kinase Cdk1 in *Saccharomyces cerevisiae*. Tartu, 2013, 157 p.
9. **Liis Karo-Astover.** Studies on the Semliki Forest virus replicase protein nsP1. Tartu, 2013, 113 p.
10. **Piret Arukuusk.** NickFects—novel cell-penetrating peptides. Design and uptake mechanism. Tartu, 2013, 124 p.
11. **Piret Villo.** Synthesis of acetogenin analogues. Asymmetric transfer hydrogenation coupled with dynamic kinetic resolution of  $\alpha$ -amido- $\beta$ -keto esters. Tartu, 2013, 151 p.
12. **Villu Kasari.** Bacterial toxin-antitoxin systems: transcriptional cross-activation and characterization of a novel *mqsRA* system. Tartu, 2013, 108 p.
13. **Margus Varjak.** Functional analysis of viral and host components of alpha-virus replicase complexes. Tartu, 2013, 151 p.
14. **Liane Viru.** Development and analysis of novel alphavirus-based multi-functional gene therapy and expression systems. Tartu, 2013, 113 p.
15. **Kent Langel.** Cell-penetrating peptide mechanism studies: from peptides to cargo delivery. Tartu, 2014, 115 p.